Dynamical Realism and Uncertainty Propagation

by

Inkwan Park

B.S., Yonsei University, 2005

M.S., Yonsei University, 2007

A thesis submitted to the

Faculty of the Graduate School of the

University of Colorado in partial fulfillment

of the requirements for the degree of

Doctor of Philosophy

Department of Aerospace Engineering Sciences

2016

This thesis entitled:
Dynamical Realism and Uncertainty Propagation
written by Inkwan Park
has been approved for the Department of Aerospace Engineering Sciences

Prof. Daniel J. Scheeres

Prof. George H. Born

Prof. Hanspeter Schaub

Prof. Brandon A. Jones

Prof. James D. Meiss

Date

The final copy of this thesis has been examined by the signatories, and we find that both the content and the form meet acceptable presentation standards of scholarly work in the above mentioned discipline.

Park, Inkwan (Ph.D., Aerospace Engineering Sciences)

Dynamical Realism and Uncertainty Propagation

Thesis directed by Prof. Daniel J. Scheeres

In recent years, Space Situational Awareness (SSA) has become increasingly important as the number of tracked Resident Space Objects (RSOs) continues their growth. One of the most significant technical discussions in SSA is how to propagate state uncertainty in a consistent way with the highly nonlinear dynamical environment. In order to keep pace with this situation, various methods have been proposed to propagate uncertainty accurately by capturing the nonlinearity of the dynamical system. We notice that all of the methods commonly focus on a way to describe the dynamical system as precisely as possible based on a mathematical perspective.

This study proposes a new perspective based on understanding dynamics of the evolution of uncertainty itself. We expect that profound insights of the dynamical system could present the possibility to develop a new method for accurate uncertainty propagation. These approaches are naturally concluded in goals of the study. At first, we investigate the most dominant factors in the evolution of uncertainty to realize the dynamical system more rigorously. Second, we aim at developing the new method based on the first investigation enabling orbit uncertainty propagation efficiently while maintaining accuracy.

We eliminate the short-period variations from the dynamical system, called a simplified dynamical system (SDS), to investigate the most dominant factors. In order to achieve this goal, the Lie transformation method is introduced since this transformation can define the solutions for each variation separately. From the first investigation, we conclude that the secular variations, including the long-period variations, are dominant for the propagation of uncertainty, i.e., short-period variations are negligible. Then, we develop the new method by combining the SDS and the higher-order nonlinear expansion method, called state transition tensors (STTs). The new method retains advantages of the SDS and the STTs and propagates uncertainty analytically and nonlinearly.

Dedication

To my wife, Antonia, and my daughter, Narin

Acknowledgements

First and foremost, I am heartily grateful to Prof. Daniel Scheeres, who has been my advisor and a life-long mentor, for supporting me throughout my PhD program. Undoubtedly, it is his guidance and help that made this dissertation exist. I also thank him for his patience and consideration that allow me the freedom to pursue my interest. Sometimes, he has also been a mentor how I can be a good father. Thank you for giving me these invaluable possessions! Also, I am very gratitude to Prof. George Born, Prof. Hanspeter Schaub, Prof. Brandon Jones, and Prof. James Meiss for agreeing to be members of the thesis committee and for providing me critical comments and helpful advice. Their valuable suggestions open my eyes to have a new perspective. Outside of the committee, I wish to especially acknowledge Martin Lara, of Polytechnic University of Madrid, for teaching me with his wealth of knowledge.

I would also like to bless with the creative members, both past and present, of the Celestial and Spaceflight Mechanics Laboratory (CSML). They have always inspired and encouraged me to keep making a step forward in my research. I particularly thank to Dr. Hyun Chul Ko for his consideration and gigantic help. My fellows who have started PhD with me, David, Antonella and Dan, I really thank you for your support. The time we have been together is really wonderful. I also want to thank to Steven Hart and Sarah Melssen, of the Colorado Center for Astrodynamics Research, for their great supports for last five years.

Above all, I appreciate inexhaustible support from my family. To my mother, Anna Lee, and father, Sewoon Park, thank you for guiding me how to live and for believing me. To my mother-in-law, Sangran Kim, and father-in-law, Sundae Hong, really appreciate for your confidence and

support. All of your supports have led me to where I am. Last but not least, especially, sincere gratitude to my wife Antonia for her love, patience, and robust faith in me and to my daughter, Narin, who makes me be the mature people and gives me as happy as I can, but no matter how much say here, I would not feel I have said enough.

Contents

Chapter

Tables

Table

Figures

Figure

Chapter 1

Introduction

1.1 Dynamical Realism in Space Situational Awareness

The term Space Situational Awareness (SSA) refers to the ability to observe, characterize, and predict the properties of natural and artificial objects orbiting the Earth [26] with the objective of avoiding collisions, identifying untracked objects, guaranteeing safety for future space missions, etc. In recent years, SSA has become increasingly important as the number of tracked Resident Space Objects (RSOs) continues their increase. Approximately 16,500 objects, generally greater than 5 cm, exist in the public two-line element (TLE) catalog maintained by the Joint Space Operations Center (JSpOC) [58] as of January 2013 and the number of objects in orbit under 1 cm in diameter is believed to be in the hundreds of thousands, with one estimate as of May 2009 at 700,000 [79]. One of the most significant technical discussions in SSA is how one can propagate state uncertainty (e.g., Figure 1.1) in a way that is consistent with the highly nonlinear dynamical environment [17, 36, 38, 62, 77]. Traditional linearized mapping techniques, e.g., the State Transition Matrix (STM) [76], assume Gaussianity of distributions over time. It has been shown, however, that the Gaussian assumption is an inconsistent description of the actual uncertainty when the dynamics are highly unstable or when propagation times become long [39, 40, 51]. Capturing this nonlinearity in a computationally efficient way is paramount in assuring future SSA capabilities as space becomes even more congested, contested, and competitive. As such, various mathematical expressions of uncertainty have been applied in the context of SSA, e.g., Gaussian sums [17, 28, 36], polynomial chaos expansions (PCEs) [38], State Transition Tensors (STTs) [27, 62, 63], and Taylor series

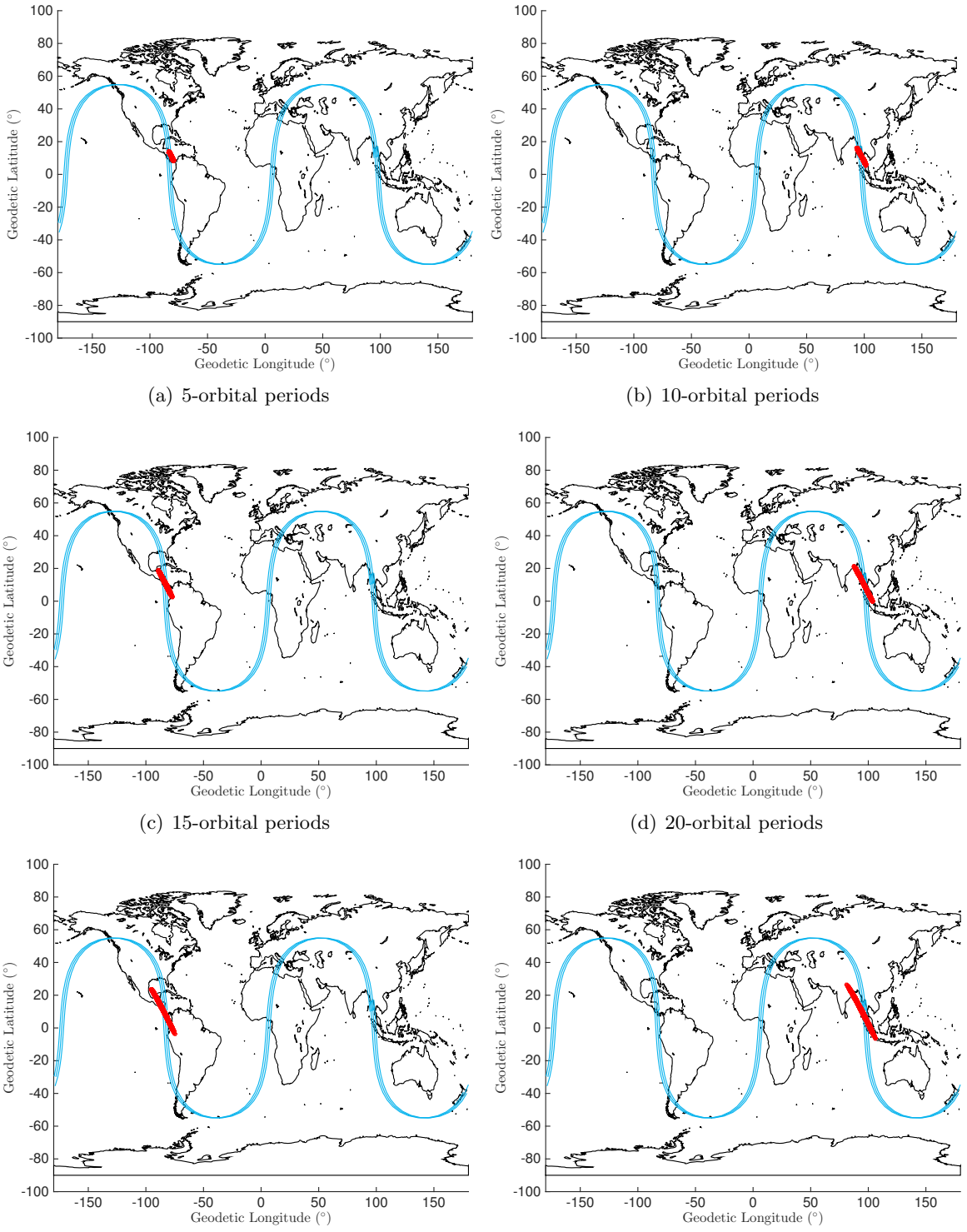

(a) 5-orbital periods

(b) 10-orbital periods

(c) 15-orbital periods

(d) 20-orbital periods

(e) 25-orbital periods

(f) 30-orbital periods

Figure 1.1: Uncertainty evolution of a GPS-like object in the Medium Earth Orbit (MEO) for 30-orbital periods of propagation ($\approx$ 15 days)

polynomial [78].

We take special note that all of the aforementioned methods are focusing on a mathematical perspective to describe the dynamics as precisely as possible. Since 1959, when Dirk Brouwer proposed the analytic solutions for the problem of the artificial satellite theory [9, 10], a lot of researchers have explored the analytic [14, 30, 33, 43, 45, 50, 71] and the semi-analytic solutions [15, 25, 46, 47, 55, 56] for describing the motion of orbiting objects around a central body with additional perturbations such as Solar Radiation Pressure (SRP), gravitational attractions due to perturbing bodies, and atmospheric drag are encountered. Moreover, analytic and semi-analytic solutions are able to provide profound insights about the dynamical system since they classify variations in the motion of an orbiting object. These facts inspire a new perspective to account for an evolution of uncertainty. In particular, if the most dominant factors are found for describing the dynamics of a satellite over time, this perception may present the possibility to develop a new method for the dynamical propagation of an object's probability density function (PDF). We address these questions in this dissertation and they naturally lead to the following thesis statement:

> The identification of the most dominant dynamical factors in the motion of orbiting objects provides the profound insight of the dynamics itself and presents the possibility of developing new methods for the efficient propagation of orbit uncertainty while ensuring accuracy. The semi-analytic solutions derived from the Deprit-Lie canonical transformation method enable these factors to be recognized, and then these solutions become the basis of a Simplified Dynamical System (SDS) that includes the dominant effects only. The new method is developed by combining the SDS with a higher-order nonlinear expansion method, i.e., STTs, and enabling orbit uncertainty propagation analytically and nonlinearly.

Let us introduce each facet of the Thesis Statement in detail.

1.1.1 The Most Dominant Factors in the Evolution of Uncertainty

One problem of concern is determining the role that the accuracy of the dynamical system plays in consistent uncertainty propagation rather than finding a mathematical description of the dynamical system as accurately as possible. This perspective simply poses the question: how accurate must the mapped dynamics be in order to appropriately model the uncertainty distribution? An original inspiration of this question is the discussion that the weak solution of Stochastic Differential Equations (SDE) has the same distribution as the sample path from the strong[1] solution but does not depend on the particular noise realization even in the stochastic case [29]. More specifically, determination of weak solutions often suffices because the first few moments of the exact and weak solutions match to within the same order of magnitude. As these low-order moments are those that are required in many engineering tasks, it is possible to employ a simplified model which is computationally efficient [53, 68, 69].

The idea of the weak solutions is borrowed in our analysis to identify the most dominant factors in the dynamical system since the propagation of uncertainty eventually maps probability density functions (PDF). We define a SDS by assuming the short-period variations as the noise, that is, the SDS plays the same role to the weak solutions of the full dynamical system. The identification of the most dominant factors is investigated based on the general perturbation theory because it divides the dynamical system into secular, short-period, and long-period variations.

In the first investigation, we introduce Brouwer's theory [9, 50] and the averaged Lagrange Planetary Equations [23, 67, 72] to idenfity the factor for a Low Earth Orbit (LEO) satellite, perturbed by J_2 gravity field harmonics, and a Medium Earth Orbit (MEO) satellite, perturbed by J_2 gravity field harmonics and gravitational attraction due to a third-body, respectively. In order to simplify the motion of equations, a pseudo-moon [23], which has a planar motion, is introduced as the perturbing body. For the each investigation, initial offset correction algorithms are implemented to get a precise initial mean conditions in order to apply the SDS accurately [54, 72]. We verify the accuracy of the propagated uncertainty with the SDS to the result from Monte Carlo simulations

[1] This solution describes actual sample paths for a given realization of the noise process.

with the full dynamical system through three statistical approaches [60, 61]: 1) a comparison of the first four moments of PDFs based on the idea of the weak solutions [29], 2) the statistical energy test for more rigorous comparison of PDFs [2, 3], and 3) a normalized standard deviation in order to show the consistency of the propagation.

As the second step, the SDS is expanded with the three objectives of improving the accuracy of the system, adopting additional perturbations, and verifying the accuracy of the SDS with additional perturbations. The Deprit-Lie transformation method [19, 42] is applied to achieve these goals since it provides a systematic way to expand solutions to higher orders and handle multiple perturbations. The expanded SDS is derived from the Deprit-Lie transformation method through two steps, i.e., simplification [18, 49] and normalization [20], and applied to map uncertainty of High Area-to-Mass Ratio (HAMR) objects [59]. The propagated uncertainty with the expanded SDS is also verified statistically. We remove the assumption, i.e., planar motion, in the first investigation by introducing the angular distance.

Throughout the above discussions, we conclude that considering the secular variations, including the long-period variations, is sufficient to capture the propagated uncertainty accurately and consistently. This conclusion identifies the most dominant factors which we posed at the beginning of this section and is herein referred to as dynamical realism. We have to remark that the ignored short-period variations can be recovered whenever necessary based on the idea of the Deprit-Lie transformation method [42].

Lastly, the SDS reduces the nonlinearity of the full dynamical system. This leads to an ability to propagate uncertainty more efficiently. The improvement of the computational efficiency is also verified through a comparison of processing times between Monte Carlo simulations with the full dynamical and the SDSs.

1.1.2 Development of a New Uncertainty Mapping Method

Another topic of recent interest is to propose a new method based on dynamical realism for the accurate and consistent representation of an observed object's uncertainty under nonlinear

dynamics [60, 61]. A motivational question of the new approach is how one can avoid using Monte Carlo simulations [51] in propagating uncertainty without losing accuracy. In this study, we propose a method by combining the advantages of the SDS and the STTs. More specifically, the STTs include higher order terms of the Taylor series expansion of a given dynamical system in order to capture nonlinearities [62, 63]. An advantage we focus on is that the STTs express a PDF at any epoch as a function of the initial PDF and the reference trajectory; thus, once we generate the STTs, we can map the initial PDF to any desired epoch directly. As we have demonstrated, the SDS reduces the nonlinearity of the full dynamical system by eliminating the short-period variations. Thus, the reference trajectory can be propagated more efficiently if the SDS is applied. The new method is defined through two steps to combine these advantages: 1) defining the SDS through the Deprit-Lie transformation method, and then 2) generating the STTs by expanding the SDS as a form of Taylor series expansion.

For the sake of verifying the new method, we incorporate multiple perturbations, such as J_2 gravity field harmonics, a direct SRP, and gravitational attractions due to the Sun and the moon, to the two-body motion. The JPL ephemeris file (DE405) has been applied to calculate the positions of the Sun from January 19, 2008 00:00:00 UCT to February 2, 2008, 23:59:59 UCT. In the same way, the propagated result from the new method is compared to that from Monte Carlo simulations with the full dynamical system statistically. We also investigate several sets of combinations to suggest an optimal set for considered examples at least. Overall, this method succeeds in accurately propagating uncertainty with decreasing the computational burden. For a proof-of-concept implementation under multiple perturbations, the optimal combination of the two ideas is found to sufficiently capture the nonlinear effects. Analytically expressed PDFs based on the STTs and the initial conditions allow one to compute the mean, variance, skewness, and kurtosis of the uncertainty, for example, with the moments of the initial PDF as inputs without any sampling.

Lastly, this study suggests us another possibility to combine the SDS to different mathematical expressions, e.g., Gaussian Mixture Model [17, 28, 36], for mapping PDFs.

1.2 Organization and Contributions

Following is a brief outline of the organization of this dissertation.

Chapter 3 *Nonlinear Mapping of System Dynamics*

Higher-order nonlinear mapping expandsion, i.e., STTs, the Fokker-Plank equation, and the evolution of the Gaussian distribution are introduced. A closed-form solution of the STTs in the Cartesian coordinate space is presented for the two-body problem to show a practical application and to verify an improvement of accuracy as an order of STTs increases. This theoretical framework is implemented numerically in MATLAB. The first two moments, mean and covariance, of a PDF are calculated with analytic expressions [62, 63]. Finally, we propose analytic expressions for the third and fourth order moments as a function of the initial mean, covariance, and STTs.

Chapter 4 *Canonical Perturbation Theory*

The Lie transformation defined by Deprit [19] and its advantageous properties are introduced. Then, more generalized expressions for applying the transformation method, proposed by Kamel [42], is presented. The symplecticity of the transformation is also discussed. Based on these theoretical frameworks, a symbolic manipulator is implemented in *Mathematica*. This manipulator is the basis of the (semi) analytic solutions applied throughout this research. Finally, the analytic solutions are tested with the problem of the artificial satellite theory [9, 10] in order to verify the feasibility and the improvement of the accuracy.

Chapter 5 *Dynamical Realism in Mapping Uncertainty*

The question "how accurate must the mapped dynamics be in order to appropriately model the uncertainty distribution?" is mainly discussed to understand the role of accuracy of the dynamical system for consistent propagation of uncertainty. A SDS is introduced by eliminating the short-period variations from the dynamical system. Implementations of this

idea are based on Brouwer's theory [9, 10] and on the averaged Lagrange Planetary Equations (LPEs) [67, 72]. For the sake of an accurate application of the SDS, a given initial condition in the osculating elements space is converted into the mean space by developing the initial offset correction algorithm. Finally, the SDS for the two-body problem with secular perturbations from J_2 gravity field harmonics and for the two-body problem with multiple perturbations, J_2 gravity field harmonics and a third-body attraction, are tested. Verification of the accuracy of uncertainty mapping and the improvement of the computational efficiency is carried out through statistical approaches and through a comparison of processing times, respectively.

Chapter 6 *Expansion of the Simplified Dynamical System through the Deprit-Lie Transformation*

Based on the discussion about the dynamical realism, the SDS is expanded based on the Deprit-Lie transformation. The new SDS uses the advantages of the transformation method in order to add higher-order solutions for the secular variation as well as to consider additional perturbations exerting on orbiting objects. The generating functions provides an analytic algorithm to define proper initial mean conditions for the SDS instead of applying the initial offset correction. Lastly, simulated examples, uncertainty of orbiting objects in the Medium Earth Orbit (MEO) and a highly elliptical orbit (Molniya), are given for verifying the expanded SDS.

Chapter 7 *Development and Application of the Hybrid Method*

A new method, called a hybrid method, is introduced to map an initial PDF directly to any desired epochs without applying Monte Carlo simulations. The hybrid method is defined by combining the advantages of the STTs and the SDS. According to an order of semi-analytic solutions and an order of the STTs, some sets of combinations are also investigated based on changes in accuracy and processing time. Finally, the hybrid method is developed and verified for the non-Keplerian motion under multiple perturbations, earth oblateness, a direct SRP, and gravitational attractions due to the Sun and moon. Recommendations for an

optimal combination of the two ideas are made based on the discussion about the accuracy and the efficiency.

Various methods have been developed and verified their capability to capture the future uncertainty. These methods are mainly focusing on describing the real dynamical system as precisely as possible with diverse mathematical approaches. Our study is initiated by proposing a different perspective – the profound insight of the dynamical system itself could present a possibility to improve our current capability – to propagate uncertainty accurately.

Our main contributions are summarized with two aspects. At first, from the new perspective, the most dominant factors in an evolution of uncertainty are identified even when the motion of an orbiting body is perturbed by gravitational and non-gravitational sources. Specifically, these dominant factors are captured by the secular dynamics of an orbit. Next, based on the identified dominant factors, we propose a hybrid method by refining the analytic nonlinear mapping technique [62, 63] with the verifications of the accuracy in mapping uncertainty and of the improvement of computational efficiency.

Lastly, it is worth noting that the current hybrid method uses the mathematical approach behind the analytic nonlinear mapping technique. This naturally suggests potential future works, that is, the dynamical realism, we address, can be combined with different well-defined mathematical approaches such as Gaussian Mixture Model (GMM) [17, 28, 36].

Chapter 2

Mathematical Background

2.1 Review of Probability

2.1.1 Probability Theory and Random Process

Definition 1 (The Probability Density Function). For a given continuous random vector $\boldsymbol{x} \in \mathcal{R}^n$, the probability of x in some volume $\mathcal{B}$ can be defined as:

$$p(\boldsymbol{x} \in \mathcal{B}) = \int_{\mathcal{B}} f(\boldsymbol{\eta})\, d\boldsymbol{\eta}, \tag{2.1}$$

where a function $f(\boldsymbol{x})$ is called as a *probability density function*(PDF). Note that

(1) $f(\boldsymbol{x})$ is non-negative for $\forall\, \boldsymbol{x}$.

(2) The area under the curve $f(\boldsymbol{x})$ has to be 1:

$$\int_{-\infty}^{\infty} f(\boldsymbol{\eta})\, d\boldsymbol{\eta} = 1$$

(3) The probability of $\boldsymbol{x}$ that belongs to a subset A is given by the integral of $f(\boldsymbol{x})$ over that interval:

$$p(\boldsymbol{x} \in A) = \int_{A} f(\boldsymbol{\eta})\, d\boldsymbol{\eta}$$

(4) For a given constant $\mathcal{C} \in \mathcal{R}^n$, a probability becomes 0:

$$p(\boldsymbol{x} = \mathcal{C}) = \int_{-\infty}^{\infty} f(\boldsymbol{\eta})\, \mathrm{d}\boldsymbol{\eta} = 0, \quad \text{for } \forall\, \boldsymbol{x}$$

Definition 2 (Moments of Probability Density Function) In statistics, the moment of PDF is a specific quantitative measure of the shape of a set of points. Table 2.1 shows significance of moments (raw, central, standardized) in connection with named properties of distributions. In particular,

Table 2.1: Definition of the moments of probability densify function

Order (k)	Raw moment	Central moment	Standardized moment
1	mean	0	0
2	-	variance	1
3	-	-	skewness
4	-	-	kurtosis
5	-	-	hyper skewness
6	-	-	hyper kurtosis

the moments up to fourth-order, i.e., mean, variance, skewness, and kurtosis, provide information about a shape of PDFs [65, 76].

Definition 3 (Mean and Covariance Matrix). The mean and covariance matrix for a given random vector $\boldsymbol{x} \in \mathcal{R}^n$ with a PDF $f(\boldsymbol{x})$ are calculated by:

$$\boldsymbol{m} = \mathbb{E}[\,\boldsymbol{x}\,] = \int_{-\infty}^{\infty} \boldsymbol{\eta}\, f(\boldsymbol{\eta})\, d\boldsymbol{\eta}, \tag{2.2a}$$

$$\mathbf{P} = \mathbb{E}[\,(\boldsymbol{x}-\boldsymbol{m})(\boldsymbol{x}-\boldsymbol{m})^T\,] = \int_{-\infty}^{\infty} (\boldsymbol{\eta}-\boldsymbol{m})(\boldsymbol{\eta}-\boldsymbol{m})^T\, f(\boldsymbol{\eta})\, d\boldsymbol{\eta}, \tag{2.2b}$$

or

$$m_i = \mathbb{E}[\,x_i\,] = \int_{-\infty}^{\infty} \eta_i\, f(\boldsymbol{\eta})\, d\boldsymbol{\eta}, \tag{2.3a}$$

$$\begin{aligned} \mathrm{P}_{ij} &= \mathbb{E}[\,(x_i - m_i)(x_j - m_j)\,] \\ &= \mathbb{E}[\,x_i x_j\,] - m_i m_j \\ &= \int_{-\infty}^{\infty} \eta_i\, \eta_j\, f(\boldsymbol{\eta}) d\,\boldsymbol{\eta} - m_i m_j. \end{aligned} \tag{2.3b}$$

Note that the variances appear along the diagonal and covariances appear in the off-diagonal elements.

Definition 4 (Skewness). The *skewness* is the third-order standardized moment,

$$\overline{\mu}_{3,i} = \frac{\mathbb{E}[\,x_i - \mathbb{E}[\,x_i\,]\,]^3}{\mu_{2,i}^{3/2}}.$$

It is a measure of symmetry, or more precisely, the lack of symmetry. Figure 2.1 shows how the skewness and the asymmetry are connected.

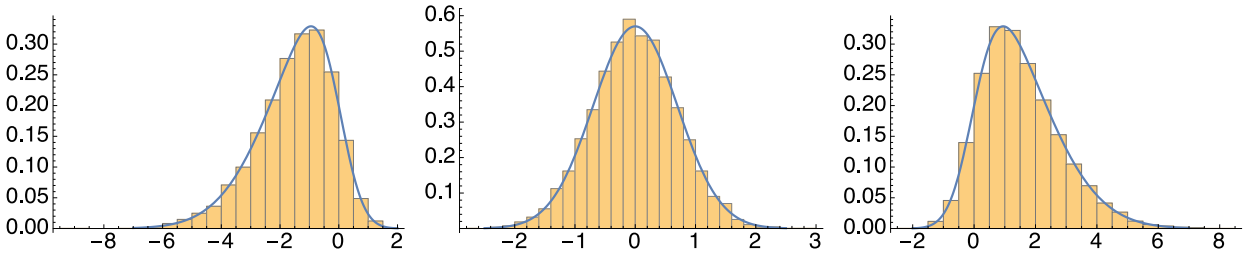

(a) $\overline{\mu}_3 = -3.0$ (b) $\overline{\mu}_3 = 0.0$ (c) $\overline{\mu}_3 = 3.0$

Figure 2.1: Example distributions with third-order standardized moments (skewness): (a) negative skewness, (b) normal distribution, and (c) positive skewness

Definition 5 (Kurtosis). The *kurtosis* is the fourth-order standardized moment,

$$\overline{\mu}_{4,i} = \frac{\mathbb{E}[\,x_i - \mathbb{E}[\,x_i\,]\,]^4}{\mu_{2,i}^2}.$$

It is a measure of whether the data are peaked or flat relative to a normal distribution.

In general, an i-th order moment can be obtained by

$$\mathbb{E}[\,x_1 x_2 \ldots x_i\,]. \tag{2.4}$$

The central moment is a moment of a probability distribution of a random variable about the random variable's mean, which can be defined as follows:

$$\mu_i = \mathbb{E}[\,(x_1 - m_1)(x_2 - m_2)\ldots(x_i - m_i)\,]. \tag{2.5}$$

Definition 6 (Characteristic Function) The *joint characteristic function*(JCF) of a continuous random vector $\boldsymbol{x} \in \mathbb{R}^N$ is defined as:

$$\chi(\boldsymbol{u}) = \mathbb{E}[e^{j\boldsymbol{u}^T\boldsymbol{x}}], \tag{2.6}$$

where $j = \sqrt{-1}$. The higher moments can be computed by

$$\mathbb{E}[\boldsymbol{x}^{\gamma_1}] = j^{-1} \left.\frac{\partial \chi(\boldsymbol{u})}{\partial \boldsymbol{u}^{\gamma_1}}\right|_{\boldsymbol{u}=\boldsymbol{0}}, \tag{2.7a}$$

$$\mathbb{E}[\boldsymbol{x}^{\gamma_1}\boldsymbol{x}^{\gamma_2}] = j^{-2} \left.\frac{\partial^2 \chi(\boldsymbol{u})}{\partial \boldsymbol{u}^{\gamma_1}\partial \boldsymbol{u}^{\gamma_2}}\right|_{\boldsymbol{u}=\boldsymbol{0}}, \tag{2.7b}$$

$$\mathbb{E}[\boldsymbol{x}^{\gamma_1}\boldsymbol{x}^{\gamma_2}\boldsymbol{x}^{\gamma_3}] = j^{-3} \left.\frac{\partial^3 \chi(\boldsymbol{u})}{\partial \boldsymbol{u}^{\gamma_1}\partial \boldsymbol{u}^{\gamma_2}\partial \boldsymbol{u}^{\gamma_3}}\right|_{\boldsymbol{u}=\boldsymbol{0}}, \tag{2.7c}$$

$$\vdots \tag{2.7d}$$

$$\mathbb{E}[\boldsymbol{x}^{\gamma_1}\boldsymbol{x}^{\gamma_2}\ldots\boldsymbol{x}^{\gamma_m}] = j^{-m} \left.\frac{\partial^m \chi(\boldsymbol{u})}{\partial \boldsymbol{u}^{\gamma_1}\partial \boldsymbol{u}^{\gamma_2}\ldots\partial \boldsymbol{u}^{\gamma_m}}\right|_{\boldsymbol{u}=\boldsymbol{0}}. \tag{2.7e}$$

2.1.2 The Gaussian Probability Distribution

Definition 7 (Gaussian Probability Density Function). Let $\boldsymbol{x}$ be a Gaussian random vector, $\boldsymbol{x} \sim \mathcal{N}(\boldsymbol{m}, \mathbf{P})$, where $\boldsymbol{m}$ is the mean vector and $\mathbf{P}$ is the covariance matrix. The *Gaussian probability density function* for $\boldsymbol{x}$ is defined as:

$$p(\boldsymbol{x}) = \frac{1}{\sqrt{(2\pi)^N |\mathbf{P}|}} \exp\left\{-\frac{1}{2}(\boldsymbol{x}-\boldsymbol{m})^T \mathbf{P}^{-1}(\boldsymbol{x}-\boldsymbol{m})\right\}, \tag{2.8}$$

where N is the dimension of the state. The Gaussian probability density function for the univariate distribution is shown in Figure 2.1(b).

First two moments, i.e., $\boldsymbol{m}$ and $\mathbf{P}$, are sufficient to describe the statistics of the Gaussian random vector $\boldsymbol{x}$ completely [21, 52, 74]. This property of the Gaussian probability distribution makes it possible to express the higher moments, e.g., $\mathbb{E}[\, x_i x_j x_k \,]$, $\mathbb{E}[\, x_i x_j x_k x_l \,]$, $\mathbb{E}[\, x_i x_j \ldots x_m \,]$, as functions of $\boldsymbol{m}$ and $\mathbf{P}$. For a nonzero mean Gaussian random vector, $\boldsymbol{x} \sim \mathcal{N}(\boldsymbol{m}, \mathbf{P})$, the higher-order moments can be obtained by substituting the Gaussian JCF

$$\chi(\boldsymbol{u}) = \exp\left\{j\boldsymbol{u}^T\boldsymbol{m} - \frac{1}{2}\boldsymbol{u}^T\mathbf{P}\boldsymbol{u}\right\} \tag{2.9}$$

into Equation (2.7). As a result, the first four moments of the Gaussian probability density function are obtained by

$$\begin{aligned}
\mathrm{E}[x_i] &= m_i \\
\mathrm{E}[x_i x_j] &= m_i m_j + P_{ij} \\
\mathrm{E}[x_i x_j x_k] &= m_i m_j m_k + (m_k P_{ij} + m_j P_{ik} + m_i P_{jk}) \\
\mathrm{E}[x_i x_j x_k x_l] &= m_i m_j m_k m_l + (m_k m_l P_{ij} + m_j m_l P_{ik} + m_j m_k P_{il} + m_i m_l P_{jk} + m_i m_k P_{jl} + m_i m_j P_{kl}) \\
&\quad + P_{il} P_{jk} + P_{ik} P_{jl} + P_{ij} P_{kl}
\end{aligned} \tag{2.10}$$

2.2 Review of Statistics

2.2.1 Goodness-of-Fit

The goodness-of-fit(GoF) of a statistical model indicates how well it fits a set of observations. In general, measures of the GoF summarize the discrepancy between the modeled and observed values in question. The GoF test can be used to make a decision in statistical hypothesis testing: to test whether two samples are obtained from identical distributions (Kolmogorov-Smirnov test), or whether outcome frequencies follow a specified distribution (Pearson's χ-squared test).

2.2.2 Hypothesis Testing

Hypothesis testing is the method to determine the probability that a given hypothesis is true. In statistics, there are two ways, "critical value approach" and "p-value approach", to determine whether the evidence is likely or unlikely given the initial assumption. We use the p-value[1] approach in this study since this approach is used more generally, such as in research, journal articles, and statistical softwares. The usual hypothesis testing consists of four steps as follows:

Step 1. Making an initial assumption, the null hypothesis H_0, and the alternative hypothesis, H_1.

[1] The p-value is the probability that a test statistic at least as significant as the one observed would be obtained assuming that the null hypothesis were true.

Step 2. Define a test statistic in order to assess the truth of the null hypothesis.

Step 3. Compute the p-value.

Step 4. Make the decision by comparing the p-value to an acceptable significance level(α.)

At the last step, we always make the decision either "reject the null hypothesis ($p \leq \alpha$)" or "fail to reject the null hypothesis ($p > \alpha$)." This implies that there is always a chance that we made an error whatever the decision is. These potential errors are called by two different names – one is a "Type I error," and the other a "Type II error." Table 2.2 shows how they correspond to the two types of errors in hypothesis testing. Here are the formal definitions of the two types of errors:

Table 2.2: Type I and II errors in the hypothesis testing

	Truth	
Decision	Null Hypothesis	Alternative Hypothesis
Fail to reject null	OK	Type II error
Reject null	Type I error	OK

· Type I error: The null hypothesis is rejected when it is true.

· Type II error: The null hypothesis is not rejected when it is false.

The significance level, α, is the probability of a Type I error: the probability of rejecting a true null hypothesis. In other words, if the null hypothesis is not rejected, it is close to the truth as large as $(1-\alpha)$, called the confidence level. The probability of a Type II error, the probability of accepting a false null hypothesis, is given by the value of β that will be small as a difference between the null hypothesis and the truth.

2.3 Statistical Approaches of Probability Density Functions Comparison

In order to verify the accuracy of the propagated uncertainty, we introduce three statistical methods: 1) comparing the moments of the PDF up to fourth-order, which has a graphical interpretation, 2) applying the statistical energy test for a more rigorous comparison of the multivariate

PDFs, and 3) defining a normalized standard deviation, which may be computed the fastest of the three methods, to prove the consistency in mapping uncertainty regardless of the propagation interval. Each of these statistical methods is briefly presented here.

2.3.1 Comparison of the Moments

In order to verify if PDFs are compatible, a natural and simple approach is to compare the first a few moments of the sample (or distribution). As demonstrated in Section 2.1.1., especially, first four moments are introduced as quantified values describing the shapes. A basic idea of this approach is to verify if PDFs are compatible based on comparing their shapes [53, 66]. We select the mean, the variance, the third-order standardized moment, and the fourth-order standardized moments among the summarized moments in Table 2.1 in the comparison. The chosen first four moments characterize the shape of most histograms as follows:

- The mean: a measure of location
- The second moment: a measure of spread
- The third moment: a measure of skewness
- The fourth moment: a measure of peakedness (or fat tails)

2.3.2 Statistical Energy Test

For the sake of comparing distributions in a more subtle way, we introduce a statistical energy test. This test measures the goodness of fit (GoF) that represents the discrepancy between observed values of a system and sample values from its model [3]. A measure of the test can be used for a statistical hypothesis testing to decide if some observed and estimated PDFs are identical. The most important property of the statistical energy test over traditional methods, e.g., the Kolmogorov-Smirnov test and Pearson's chi-squared test, is to provide a manageable way to measure the GoF of a distribution of multivariate random variable [2, 3].

A basic assumption of the statistical energy test is that statistical observations have similar relationship to the notion of electrostatic potential energy [2, 75]. Equation (2.11) shows a total energy of a continuous charge density distribution ρ.

$$\mathfrak{K} = \frac{1}{8\pi\,\epsilon_0} \int\int \frac{\rho(\boldsymbol{r})\rho(\boldsymbol{r}')}{|\boldsymbol{r}-\boldsymbol{r}'|}\, d\boldsymbol{r}d\boldsymbol{r}' \tag{2.11}$$

Suppose that there exists an external continuous charge density distribution, ρ_{ex}, as seen in

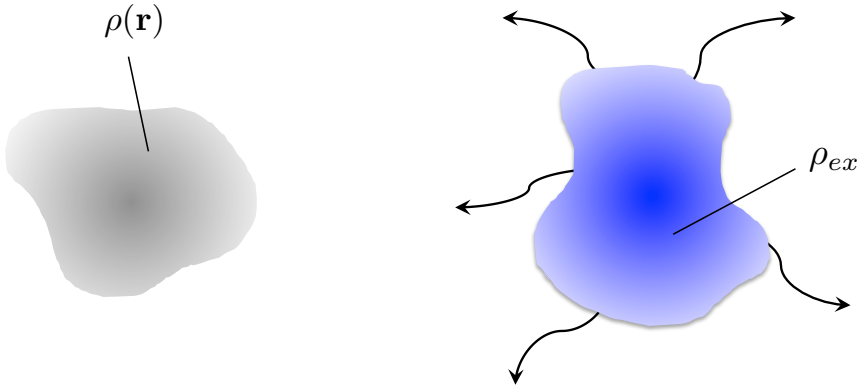

Figure 2.2: Two continuous charge density distributions

Figure 2.2. The total energy $\mathfrak{V}$ of ρ_{ex} with ρ can be calculated by Equation (2.11):

$$\mathfrak{V} = \frac{1}{8\pi\,\epsilon_0} \int\int \frac{[\,\rho(\boldsymbol{r}) + \rho_{ex}(\boldsymbol{r})\,][\,\rho(\boldsymbol{r}') + \rho_{ex}(\boldsymbol{r}')\,]}{|\boldsymbol{r}-\boldsymbol{r}'|}\, d\boldsymbol{r}d\boldsymbol{r}'. \tag{2.12}$$

Then, by considering a system as a positively continuous charge density distribution ρ and a negatively external continuous charge density distribution $-\rho_{ex}$ with

$$\int [\,\rho(\boldsymbol{r}) - \rho_{ex}(\boldsymbol{r})\,] d\boldsymbol{r} = 0, \tag{2.13}$$

we can make the total energy to be zero, i.e., free of charges. This property is applied to compare statistical distributions through the statistical energy test by replacing probability density functions, ρ and ρ_{ex}, with obervations [2, 3].

Definition 8 (Test Statistic) The *test statistic*(Ψ) is a quantity, the energy, which measures the difference between two PDFs $f_0(\boldsymbol{x})$ and $f(\boldsymbol{x})$, $\boldsymbol{x} \in \mathbb{R}^d$, by

$$\Psi = \frac{1}{2} \int\int [\,f(\boldsymbol{x}) - f_0(\boldsymbol{x})\,][\,f(\boldsymbol{x}') - f_0(\boldsymbol{x}')\,]\, R(\boldsymbol{x},\, \boldsymbol{x}')\, d\boldsymbol{x}d\boldsymbol{x}'. \tag{2.14}$$

The distance function $R(\boldsymbol{x}, \boldsymbol{x}')$ is a continuous, monotonic decreasing function of the Euclidian distance between the charges, $|\boldsymbol{x} - \boldsymbol{x}'|$. Equation (2.14) becomes a form of the electrostatic energy of two charge distributions f and f_0 of opposite sign when $R(\boldsymbol{x}, \boldsymbol{x}') = 1/|\boldsymbol{x} - \boldsymbol{x}'|$, which is minimum if the charges neutralize each other.

In order to calculate the test statistic conveniently, we rewrite Equation (2.14) as a function of the expectation values of the distance function R:

$$\begin{aligned}\Psi &= \frac{1}{2}\int\int [\, f(\boldsymbol{x})f(\boldsymbol{x}') + f_0(\boldsymbol{x})f_0(\boldsymbol{x}') - 2f(\boldsymbol{x})f_0(\boldsymbol{x}')\,]\, R\big(|\boldsymbol{x} - \boldsymbol{x}'|\big)\, d\boldsymbol{x}d\boldsymbol{x}' \\ &= \frac{1}{2}\mathbb{E}_1 + \frac{1}{2}\mathbb{E}_2 - \mathbb{E}_3.\end{aligned} \tag{2.15}$$

Since finite samples are considered in statistics, e.g., Monte Carlo approach, for a practical calculation, the integrals in Equation (2.15) can be replaced with corresponding sample means. Therefore, by assuming the number of samples of the reference M and that of the other N, the test statistic, Ψ_{NM}, can be obtained through

$$\begin{aligned}\Psi_{NM} = &\frac{1}{N(N-1)}\sum_{i<j}^{N} R\big(|\boldsymbol{x}_i - \boldsymbol{x}_j|\big) + \frac{1}{M(M-1)}\sum_{i<j}^{M} R\big(|\boldsymbol{y}_i - \boldsymbol{y}_j|\big) \\ &- \frac{1}{NM}\sum_{i=1}^{n}\sum_{j=1}^{M} R\big(|\boldsymbol{x}_i - \boldsymbol{y}_j|\big).\end{aligned} \tag{2.16}$$

The distance function for the electrostatic energy follows inverse power laws, $1/r$. There exist, however, more options since the distance function R should be adjusted to a specific statistical problem [2]. Throughout this research, we use a different distance function, called logarithmic distance function,

$$R\big(|\boldsymbol{x} - \boldsymbol{x}'|\big) = -\ln\big(|\boldsymbol{x} - \boldsymbol{x}'| + \epsilon\big). \tag{2.17}$$

ϵ is applied to avoid the singularity of the logarithm for $\ln 0$. This new distance function allows the test is scale invariant, has no free parameter, and offers a good rejection power against many alternatives to the null hypothesis [81].

As demonstrated above, the statistical energy test measures the GoF for the hypothesis testing. A practical application of the test statistic from Equation (2.16) is as follows:

(1) set the null and alternate hypotheses:

$$\begin{aligned} H_0: &\quad f(\boldsymbol{x}) = f_0(\boldsymbol{x}), \\ H_1: &\quad f(\boldsymbol{x}) \neq f_0(\boldsymbol{x}). \end{aligned} \tag{2.18}$$

(2) assume a significance level α (5% in general.)

(3) estimate a critical energy value Ψ_c with a Monte Carlo approach [3, 24, 34].

(4) acquire the p-value by comparing the test statistic to its critical value:

two distributions are compatible at level α if the statistical energy Ψ_{NM} is less than Ψ_c.

As a result of these steps, we can conclude if two distributions are compatible, i.e., the null hypothesis is accepted, (or incompatible, i.e., the alternate hypothesis is accepted) with a $(1-\alpha)$ confidence level.

2.3.3 Normalized Standard Deviation

We are interested in a comparison of the positional standard deviations of the propagated uncertainties. The dynamics, however, tend to enlarge the positional uncertainty over time, i.e., the standard deviation increases, making an absolute comparison unsuitable to show the consistency of a propagation. For this reason, we define a normalized standard deviation (normalized STD) as a relative metric so as to account for this intrinsic growth in positional uncertainty. By defining the normalized STD as Equation (2.19), we will show the consistency of the proposed propagation method in uncertainty propagation regardless of the propagation interval. Let us assume that the result from the Monte Carlo simulation with a full dynamical system be the truth, $\boldsymbol{X}_{num}(t)$.

$$\text{Normalized STD} = \frac{\sigma(\Delta\delta\mathbf{x})}{\sigma(\delta\mathbf{x}_{\text{num}})}, \tag{2.19}$$

where $\delta\mathbf{x}$ and $\Delta\delta\mathbf{x}$ represent a deviation with respect to the reference trajectory based on the proposed method, which is a propagated state from a given initial state, and the error of each

component($\delta\mathbf{x} - \delta\mathbf{x}_{\text{num}}$), respectively. $\delta\boldsymbol{x}_{num}$ means a true deviation with respect to the true reference trajectory, $\boldsymbol{X}_{num}(t)$.

2.4 Review of Hamiltonian Systems

2.4.1 Dynamics and Properties of the System

Definition 9 (Lagrangian Equations). The Lagrangian equations are defined as

$$\frac{d}{dt}\left(\frac{\partial L}{\partial \dot{q}_i}\right) - \frac{\partial L}{\partial q_i} = 0, \qquad i \in \{1, 2, \ldots, n\} \tag{2.20}$$

where the scalar function $L = L(\boldsymbol{q}, \dot{\boldsymbol{q}}, t)$ and q_i are the Lagrangian function and the generalized coordinates, respectively. The Lagrangian function is a combination of the kinetic energy, T, and potential energy, V, as

$$L(\boldsymbol{q}, \dot{\boldsymbol{q}}, t) = T(\boldsymbol{q}, \dot{\boldsymbol{q}}) - V(\boldsymbol{q}, t)$$

Definition 10 (Hamiltonian Equations). The hamiltonian can be obtained from the Lagrangian through the *Legendre transformation*.

$$\mathcal{H}(\boldsymbol{q}, \boldsymbol{p}, t) = \dot{\boldsymbol{q}} \cdot \boldsymbol{p} - L(\boldsymbol{q}, \dot{\boldsymbol{q}}, t) \tag{2.21}$$

By substituting Equation (2.21) into the Equation (2.20),

$$\frac{d}{dt}\left[\frac{\partial L(\boldsymbol{q}, \dot{\boldsymbol{q}}, t)}{\partial \dot{\boldsymbol{q}}}\right] - \frac{\partial L(\boldsymbol{q}, \dot{\boldsymbol{q}}, t)}{\partial \boldsymbol{q}} = 0, \tag{2.22}$$

we can get

$$\frac{d}{dt}\left[\frac{\partial}{\partial \dot{\boldsymbol{q}}}(\dot{\boldsymbol{q}} \cdot \boldsymbol{p} - \mathcal{H}(\boldsymbol{q}, \boldsymbol{p}, t))\right] - \frac{\partial}{\partial \boldsymbol{q}}(\dot{\boldsymbol{q}} \cdot \boldsymbol{p} - \mathcal{H}(\boldsymbol{q}, \boldsymbol{p}, t)) = 0. \tag{2.23}$$

As a result, the Hamiltonian equations are defined as

$$\dot{q}_i = \frac{\partial \mathcal{H}}{\partial p_i}, \quad \dot{p}_i = -\frac{\partial \mathcal{H}}{\partial q_i}. \tag{2.24}$$

The Hamiltonian is the natural mathematical structure in which to develop the theory of conservative mechanical system; and a system that satisfies Hamiltonian equations is called *canonical*.

Note that the Hamiltonian equations can be written with the symplectic unit matrix as

$$\begin{bmatrix} \dot{\boldsymbol{q}} \\ \dot{\boldsymbol{p}} \end{bmatrix} = \mathbf{J} \begin{bmatrix} \frac{\partial \mathcal{H}}{\partial q_i} \\ \frac{\partial \mathcal{H}}{\partial p_i} \end{bmatrix}. \tag{2.25}$$

Definition 11 (Symplecticity). For a given $2n \times 2n$ matrix $\mathbf{A}$, the matrix is called *symplectic* if it satisfies

$$\boldsymbol{A}^T \mathbf{J} \boldsymbol{A} = \mathbf{J}, \tag{2.26}$$

where

$$\mathbf{J} = \mathbf{J}_{2n \times 2n} = \begin{bmatrix} \mathbf{0}_{n \times n} & \mathbf{I}_{n \times n} \\ -\mathbf{I}_{n \times n} & \mathbf{0}_{n \times n} \end{bmatrix}. \tag{2.27}$$

$\mathbf{J}$ is the symplectic unit matrix.

Properties of the symplectic unit matrix are

$$\mathbf{J}^T \mathbf{J} = -\mathbf{J}\mathbf{J} = \mathbf{I}, \tag{2.28a}$$

$$\mathrm{J}_{\alpha i} \mathrm{J}_{\alpha j} = -\mathrm{J}_{i\alpha} \mathrm{J}_{\alpha j} = \delta_{ij}, \tag{2.28b}$$

$$\det(\mathbf{J}) = 1, \tag{2.28c}$$

where δ_{ij} represent the Kronecker delta function. Note that the the inverse of the symplectic matrix, e.g., $\boldsymbol{A}^{-1}$, can be obtained without a matrix inversion as:

$$\boldsymbol{A}^{-1} = -\mathbf{J} \boldsymbol{A}^T \mathbf{J}. \tag{2.29}$$

Definition 12 (Canonical Transformations). The *canonical transformations* change the given variables $(q_i,\, p_i)$ into a new set $(Q_i,\, P_i)$

$$(q_i,\, p_i) \;\longmapsto\; (Q_i,\, P_i) \tag{2.30}$$

while preserving the canonical form of the equations.

$$\dot{q}_i = \frac{\partial \mathcal{H}}{\partial p_i}, \quad \dot{p}_i = -\frac{\partial \mathcal{H}}{\partial q_i} \;\longmapsto\; \dot{Q}_i = \frac{\partial \mathcal{H}^*}{\partial P_i}, \quad \dot{P}_i = -\frac{\partial \mathcal{H}^*}{\partial Q_i}, \tag{2.31}$$

where $\mathcal{H}$ and $\mathcal{H}^*$ represent the given Hamiltonian and a new Hamiltonian, respectively.

2.4.2 Poisson Brackets

The Poisson bracket, $\{-,-\}$, for two functions of the canonical variables can be defined as

$$\{F,\, G\} = \sum_{i=1}^{n} \left(\frac{\partial F}{\partial q_i}\frac{\partial G}{\partial p_i} - \frac{\partial G}{\partial q_i}\frac{\partial F}{\partial p_i} \right), \tag{2.32}$$

where $\boldsymbol{q} = (q_1, \ldots, q_n)$ and $\boldsymbol{p} = (p_1, \ldots, p_n)$ are generalized coordinates. It is worth mentioning that Hamiltonian equations, Equation (2.24), can be rewritten with the Poisson brackets as

$$\begin{aligned} \dot{q}_i &= \{q_i,\, \mathcal{H}\}, \\ \dot{p}_i &= \{p_i,\, \mathcal{H}\}, \end{aligned} \tag{2.33}$$

where the Hamiltonian $\mathcal{H} = \mathcal{H}(\boldsymbol{q},\, \boldsymbol{p})$. The Poisson brackets can be rewritten with the symplectic matrix, $\mathbf{J}$, as

$$\{F,\, G\} = \triangledown F \cdot (\mathbf{J} \cdot \triangledown G) = \left(\frac{\partial F}{\partial \boldsymbol{z}}\right) \cdot \mathbf{J} \cdot \left(\frac{\partial G}{\partial \boldsymbol{z}}\right)^{T}, \tag{2.34}$$

where $z_i = q_i$ and $z_{i+n} = p_i$. Lastly, the Poisson brackets have four useful properties as follows:

(1) The Skew-symmetry (antisymmetry)

$$\{F,\, G\} = -\{G,\, F\}. \tag{2.35}$$

(2) The linearity and bilinearity

$$\begin{aligned} \{\alpha_1 F_1 + \alpha_2 F_2,\, G\} &= \alpha_1\{F_1,\, G\} + \alpha_2\{F_2,\, G\}, \\ \{\alpha_1 F_1 + \alpha_2 F_2,\, \beta_1 G_1 + \beta_2 G_2\} &= \alpha_1\beta_1\{F_1,\, G_1\} + \alpha_1\beta_2\{F_1,\, G_2\} \\ &\quad + \alpha_2\beta_1\{F_2,\, G_1\} + \alpha_2\beta_2\{F_2,\, G_2\}. \end{aligned} \tag{2.36}$$

(3) The Leibnitz property (product rule)

$$\{F,\, GH\} = G\{F,\, H\} + \{F,\, G\}H. \tag{2.37}$$

(4) The Jacobi identity

$$\{F,\, \{G,\, H\}\} + \{G,\, \{H,\, F\}\} + \{H,\, \{F,\, G\}\} = 0. \tag{2.38}$$

2.4.3 The Extended Phase Space

The extended phase space is necessary when we consider non-autonomous Hamiltonian dynamics, which is a particular case of autonomous Hamiltonian dynamics. For a given non-autonomous Hamiltonian in $2n$-dimensional phase space, the extended phase space can be defined by introducing the time, t, and its conjugate momenta, p_t into the original phase space as seen in Equation (2.39).

$$\boldsymbol{q} = (q_1,\, q_2, \ldots, q_n,\, t), \tag{2.39a}$$

$$\boldsymbol{p} = (p_1,\, p_2, \ldots, p_n,\, p_t). \tag{2.39b}$$

By assuming that the generalized coordinates are a function of a parameter τ, the Hamilton's equations become

$$\frac{dq_i}{d\tau} = t'\frac{\partial \mathcal{H}}{\partial p_i}, \qquad \frac{dp_i}{d\tau} = -t'\frac{\partial \mathcal{H}}{\partial q_i} \qquad (i = 1,\, 2, \ldots, n) \tag{2.40}$$

where t' denotes the derivative of t with respect to τ. As t' is independent of the variables q_i and p_i, Equation (2.40) can be rewritten as

$$\frac{dq_i}{d\tau} = \frac{\partial(\mathcal{H}t')}{\partial p_i}, \qquad \frac{dp_i}{d\tau} = -\frac{\partial(\mathcal{H}t')}{\partial q_i} \tag{2.41}$$

If p_t is the conjugate momentum of the time t, a complementary differential equation may be introduced based on the Hamilton's equations as

$$t' = \frac{dt}{d\tau} = \frac{\partial(t'p_t)}{\partial p_t}. \tag{2.42}$$

An unified form of these equations becomes

$$\frac{dq_i}{d\tau} = \frac{\partial \mathcal{K}}{\partial p_i}, \qquad \frac{dp_i}{d\tau} = -\frac{\partial \mathcal{K}}{\partial q_i}, \tag{2.43a}$$

$$\frac{dt}{d\tau} = \frac{\partial \mathcal{K}}{\partial p_t}, \qquad \frac{dp_t}{d\tau} = -\frac{\partial \mathcal{K}}{\partial t}, \tag{2.43b}$$

where

$$\mathcal{K}\big(q_i,\, t,\, p_i,\, p_t\big) = t'\mathcal{H} + t'p_t. \tag{2.44}$$

$\mathcal{K}$ is the new Hamiltonian of the given system in the extended phase space. In practical applications, the relation between the time t and the parameter τ is an identity; thus, $t' = 1$ in general. The moment conjugates to the time, p_t, is usually an opposite energy, i.e., $-\mathcal{H}$.

Chapter 3

Nonlinear Mapping of System Dynamics

In this chapter, we discuss an analytic method of nonlinear uncertainty propagation and of an evolution of PDF. A special solution to the Fokker-Planck equations for deterministic systems and the concept of the State Transition Tensors (STTs) are combined so that, given an analytical expression of both the initial probability distribution and the dynamics, the probability distribution may be expressed analytically for all time. Moreover, the analytic expressions for calculating the third and fourth order moments are introduced as an expansion of the previous studies [27, 62, 63]. In order to understand the STTs more clearly, the two-body dynamics is applied to the above framework.

The outline of this chapter is as follows. A brief review of the STTs is presented. Then, the solution of the Fokker-Planck equation for a deterministic dynamical system is discussed with a focus on the integral invariance. This property provides a theoretical background to define the analytic expressions of an evolution of the Gaussian distribution. Additional analytic expressions to compute the third and fourth order moments are introduced. Then, finally, this theoretical framework is implemented numerically in MATLAB. Lastly, by taking an example with a two-body problem, the accuracy of the propagated uncertainty and the PDF from STTs with different orders (up to fourth order) are investigated.

3.1 Higher Order Nonlinear Mapping Expansion

Suppose that dynamics of an orbiting object is governed by the equations of motion as

$$\dot{\boldsymbol{x}}(t) = \boldsymbol{f}(t,\, \boldsymbol{x}(t)), \tag{3.1}$$

where $\boldsymbol{x}$ and $\boldsymbol{f}$ represent state vector and the equations of motion [27, 62], respectively.

Definition 13 (Solution Flow) A *solution flow* maps an initial state $\boldsymbol{x}^0$ $(t = t^0)$ to a state $\boldsymbol{x}(t)$ at any time $t = t$. A solution of Equation (3.1) can be expressed as a function of the solution flow, ϕ, as follows:

$$\boldsymbol{x}(t) = \phi(t\,;\, \boldsymbol{x}^0,\, t^0). \tag{3.2}$$

Then, the solution flow satisfies

$$\begin{aligned} \frac{d\phi}{dt} &= \boldsymbol{f}(t,\, \phi(t\,;\, \boldsymbol{x}^0, t^0)), \\ \phi(t^0\,;\, \boldsymbol{x}^0,\, t^0) &= \boldsymbol{x}(t^0). \end{aligned} \tag{3.3}$$

Definition 14 (Phase Volume) A *phase volume* is a subset of Euclidean space $\mathbb{R}^N$ that is closed and bounded. Suppose that the phase volume of any given initial distribution is $\mathcal{B}_0$, then a phase volume at time t is

$$\mathcal{B}(t) = \{\boldsymbol{x}(t) | \boldsymbol{x}(t) = \phi(t\,;\, \boldsymbol{x}^0,\, t^0),\ \forall\, \boldsymbol{x}^0 \in \mathcal{B}_0\}. \tag{3.4}$$

Since the solution flow describes a future state as a function of the initial conditions, it allows to express an evolution of distribution more conveniently. For a given reference initial condition $\boldsymbol{x}_0$, the relative motion of $\delta\boldsymbol{x}(t)$ with respect to the reference (nominal) trajectory becomes

$$\delta\boldsymbol{x}(t) = \phi(t\,;\, \boldsymbol{x}_0 + \delta\boldsymbol{x}^0, t^0) - \phi(t\,;\, \boldsymbol{x}^0, t^0), \tag{3.5}$$

where $\delta\boldsymbol{x}_0$ represents a deviation in $\boldsymbol{x}_0$. Then, the relative motion satisfies the equation of motion shown in Equation (3.5):

$$\delta\dot{\boldsymbol{x}}(t) = \boldsymbol{f}(t,\, \phi(t\,;\, \boldsymbol{x}^0 + \delta\boldsymbol{x}^0, t^0)) - \boldsymbol{f}(t,\, \phi(t\,;\, \boldsymbol{x}^0, t^0)). \tag{3.6}$$

Definition 15 (Taylor Series Expansion) Suppose that a given equation, $\boldsymbol{\mathcal{F}}(\boldsymbol{x})$, is an infinitely differentiable and real function with $(\boldsymbol{\mathcal{F}}(\boldsymbol{x}),\, \boldsymbol{x}) \in \mathbb{R}^N$, the Taylor series expansion about a point $\boldsymbol{x} = \boldsymbol{a}$ is defined as:

$$\mathcal{F}^i\left(x^1, \ldots, x^N\right) = \sum_{j=0}^{\infty} \frac{1}{j!} \left[\sum_{k=1}^{N} \left(x^k - a^k\right) \frac{\partial}{\partial \xi^k} \right]^j \mathcal{F}^i\left(\xi^1, \ldots, \xi^N\right) \Bigg|_{\xi^l = a^l}, \tag{3.7}$$

where $\boldsymbol{\xi}$ represents a dummy variable.

By substituting Equation (3.5) or (3.6) into $\boldsymbol{\mathcal{F}}(\boldsymbol{x})$ and expanding it with respect to the initial state $\boldsymbol{x}^0$, the relative motion and the relative trajectory dynamics, respectively, can be rewritten using the Einstein summation convention as:

$$\delta\boldsymbol{x}(t) = \sum_{p=1}^{m} \frac{1}{p!} \Phi_{i,k_1 \ldots k_p} \delta\boldsymbol{x}^0_{k_1} \ldots \delta\boldsymbol{x}^0_{k_p}, \tag{3.8a}$$

$$\delta\dot{\boldsymbol{x}}(t) = \sum_{p=1}^{m} \frac{1}{p!} \mathrm{A}_{i,k_1 \ldots k_p} \delta\boldsymbol{x}_{k_1} \ldots \delta\boldsymbol{x}_{k_p}, \tag{3.8b}$$

where $k_j \in \{1, 2, \ldots, N\}$, k_j represents the k_j-th component of the state vector.

$$\Phi_{i,k_1 \ldots k_p} = \frac{\partial^p \phi^i(t\,;\, \boldsymbol{x}^0,\, t^0)}{\partial \boldsymbol{x}^0_{k_1} \ldots \partial \boldsymbol{x}^0_{k_p}}, \tag{3.9}$$

$$\mathrm{A}_{i,k_1 \ldots k_p} = \left. \frac{\partial^p \boldsymbol{f}^i(t,\, \boldsymbol{x}(t))}{\partial \boldsymbol{x}_{k_1} \ldots \partial \boldsymbol{x}_{k_p}} \right|_{\boldsymbol{x} = \boldsymbol{x}^*}, \tag{3.10}$$

denote STTs and a local dynamics tensor (LDT) [27], evaluated along the nominal trajectory $\boldsymbol{x}^*$. The STT in Equation (3.9) is equivalent to the State Transition Matrix (STM) [76] where $m = 1$. In general, since we may have dynamics model rather than the solution flow, it is impossible to generate the STT directly in most cases. For that reason, in order to get the STT, we need to use two different expressions of the relative trajectory dynamics $\delta\dot{\boldsymbol{x}}(t)$. The first expression is from a time derivative of Equation (3.8a) as follows:

$$\delta\dot{\boldsymbol{x}}(t) = \sum_{p=1}^{m} \frac{1}{p!} \dot{\Phi}_{i,k_1 \ldots k_p} \delta\boldsymbol{x}^0_{k_1} \ldots \delta\boldsymbol{x}^0_{k_p}. \tag{3.11}$$

The other is to substitute Equation (3.8a) into Equation (3.8b), then the relative trajectory dynamics can be defined as a function of the STT and initial deviations. By comparing it to Equation (3.11), one can obtain the differential equations of the STT, which are given below up to fourth

order.

$$\dot{\Phi}^{i,a} = A^{i,\alpha}\Phi^{\alpha,a}, \tag{3.12a}$$

$$\dot{\Phi}^{i,ab} = A^{i,\alpha}\Phi^{\alpha,ab} + A^{i,\alpha\beta}\Phi^{\alpha,a}\Phi^{\beta,b}, \tag{3.12b}$$

$$\dot{\Phi}^{i,abc} = A^{i,\alpha}\Phi^{\alpha,abc} + A^{i,\alpha\beta}(\Phi^{\alpha,a}\Phi^{\beta,bc} + \Phi^{\alpha,ab}\Phi^{\beta,c} + \Phi^{\alpha,ac}\Phi^{\beta,b}) + A^{i,\alpha\beta\gamma}\Phi^{\alpha,a}\Phi^{\beta,b}\Phi^{\gamma,c}, \tag{3.12c}$$

$$\begin{aligned}\dot{\Phi}^{i,abcd} &= A^{i,\alpha}\Phi^{\alpha,abcd} + A^{i,\alpha\beta}(\Phi^{\alpha,abc}\Phi^{\beta,d} + \Phi^{\alpha,abd}\Phi^{\beta,c} + \Phi^{\alpha,acd}\Phi^{\beta,b} + \Phi^{\alpha,ab}\Phi^{\beta,cd} \\ &+ \Phi^{\alpha,ac}\Phi^{\beta,bd} + \Phi^{\alpha,ad}\Phi^{\beta,bc} + \Phi^{\alpha,a}\Phi^{\beta,bcd}) + A^{i,\alpha\beta\gamma}(\Phi^{\alpha,ab}\Phi^{\beta,c}\Phi^{\gamma,d} + \Phi^{\alpha,ac}\Phi^{\beta,b}\Phi^{\gamma,d} \\ &+ \Phi^{\alpha,ad}\Phi^{\beta,b}\Phi^{\gamma,c} + \Phi^{\alpha,a}\Phi^{\beta,bc}\Phi^{\gamma,d} + \Phi^{\alpha,a}\Phi^{\beta,bd}\Phi^{\gamma,c} + \Phi^{\alpha,a}\Phi^{\beta,b}\Phi^{\gamma,cd}) + A^{i,\alpha\beta\gamma\delta}\Phi^{\alpha,a}\Phi^{\beta,b}\Phi^{\gamma,c}\Phi^{\delta,d}\end{aligned} \tag{3.12d}$$

The initial conditions for STT can be simply defined identity tensors because $\Phi^0_{i,a} = 1$, *iff* $i = a$, otherwise $\Phi^0_{i,a} = 0$. After solving for the STT, one can compute deviations at time $t\,(t > t^0)$ analytically by adding the higher-order solution to the nominal trajectory, $\boldsymbol{x}_i(t) = \boldsymbol{x}^*_i(t) + \boldsymbol{\Phi}\cdot\delta\boldsymbol{x}^0_i = \boldsymbol{x}^*_i(t) + \delta\boldsymbol{x}_i(t)$.

3.2 Solution of the Fokker-Planck Equation for a Deterministic Dynamics

Orbital dynamics problems entailing uncertainty can be expressed with the Itô stochastic differential equation,

$$\delta\boldsymbol{x}(t) = f(\boldsymbol{x}(t), t)\,\mathrm{d}t + \boldsymbol{G}(\boldsymbol{x}(t), t)\,\mathrm{d}\boldsymbol{\beta}(t), \tag{3.13}$$

where $\boldsymbol{G}$ and $\boldsymbol{\beta}$ are an n-by-m matrix characterizing the diffusion and the diffusion vector, respectively. Suppose that a given system satisfying the Itô stochastic differential equation, the time evolution of a probability density function (PDF), $p(\boldsymbol{x}, t)$, over $\boldsymbol{x}$ at time t is described by the Fokker-Planck equation [51],

$$\frac{\partial p(\boldsymbol{x},t)}{\partial t} = -\sum_{i=1}^{N}\frac{\partial}{\partial x_i}[p(\boldsymbol{x},\,t)\boldsymbol{f}_i(\boldsymbol{x},\,t)] + \frac{1}{2}\sum_{i=1}^{N}\sum_{j=1}^{N}\frac{\partial^2}{\partial x_i\partial x_j}\left[p(\boldsymbol{x},t)\{\boldsymbol{G}(\boldsymbol{x},t)\boldsymbol{Q}(t)\boldsymbol{G}^T(\boldsymbol{x},t)\}^{ij}\right], \tag{3.14}$$

where a single subscript and a double subscript indicate vector components and matrix components, respectively. If one defined the Fokker-Planck equation without the diffusion terms, i.e., $\boldsymbol{\beta}(t) = 0$,

it would become simpler as

$$\frac{\partial p(\boldsymbol{x}, t)}{\partial t} = -\sum_{i=1}^{N} \frac{\partial}{\partial x_i}[\, p(\boldsymbol{x},\, t)\boldsymbol{f}_i(\boldsymbol{x},\, t)]. \tag{3.15}$$

Note that solutions of the FPE give the true evolution of the probability density function. However, including these partial differential equations in the trajectory navigation problem introduces additional difficulties and is usually avoided for practical reasons. In this thesis, we consider systems with no process noise and the probability density function satisfies the Fokker-Planck equation defined in Equation (3.15). This is a reasonable model for astrodynamics problems with no thrusters and no dissipative forces acting on the spacecraft.

Definition 16 (Integral Invariance) Consider a dynamical system with the governing equations of motion $\dot{\boldsymbol{x}} = \boldsymbol{g}(\boldsymbol{x},\, t)$ and let $I(\boldsymbol{x},\, t)$ be an integral of a vector field $M(\boldsymbol{x},\, t)$ over some volume $\mathcal{B}$:

$$I(\boldsymbol{x},\, t) = \int_{\mathcal{B}} M(\boldsymbol{x},\, t)\, d\boldsymbol{x}. \tag{3.16}$$

The integral $I(\boldsymbol{x},\, t)$ is called an integral invariant if it is constant for all time, i.e., $dI/dt = 0$. In general, the sufficiency condition for integral invariance can be explicitly stated as

$$\frac{\partial M(\boldsymbol{x},\, t)}{\partial t} = -\sum_{i=1}^{N} \frac{\partial}{\partial x^i} \left[\, M(\boldsymbol{x},\, t)\, g^i(\boldsymbol{x},\, t) \,\right], \tag{3.17}$$

which is known as Liouville's equation.

By comparing Equation (3.15) with Equation (3.17), we see that $p(\boldsymbol{x},\, t)$ satisfies the sufficiency condition for the probability to be an integral invariant. Hence, this implies that probability of any dynamical system with no diffusion term is an integral invariant.

The integral invariant can be shown as well by using the deterministic Hamiltonian. Let us consider a Hamiltonian $\mathcal{H}(\boldsymbol{q},\, \boldsymbol{p})$, which is a function of n-dimensional generalized coordinate $\boldsymbol{q}$ and conjugate moment $\boldsymbol{p}$. The equation of motion, $\dot{\boldsymbol{x}}(t)$, can be written with the symplectic identity matrix $\mathbf{J}$ as follows:

$$\dot{\boldsymbol{x}}(t) = \mathbf{J}\mathcal{H}_{\boldsymbol{x}}^{\mathrm{T}}, \tag{3.18}$$

where $\boldsymbol{x} = [\,\boldsymbol{q}^{\mathrm{T}} \quad \boldsymbol{p}^{\mathrm{T}}\,]$. Assuming a deterministic Hamiltonian, the Fokker-Planck equation in Equation (3.15) can be written as follow.

$$\frac{\partial p(\boldsymbol{x}, t)}{\partial t} = -\sum_{i=1}^{N} \left[\frac{\partial p(\boldsymbol{x},\, t)}{\partial x_i}\, \dot{\boldsymbol{x}}_i + p(\boldsymbol{x},\, t)\, \mathrm{tr}\left(\mathbf{J}\mathcal{H}_{\boldsymbol{xx}}^{\mathrm{T}}\right) \right], \tag{3.19}$$

where $\mathrm{tr}(\cdot)$ represents the trace of a matrix, i.e., a summation of diagonal elements. The second term on the right-hand side is

$$\mathrm{tr}\left(\mathbf{J}\mathcal{H}_{\boldsymbol{xx}}^{\mathrm{T}}\right) = \mathrm{tr} \begin{bmatrix} \mathcal{H}_{\boldsymbol{pq}} & \mathcal{H}_{\boldsymbol{pp}} \\ -\mathcal{H}_{\boldsymbol{qq}} & -\mathcal{H}_{\boldsymbol{qp}} \end{bmatrix} = 0.$$

This fact reduces the Fokker-Planck equation to:

$$\frac{d\, p(\boldsymbol{x}, t)}{dt} = 0. \tag{3.20}$$

Thus, the solution of the Fokker-Planck equation is:

$$p(\boldsymbol{x},\, t) = p\left[\, \phi(t\,;\, \boldsymbol{x}^0,\, t^0),\, t\,\right] = p(\boldsymbol{x}^0,\, t), \tag{3.21}$$

where $p(\boldsymbol{x}^0,\, t^0)$ is assumed to be specified. A time invariance in Equation (3.20) shows that the probability of the state in some phase volume $\mathcal{B}(t)$ is an integral invariant. Then, this lead to

$$\begin{aligned} \Pr(\boldsymbol{x} \in \mathcal{B}) &= \int_{\mathcal{B}} p(\boldsymbol{x},\, t)\, d\boldsymbol{x} \\ &= \int_{\mathcal{B}_0} p(\phi(t\,;\, \boldsymbol{x}^0,\, t^0),\, t) \left| \frac{\partial \boldsymbol{x}}{\partial \boldsymbol{x}^0} \right| d\boldsymbol{x}^0 \\ &= \int_{\mathcal{B}_0} p(\boldsymbol{x}^0, t^0)\, d\boldsymbol{x}^0, \end{aligned} \tag{3.22}$$

which gives

$$p(\phi(t\,;\, \boldsymbol{x}^0,\, t^0),\, t) \left| \frac{\partial \boldsymbol{x}}{\partial \boldsymbol{x}^0} \right| = p(\boldsymbol{x}^0, t^0). \tag{3.23}$$

Since the mapping from $\boldsymbol{x}^0$ to $\boldsymbol{x}$ is canonical in the Hamiltonian system, the determinant $\left|\partial \boldsymbol{x}/\partial \boldsymbol{x}^0\right|$ becomes 1. Equation (3.23) indicates that the PDF at a specific epoch t ($t \neq t^0$) can be characterized by the initial PDF; thus, if the solution is known as a function of initial conditions and the PDF is known at any arbitrary epoch, the PDFs for all time can be found.

3.3 Nonlinear Mapping of the Gaussian Distribution

Using the aforementioned property, shown in Equation (3.23), the mean of PDFs at any arbitrary epoch can be rewritten as a function of the initial conditions as

$$\begin{aligned} \mathrm{E}[\boldsymbol{x}(t)] &= \int_{\infty} \boldsymbol{x}(t)\, p(\boldsymbol{x}, t)\, d\boldsymbol{x} \\ &= \int_{\infty} \phi(t; \boldsymbol{x}^0, t^0) p(\boldsymbol{x}^0, t^0)\, d\boldsymbol{x}^0 \end{aligned} \tag{3.24}$$

We observe that Equation (3.24) is suitable for computation of the state uncertainties using the STT formulation because the solution flow can be expanded using the Taylor series and higher moments can be computed using the joint conditional function(JCF) of the initial Gaussian distribution [62]. Consider the Gaussian boundary condition for the PDF. The PDF for the state $\delta\boldsymbol{x}^0$ can be obtained via a linear transformation, $\boldsymbol{x}^0 = \delta\boldsymbol{x}^0 + \boldsymbol{m}^0 - \delta\boldsymbol{m}^0$, where $\boldsymbol{m}^0$ is the initial mean and $\delta\boldsymbol{m}^0$ is the initial mean of the deviation by assuming a nonzero mean for the initial state. By substituting these relations into Equation (2.8), the PDF yields

$$p(\delta\boldsymbol{x}^0,\, t^0) = \frac{1}{\sqrt{(2\pi)^n \det \mathbf{P}^0}} \exp\left\{ -\frac{1}{2} (\delta\boldsymbol{x}^0 - \delta\boldsymbol{m}^0)^{\mathrm{T}} \boldsymbol{\Lambda}^0 (\delta\boldsymbol{x}^0 - \delta\boldsymbol{m}^0) \right\}. \tag{3.25}$$

Since the expectation of the nominal trajectory does not change, by definition, it is easier to instead analyze the statistics of the deviated state. As seen in Equation (3.8a), a state at future can be mapped with the STTs and initial deviations. The nominal trajectory is fixed in time, thus the current state mean and covariance are defined with the deviated state and STTs

$$\delta\boldsymbol{m}_i(t) = \sum_{p=1}^{m} \frac{1}{p!} \Phi_{i,k_1\ldots k_p}\, \mathbb{E}[\delta\boldsymbol{x}^0_{k_1} \ldots \delta\boldsymbol{x}^0_{k_p}], \tag{3.26a}$$

$$\begin{aligned} \mathrm{P}_{ij}(t) = &\left(\sum_{p=1}^{m} \sum_{q=1}^{m} \frac{1}{p!\, q!} \Phi_{i,k_1\ldots k_p} \Phi_{j,l_1\ldots l_p}\, \mathbb{E}[\delta\boldsymbol{x}^0_{k_1} \ldots \delta\boldsymbol{x}^0_{k_p} \delta\boldsymbol{x}^0_{l_1} \ldots \delta\boldsymbol{x}^0_{l_p}] \right) \\ &- \delta\boldsymbol{m}_i(t) \delta\boldsymbol{m}_j(t), \end{aligned} \tag{3.26b}$$

where $\{k_j,\, l_j\} \in \{1, \ldots, 2n\}$ and m is the order of the expansion of the dynamics. Consequentially, Equation (3.26) gives an analytic method to compute the mean and covariance of a current PDF directly.

Up to $2m$-order moment of the initial PDF is required to propagate the covariance matrix, where an n-th order moment, $\kappa^{\gamma_1,\ldots,\gamma_n}$, is defined Equation (2.5) [35, 52] as

$$\kappa^{\gamma_1,\ldots,\gamma_n} = \mathbb{E}[\,(x_{\gamma_1} - m_{\gamma_1})(x_{\gamma_2} - m_{\gamma_2})\ldots(x_{\gamma_i} - m_{\gamma_i})\,].$$

In this research, we derive the third and fourth order central moments based on the above equation as follows:

$$\begin{aligned}
\mu_3^{ijk}(t) = &\left(\sum_{p=1}^{m}\sum_{q=1}^{m}\sum_{r=1}^{m} \frac{1}{p!q!r!}\Phi_{i,k_1\ldots k_p}\Phi_{j,l_1\ldots l_q}\Phi_{k,m_1\ldots m_r}\times \right. \qquad (3.27a)\\
&\left. \mathbb{E}[\delta x^0_{k_1}\ldots\delta x^0_{k_p}\delta x^0_{l_1}\ldots\delta x^0_{l_q}\delta x^0_{m_1}\ldots\delta x^0_{m_r}] \right) - \Big(\delta m^i(t)P^{jk}(t) + \delta m^j(t)P^{ik}(t) + \delta m^k(t)P^{ij}(t) \Big)\\
&- \delta m^i(t)\delta m^j(t)\delta m^k(t),\\
\mu_4^{ijkl}(t) = &\left(\sum_{p=1}^{m}\sum_{q=1}^{m}\sum_{r=1}^{m}\sum_{s=1}^{m} \frac{1}{p!q!r!s!}\Phi_{i,k_1\ldots k_p}\Phi_{j,l_1\ldots l_q}\Phi_{k,m_1\ldots m_r}\Phi_{l,n_1\ldots n_s} \right. \qquad (3.27b)\\
&\left. \times\, \mathbb{E}[\delta x^0_{k_1}\ldots\delta x^0_{k_p}\delta x^0_{l_1}\ldots\delta x^0_{l_q}\delta x^0_{m_1}\ldots\delta x^0_{m_r}\delta x^0_{n_1}\ldots\delta x^0_{n_s}] \right) - \Big\{ \delta m^i(t)\delta m^j(t)P^{kl}(t)\\
&+\delta m^i(t)\delta m^k(t)P^{jl}(t) + \delta m^j(t)\delta m^k(t)P^{il}(t) + \delta m^i(t)\delta m^l(t)P^{jk}(t) + \delta m^j(t)\delta m^l(t)P^{ik}(t)\\
&+\delta m^k(t)\delta m^l(t)P^{ij}(t) \Big\} - (P^{ij}P^{kl} + P^{ik}P^{jl} + P^{il}P^{jk}) - \delta m^i(t)\delta m^j(t)\delta m^k(t)\delta m^l(t).
\end{aligned}$$

3.4 Uncertainty Propagation Using State Transition Tensors

In this section, results of MATLAB implementations of the analytic theory discussed above are shown. Then, the moments of PDF are calculated with Equations (3.26)-(3.27). An initial

condition is defined as:

$$\mathbf{X}_0 = \begin{pmatrix} \boldsymbol{r}_0 \\ \boldsymbol{v}_0 \end{pmatrix} = \begin{pmatrix} 757700.301 \\ 5222606.566 \\ 4851499.770 \\ 2213.250611 \\ 4678.372741 \\ -5371.314404 \end{pmatrix}, \tag{3.28}$$

where position and velocity are defined in m and m/s, respectively. For the Monte Carlo simulations, 10,000 samples, normally distributed within some specified 3-σ region, are generated with respect to the initial state in the Cartesian based on 1-σ Gaussian error

$$diag\left(\mathbf{P}_0\right) = \left[1000.0^2, \quad 1000.0^2, \quad 1000.0^2, \quad 2.5^2, \quad 2.5^2, \quad 2.5^2\right]. \tag{3.29}$$

For this analysis, the initial uncertainty is propagated with the two-body dynamics for 12 and 48 hours with the STTs up to the fourth-order. Figures 3.1-3.2 show the results of the propagation for each period. Even though the simple two-body dynamics are introduced, the first-order STT, i.e., STM, does not describe the uncertainty accurately. However, about fourth order, the STT approximation is close enough to the full dynamical system. Also, the nonlinearity grows as the propagation time is made longer, as expected. Figure 3.2 is a representation of the Monte Carlo simulations result after 48 hours. The second order STT could follow the nonlinear evolution of the full dynamical system. Note that higher STTs continue to be sufficient approximations to the complete two-body dynamics even after such long propagation times. In summary, the STT propagation, particularly above third order, continues to retain uncertainty consistency after 48 hours. It is also more clear for this case how the expansion of the dynamics converges upon the true dynamics as one includes higher order effects. Tables 3.1-3.4 summarize the relative errors of the mean of deviations and of the diagonal terms of covariance matrices obtained from each order of STTs in percentages from Equations (3.26)-(3.27). As seen in Table 3.1, after 12 hours of propagation, the propagated uncertainty with the STM is inaccurate. On the other hand, the relative errors imply that the STTs above the second order are sufficient to map the initial

Table 3.1: Relative errors in δm on each direction with respect to the order of STTs after 12 hours of propagation (%)

	STM	STTs		
		2nd	3rd	4th
δm_x	109.9525	18.0257e-3	17.35032e-3	26.8396e-6
δm_y	95.2005	12.9850e-3	13.6389e-3	6.7264e-6
δm_z	1.42828e3	686.7043e-3	390.9971e-3	2.3752e-3
$\delta m_{\dot{x}}$	59.3448	10.4839e-3	1.1685e-3	53.6116e-6
$\delta m_{\dot{y}}$	912.2435	426.8609e-3	264.8679e-3	1.3774e-3
$\delta m_{\dot{z}}$	96.67917	10.9573e-3	11.0970e-3	11.7053e-6

uncertainty. After 4 days of propagation, the relative errors in the mean of deviations are presented

Table 3.2: Relative errors in variances(diagonal terms of a covariance matrix) on each direction with respect to the order of STTs after 12 hours of propagation (%)

	STM	STTs		
		2nd	3rd	4th
P_{xx}	348.6960e-3	46.0766e-3	37.5546e-6	240.2988e-6
P_{yy}	438.9232e-3	99.8500e-3	615.5324e-6	353.0359e-6
P_{zz}	61.0509e-3	66.7837e-3	9.0025e-6	12.6218e-6
$P_{\dot{x}\dot{x}}$	67.4613e-3	64.5812e-3	28.7991e-6	31.1886e-6
$P_{\dot{y}\dot{y}}$	55.5510e-3	61.3321e-3	3.9085e-6	7.3276e-6
$P_{\dot{z}\dot{z}}$	812.6804e-3	99.9410e-3	793.3978e-6	440.4987e-6

in Table 3.3. The results also imply that the second order STT propagates the initial uncertainty with the sufficient accuracy. It is worth noting that the propagated uncertainty from the fourth order STT describes the full dynamical system most accurately.

Table 3.3: Relative errors in δm on each direction with respect to the order of STTs after 48 hours of propagation (%)

	STM	STTs		
		2nd	3rd	4th
δm_x	104.7124	311.7035e-3	295.9309e-3	384.3329e-6
δm_y	100.9504	296.8674e-3	292.9992e-3	483.8280e-6
δm_z	81.7932	214.1611e-3	279.4905e-3	1.0148e-3
$\delta m_{\dot{x}}$	94.6232	292.6597e-3	313.6472e-3	892.9517e-6
$\delta m_{\dot{y}}$	79.9286	276.5333e-3	349.0988e-3	1.6933e-3
$\delta m_{\dot{z}}$	101.2280	301.0879e-3	295.8066e-3	515.3685e-6

Table 3.4: Relative errors in variances(diagonal terms of a covariance matrix) on each direction with respect to the order of STTs after 48 hours of propagation (%)

	STM	STTs		
		2nd	3rd	4th
P_{xx}	362.9316e-3	1.1741	3.8953e-3	3.6849e-3
P_{yy}	12.3554	1.2165e	124.9981e-3	6.0906e-3
P_{zz}	1.1441	1.1500	2.6303e-3	2.7136e-3
$P_{\dot{x}\dot{x}}$	818.0988e-3	1.1262	1.3458e-3	2.0978e-3
$P_{\dot{y}\dot{y}}$	1.1560	1.1588	2.7633e-3	2.8364e-3
$P_{\dot{z}\dot{z}}$	7.0179	1.3374	74.0184e-3	7.2554e-3

3.5 Conclusion

In this chapter, an analytic method of nonlinear uncertainty propagation is discussed. A special solution to the Fokker-Planck equations for deterministic systems and the concept of the State Transition Tensors (STTs) are combined so that, given an analytic expression of both the initial probability distribution and the dynamics, the probability distribution may be expressed analytically for all time. Propagation of uncertainty is then only a matter of changing the time parameter t. In particular, two-body dynamics is applied to the above framework. The propagation results are compared with numerical Monte Carlo simulations. This example demonstrated the potential efficiency and accuracy of analytic uncertainty propagation even when compared to numerical results employing realistic parameter models. Lastly, the good agreement between the analytic and Monte Carlo results implies that further investigation in analytic uncertainty propagation may indeed be beneficial.

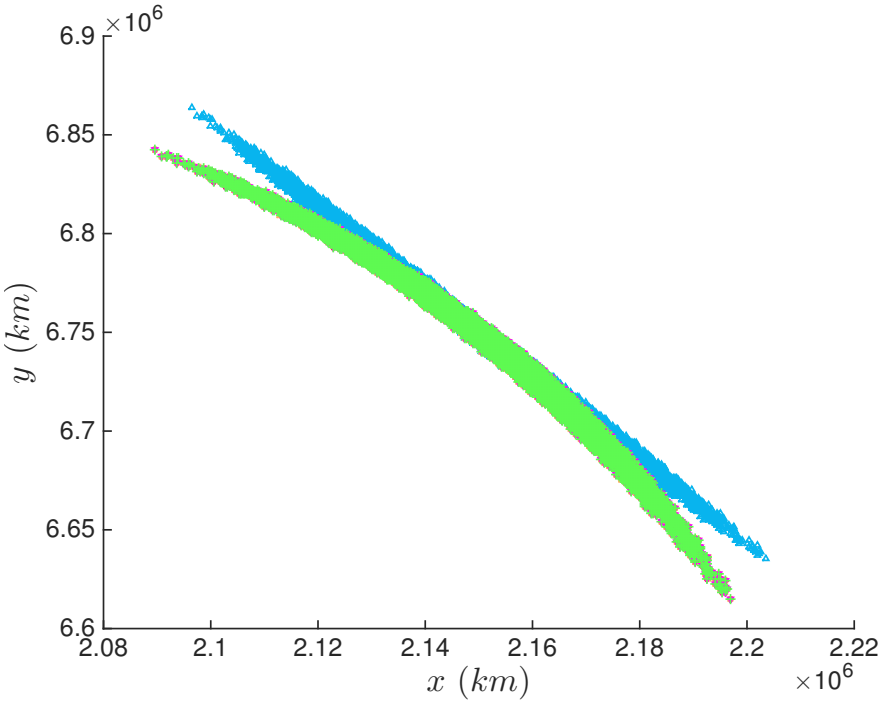

(a) Propagated uncertainty on the x-y phase space after 12 hrs

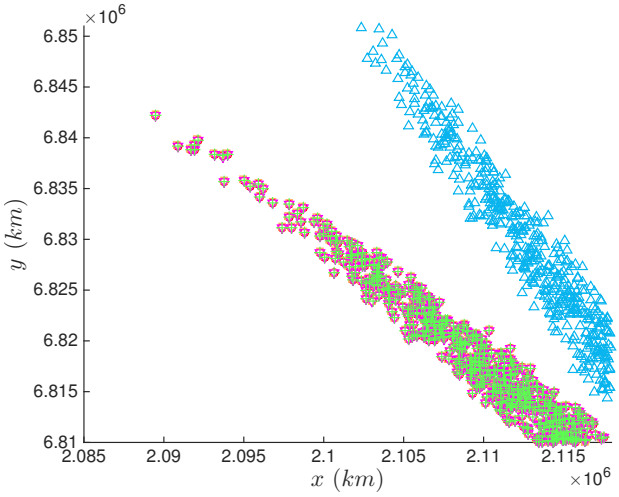

(b) Zoom up near the left tail

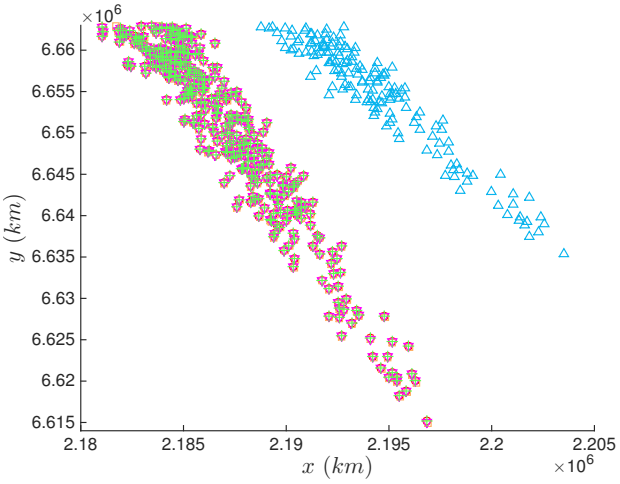

(c) Zoom up near the right tail

Figure 3.1: Comparison of the propagated uncertainty on x-y phase space with the STTs up to the fourth order after 12 hours. The accuracy of the propagated uncertainty with the higher-order STT is higher. A magnified plot of the left tail (bottom-left) depicts that the fourth-order STT (green crosses) maps the initial uncertainty with the highest accuracy: a result from the full dynamical system, the second, and the third-order STTs is plotted in red circles, orange squares and in magenta triangles, respectively.

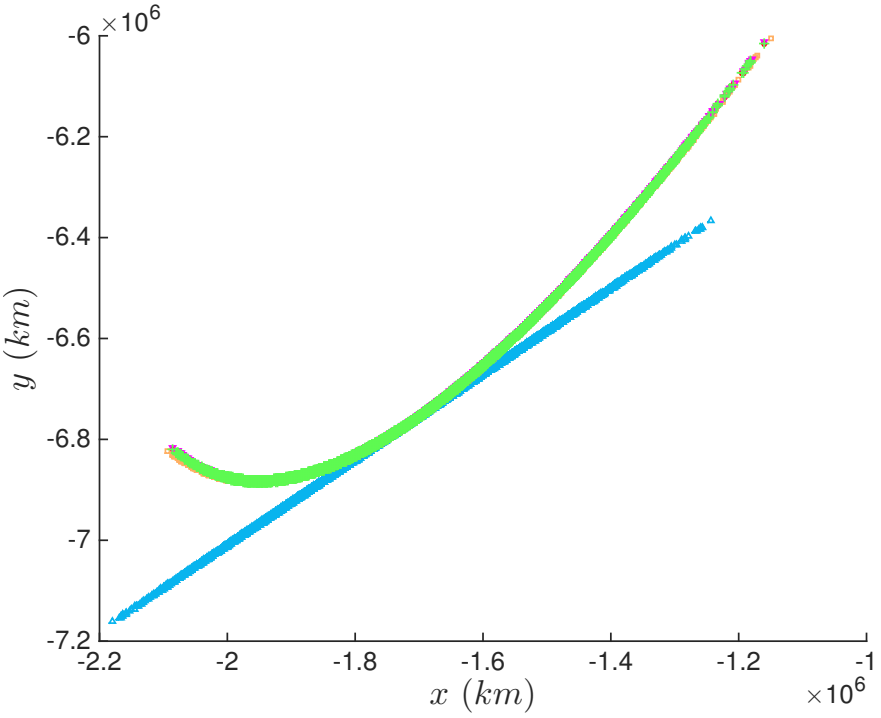

(a) Propagated uncertainty on the x-y phase space after 48 hrs

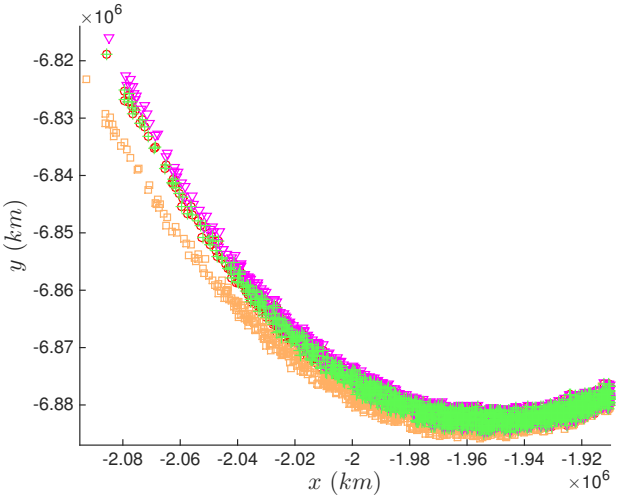

(b) Zoom up near the left tail

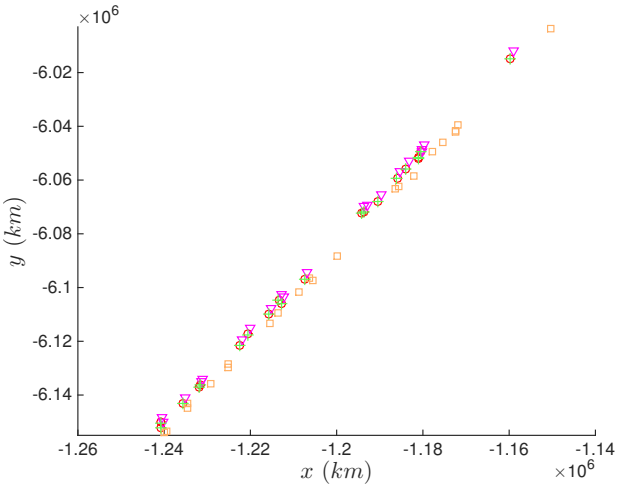

(c) Zoom up near the right tail

Figure 3.2: Comparison of the propagated uncertainty on x-y phase space with the STTs up to the fourth order after 48 hours. The accuracy of the propagated uncertainty with the higher-order STT is higher. A magnified plot of the left tail (bottom-left) depicts that the fourth-order STT (green crosses) maps the initial uncertainty with the highest accuracy: a result from the full dynamical system, the second, and the third-order STTs is plotted in red circles, orange squares and in magenta triangles, respectively.

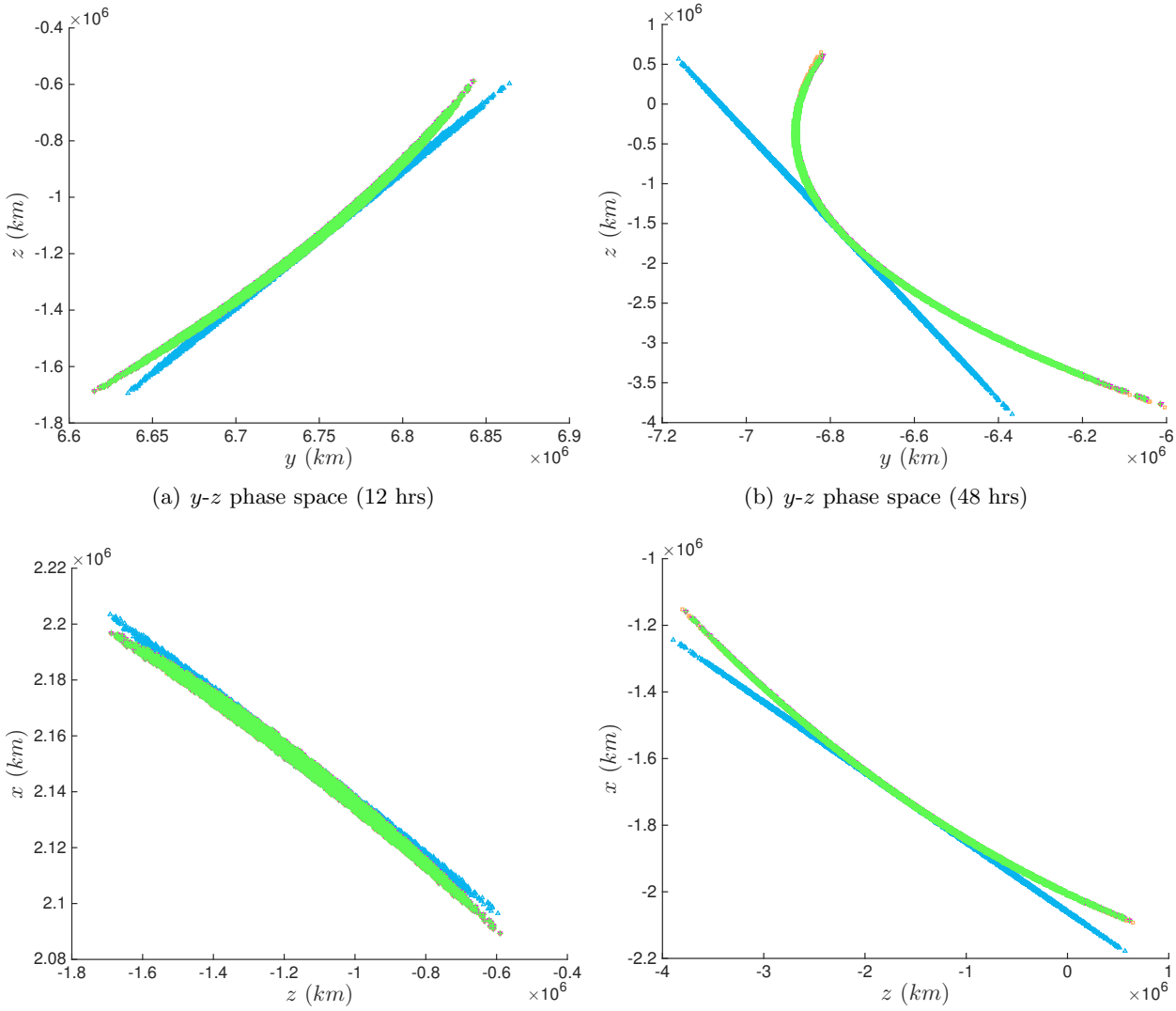

(a) y-z phase space (12 hrs)

(b) y-z phase space (48 hrs)

(c) z-x phase space (12 hrs)

(d) z-x phase space (48 hrs)

Figure 3.3: Propagated uncertainty with the STTs on y-z and z-x phase spaces after 12 hours (left column) and 48 hours (right column). The accuracy of the propagated uncertainty gets higher by introducing a higher-order STT.

Chapter 4

Canonical Perturbation Theory

Historically, the first methods were developed in the non-canonical framework[1] . The perturbative methods, usually applied to deal with nonlinear dynamical problems, are defined based on an expansion in power series of a "small" parameter with respect to the "known" solution of a problem; thus, the "perturbed" and "unperturbed" systems differ in "small" quantities. Since about a century ago, problems of celestial mechanics are exclusively dealt with the perturbative methods; this celestial mechanical origin has characterized the structure of perturbation theory [7]. This historical background makes the perturbation techniques a powerful tool to obtain a solution for a perturbed system for which there is already known non-perturbed solution, e.g., the two-body motion. In this study, we use the canonical framework, originally suggested by Hamilton, since it has the advantage that the equations of motion are written in a very simple form [7].

In this chapter, we summarize further details of the perturbation theory with a focus on the Lie transformation method defined by Deprit [19, 42]. The properties of the transformation method, such as

· providing a systematic way to derive higher-order solutions,

· deriving the solutions for the secular, short-period, and long-period variations separately,

inspire us to apply this specific transformation method instead of the classical Von Zeipel method applied by Brouwer [9, 10, 50]. Advantages of the Deprit-Lie transformation method over the

[1] The first person introduced perturbative methods, even if they were exclusively geometric, was Isaac Newton in Book III of the *Principia* to deal with the irregularities of lunar motions.

Von Zeipel method are from these properties. The feasibility and advantages of the Deprit-Lie transformation method are verified by revisiting the problem originally addressed by Brouwer [9, 10]. Lastly, it is worth mentioning that, in 1966, Hori also defined the perturbation theory based on the Lie theory [33] and, after the Deprit's work [19], Campbell showed that both methods were mathematically equivalent [13].

The outline of this chapter is as follows. A general definition of the Deprit-Lie transformation method and its advantageous properties are introduced [7, 19]. Then, the generalized expressions proposed by Kamel [42] and the symplecticity of the transformation method are addressed. Finally, we present a practical example by revisiting the problem of the artificial satellite problem [9, 10]. From the example, the analytic solutions from the Deprit-Lie transformation method are tested to guarantee the feasibility and the improvement of the accuracy.

4.1 Lie Transformation Method

We overview the Lie series and transformations in brief, and specifically address the algorithm of Lie transformation defined by Deprit[19] to investigate the Hamiltonian of the problem; then, we present a generalized algorithm by Kamel[42] for solving a *homological equations*. The primary feature of the Deprit-Lie transformation method is the application of the Lie transform operator to construct a canonical transformation in expanded form.

Definition 17 (Lie Operator). For given two analytic functions $f(\boldsymbol{q}, \boldsymbol{p})$ and $\mathcal{W}(\boldsymbol{q}, \boldsymbol{p})$ bounded in a domain Ω of phase space, *Lie derivative* of the function f generated by $\mathcal{W}$ is defined as a form of the Poisson bracket $\{f, \mathcal{W}\}$, which we now denote by the symbol

$$\mathcal{L}_{\mathcal{W}} f = \{f, \mathcal{W}\} = \sum_{i=1}^{n} \left(\frac{\partial f}{\partial q_i} \frac{\partial \mathcal{W}}{\partial p_i} - \frac{\partial f}{\partial p_i} \frac{\partial \mathcal{W}}{\partial q_i} \right), \tag{4.1}$$

where $\mathcal{L}_{\mathcal{W}}$ is called the *Lie operator*.

For Hamiltonian systems, the Lie transform between two functions $\mathcal{H}$ and $\mathcal{W}$ is equivalent to the classic Poission bracket as seen in Equation (4.1), which is generally referred to as the Lie derivative

of $\mathcal{H}$ generated by $\mathcal{W}$. Further, the n-th Lie derivative is defined as $\mathcal{L}^n_{\mathcal{W}}\mathcal{H} = \mathcal{L}_{\mathcal{W}}\left(\mathcal{L}^{n-1}_{\mathcal{W}}\mathcal{H}\right)$ and the zeroth order derivative is the identity operator, i.e., $\mathcal{L}^0_{\mathcal{W}}\mathcal{H} = \mathcal{H}$. As mentioned in Definition 17, the functions $\mathcal{H}$ and $\mathcal{W}$ are assumed real and analytic in a bounded domain of the phase space, i.e., Ω. This guarantees a convergent, real-valued series expansion for the resultant canonical transformation in a neighborhood of the unperturbed system. Detailed properties and descriptions about the Lie series and Lie transformation can be found in Appendix D.

In the original formulation, given Hamiltonian and generating functions are represented by the series expansion about the small parameter ϵ as follows:

$$\mathcal{H}(\boldsymbol{\zeta}\,;\,\epsilon) = \sum_{n=0}^{\infty} \frac{\epsilon^n}{n!}\mathcal{H}_n(\boldsymbol{\zeta}\,;\,0), \tag{4.2a}$$

$$\mathcal{W}(\boldsymbol{\zeta}\,;\,\epsilon) = \sum_{n=0}^{\infty} \frac{\epsilon^n}{n!}\mathcal{W}_{n+1}(\boldsymbol{\zeta}\,;\,0). \tag{4.2b}$$

The $2n$-dimensional vector $\boldsymbol{\zeta}$ is defined as $\boldsymbol{\zeta} = (\boldsymbol{q}, \boldsymbol{p})$, where q_i and p_i are generalized coordinates and conjugate momenta. Then, it is possible to obtain

$$\frac{\partial\mathcal{H}}{\partial\epsilon}(\boldsymbol{\zeta}\,;\,\epsilon) = \sum_{n=0}^{\infty} \frac{\epsilon^n}{n!}\mathcal{H}_{n+1}(\boldsymbol{\zeta}\,;\,0), \tag{4.3a}$$

$$\mathcal{L}_{\mathcal{W}}\mathcal{H}(\boldsymbol{\zeta}\,;\,\epsilon) = \sum_{n=0}^{\infty} \frac{\epsilon^n}{n!}\sum_{m=0}^{n}\binom{n}{m}\mathcal{L}_{m+1}\mathcal{H}_{n-m}(\boldsymbol{\zeta}\,;\,0). \tag{4.3b}$$

For the sake of simple notations, let us put $\mathcal{L}_{\mathcal{W}_\xi} = \mathcal{L}_\xi$. A subscript ξ denotes an order of generating function. The Lie transformation $\Delta_{\mathcal{W}} f$ [7, 19] is represented by the formal series as

$$\Delta_{\mathcal{W}}\mathcal{H} = \sum_{n=0}^{\infty} \frac{\epsilon^n}{n!}\mathcal{H}^{(1)}_n(\boldsymbol{\zeta}\,;\,0), \tag{4.4}$$

and the recurrence extends to any n ($n \geq 0$) is given by

$$\Delta^k_W\mathcal{H} = \sum_{n=0}^{\infty} \frac{\epsilon^n}{n!}f^{(k)}_n(\boldsymbol{\zeta}\,;\,0). \tag{4.5}$$

Equation (4.5) can be rewritten as a generalized form as

$$\mathcal{H}^{(k)}_n(\boldsymbol{\zeta}) = \mathcal{H}^{(k-1)}_{n+1} + \sum_{m=0}^{n}\binom{n}{m}L_{m+1}\mathcal{H}^{(k-1)}_{n-m}. \tag{4.6}$$

In particular,

$$\mathcal{H}^{(k)}(\boldsymbol{\zeta}\,;0) = \mathcal{H}_0^{(k)}(\boldsymbol{\zeta}\,;\epsilon) = \mathcal{H}_1^{(k-1)} + \mathcal{L}_1\mathcal{H}^{(k-1)}. \tag{4.7}$$

Lastly, the recursion Equation (4.6) is easily visualized as shown in Figure 4.1. The figure is called

$$\begin{array}{ccccccccccc}
\mathcal{H}_{0,0} & & & & & & & & & & \\
| & & & & & & & & & & \\
\mathcal{H}_{1,0} & - & \mathcal{H}_{0,1} & & & & & & & & \\
| & & | & & & & & & & & \\
\mathcal{H}_{2,0} & - & \mathcal{H}_{1,1} & - & \mathcal{H}_{0,2} & & & & & & \\
| & & | & & | & & & & & & \\
\mathcal{H}_{3,0} & - & \mathcal{H}_{2,1} & - & \mathcal{H}_{1,2} & - & \mathcal{H}_{0,3} & & & & \\
| & & | & & | & & | & & & & \\
\mathcal{H}_{4,0} & - & \mathcal{H}_{3,1} & - & \mathcal{H}_{2,2} & - & \mathcal{H}_{1,3} & - & \mathcal{H}_{0,4} & & \\
| & & | & & | & & | & & | & & \\
\mathcal{H}_{5,0} & - & \mathcal{H}_{4,1} & - & \mathcal{H}_{3,2} & - & \mathcal{H}_{2,3} & - & \mathcal{H}_{1,4} & - & \mathcal{H}_{0,5}
\end{array}$$

Figure 4.1: Recursive transformation of an analytic function under the Lie transformation (Deprit's triangle)

the *Deprit's triangle* and provides a simple way to compute transformed Hamiltonian functions, $\mathcal{H}_n^{(k)}$. Some examples from the Deprit's triangle are given below:

$$\begin{aligned}
&\mathcal{O}(\epsilon^0):\ \mathcal{H}_0^{(0)} = \mathcal{H}_{0,0},\\
&\mathcal{O}(\epsilon^1):\ \mathcal{H}_0^{(1)} = \mathcal{H}_{0,1} = \mathcal{H}_{1,0} + \mathcal{L}_{\mathcal{W}_1}\mathcal{H}_{0,0},\\
&\mathcal{O}(\epsilon^2):\ \mathcal{H}_0^{(2)} = \mathcal{H}_{0,2} = \mathcal{H}_{1,1} + \mathcal{L}_{\mathcal{W}_1}\mathcal{H}_{0,1} = \mathcal{H}_{2,0} + \mathcal{L}_{\mathcal{W}_1}(\mathcal{H}_{1,0} + \mathcal{H}_{0,1}) + \mathcal{L}_{\mathcal{W}_2}\mathcal{H}_{0,0},\\
&\mathcal{O}(\epsilon^3):\ \mathcal{H}_0^{(3)} = \mathcal{H}_{0,3} = \mathcal{H}_{3,0} + \mathcal{L}_{\mathcal{W}_1}(2\mathcal{H}_{2,0} + \mathcal{H}_{0,2}) + \mathcal{L}_{\mathcal{W}_2}(2\mathcal{H}_{1,0} + \mathcal{H}_{0,1}) + \mathcal{L}_{\mathcal{W}_3}\mathcal{H}_{0,0}\\
&\qquad\qquad + \mathcal{L}_{\mathcal{W}_1}\mathcal{L}_{\mathcal{W}_1}\mathcal{H}_{1,0} + \mathcal{L}_{\mathcal{W}_1}\mathcal{L}_{\mathcal{W}_2}\mathcal{H}_{0,0},\\
&\qquad\qquad\qquad\qquad \vdots
\end{aligned} \tag{4.8}$$

Lastly, for every order of ϵ shown in Equation (4.8), the generating functions can be written as a form of the PDE (partial differential equation) as follows, which is called the *homological equation* [19, 42].

$$\mathcal{L}_0(\mathcal{W}_n) + \mathcal{K}_n = \widetilde{\mathcal{H}}_{0,n}, \tag{4.9}$$

where $\widetilde{\mathcal{H}}_{0,n}$, $\mathcal{K}_n$, and $\mathcal{L}_0(-)$ are a collection of all terms known from the previous order, transformed Hamiltonians, and $\{-,\,\mathcal{H}_0\}$, respectively. A purpose of the homological equation is to separate the

given Hamiltonian into two parts, constant and varying terms with respect to a specific variable. The constant terms may be assigned as the transformed Hamiltonian, and the generating function, $\mathcal{W}_n$, is defined as a function including the varying terms.

For the sake of applying the Deprit-Lie transformation method, the generalized algorithm proposed by Kamel [42] is discussed in this section. Based on the transformed Hamiltonian and generating functions, i.e., $\mathcal{K}_n$ and $\mathcal{W}_n$, the (semi) analytic solutions can be obtained based on the definition of the perturbation theory. Let us assume an original set of variables as ($\boldsymbol{x}$, $\boldsymbol{X}$) and a transformed set of variables as ($\boldsymbol{y}$, $\boldsymbol{Y}$). The transformation is a near-identity canonical transformation $\psi : (\boldsymbol{y}, \boldsymbol{Y}; \epsilon) \longmapsto (\boldsymbol{x}, \boldsymbol{X})$, defined by the solution $\boldsymbol{x}(\boldsymbol{y}, \boldsymbol{Y}; \epsilon)$ and $\boldsymbol{X}(\boldsymbol{y}, \boldsymbol{Y}; \epsilon)$. The solutions satisfy that

$$\frac{d\boldsymbol{x}}{d\epsilon} = \frac{\partial \mathcal{W}}{\partial \boldsymbol{X}}, \qquad \frac{d\boldsymbol{X}}{d\epsilon} = -\frac{\partial \mathcal{W}}{\partial \boldsymbol{x}} \tag{4.10}$$

with initial conditions $\boldsymbol{x}(\boldsymbol{y}, \boldsymbol{Y}; 0) = \boldsymbol{y}$ and $\boldsymbol{X}(\boldsymbol{y}, \boldsymbol{Y}; 0) = \boldsymbol{Y}$ [19]. In the original set of variables space, an Hamiltonian, $\mathcal{H}(\boldsymbol{x}, \boldsymbol{X}; \epsilon)$, and generating, $\mathcal{W}(\boldsymbol{x}, \boldsymbol{X}; \epsilon)$, functions are defined as a power series of the small parameter ϵ

$$\mathcal{H}(\boldsymbol{x}, \boldsymbol{X}; \epsilon) = \sum_{n \geq 0} \frac{\epsilon^n}{n!} \mathcal{H}_n(\boldsymbol{x}, \boldsymbol{X}) = \sum_{n \geq 0} \frac{\epsilon^n}{n!} \mathcal{H}_{n,0}(\boldsymbol{x}, \boldsymbol{X}), \tag{4.11a}$$

$$\mathcal{W}(\boldsymbol{x}, \boldsymbol{X}; \epsilon) = \sum_{n \geq 0} \frac{\epsilon^n}{n!} \mathcal{W}_{n+1}(\boldsymbol{x}, \boldsymbol{X}), \tag{4.11b}$$

both of them are based on Equation (4.2). The given Hamiltonian function can be transformed term by term up to required order in a recursive way through Equation (4.6). This procedure is carried out systematically by solving the *homological equation*.

Then, suppose that the transformed Hamiltonian, $\mathcal{K}$, is

$$\mathcal{K}(\boldsymbol{y}, \boldsymbol{Y}; \epsilon) = \sum_{n=0}^{\infty} \frac{\epsilon^n}{n!} \mathcal{K}_n(\boldsymbol{y}, \boldsymbol{Y}) = \sum_{n=0}^{\infty} \frac{\epsilon^n}{n!} \mathcal{H}_{0,n}(\boldsymbol{y}, \boldsymbol{Y}). \tag{4.12}$$

If the variables satisfy the canonical equations, one can get relations from the transformed Hamiltonian

$$\frac{d\boldsymbol{y}_i}{dt} = \frac{\partial \mathcal{K}_n}{\partial \boldsymbol{Y}_i}, \qquad \frac{d\boldsymbol{Y}_i}{dt} = -\frac{\partial \mathcal{K}_n}{\partial \boldsymbol{y}_i}, \qquad (i{=}1, \ldots, m) \tag{4.13}$$

where $\boldsymbol{y}_i$ and $\boldsymbol{Y}_i$ indicate the generalized coordinates, and conjugate momenta. m represents the number of variables. Figure 4.2 shows a procedure of the transformation. In general, the motion

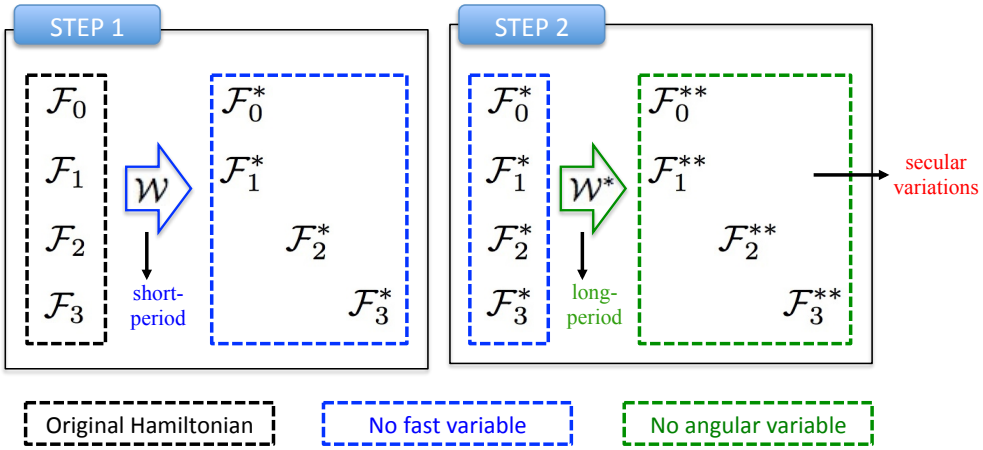

Figure 4.2: Two steps in the canonical transformation for eliminating the periodic variations from a given Hamiltonian dynamics: 1) $\mathcal{W}$ extracts all terms dependent on the fast variable, e.g., mean anomaly, from the given Hamiltonian $\mathcal{F}$ in order to remove the short-period variation, and 2) the long-period variation is eliminated by $\mathcal{W}^*$ from a transformed Hamiltonian in the first step, i.e., $\mathcal{F}^*$. As a result of this procedure, the Hamiltonian at the final stage, $\mathcal{F}^{**}$, has no variations which evolve periodically.

of an orbiting object around a central body includes two different periodic variations, that is, the short-period and long-period variations. Through the two-step transformations, these periodic variations can be eliminated.

4.1.1 The Secular Variations

After completing the transformations, the transformed Hamiltonian can be expressed by Equation (4.12) based on the relation given below.

$$\begin{aligned}
\mathcal{K}_0 &= \mathcal{H}_{0,0} = \mathcal{F}_0^{**}, \\
\mathcal{K}_1 &= \mathcal{H}_{0,1} = \mathcal{F}_1^{**}, \\
\mathcal{K}_2 &= \mathcal{H}_{0,2} = \mathcal{F}_2^{**}, \\
\mathcal{K}_3 &= \mathcal{H}_{0,3} = \mathcal{F}_3^{**}, \\
&\vdots
\end{aligned} \tag{4.14}$$

Then, the transformed Hamiltonian $\mathcal{K}$ has no periodic variations; thus, one can get the analytic solutions for the secular motion of an orbiting object through Equation (4.13).

The semi-analytic solutions eliminates only the short-period variations; thus, these solutions can be defined by replacing $\mathcal{F}_n^{**}$ in Equation (4.14) with $\mathcal{F}_n^{*}$, i.e., transformed Hamiltonians after the first step. In particular, we focus on the semi-analytic solutions in analyzing the dynamical realism since a magnitude of the long-period variations may be greater than that of the short-period variations. In other words, it may be impossible to assume the magnitude of the long-period variations as a noise. Lastly, here are advantages of the semi-analytic solutions.

- the semi-analytic solutions have advantages over the full analytic solutions when we consider the resonances.
- the accuracy of a propagation with the semi-analytic solutions is better since there is no truncation of higher-order terms, occurred in the second transformation.

4.1.2 The Periodic Variations

Based on the property of the canonical transformation, the generating function provides information about non-constant parts; thus, the analytic solutions for the periodic variations are derived from the generating functions. In this section, we summarize the generalized expressions by Kamel [42] for the periodic variations. Note that the original set of variables, e.g., osculating elements, and the transformed one, e.g., mean elements, are ($\boldsymbol{x}$, $\boldsymbol{X}$) and ($\boldsymbol{y}$, $\boldsymbol{Y}$), respectively.

The transformation which recovers the periodic variations, converting the space from the mean to osculating, is defined as follows:

$$\boldsymbol{x} = \boldsymbol{y}_0^{(0)} + \sum_{n\geq 1} \frac{\epsilon^n}{n!} \mathcal{L}_{\mathcal{W}}^n(\boldsymbol{y}) = \boldsymbol{y}_0^{(0)} + \sum_{n\geq 1} \frac{\epsilon^n}{n!} \boldsymbol{y}_0^{(n)}, \tag{4.15a}$$

$$\boldsymbol{X} = \boldsymbol{Y}_0^{(0)} + \sum_{n\geq 1} \frac{\epsilon^n}{n!} \mathcal{L}_{\mathcal{W}}^n(\boldsymbol{Y}) = \boldsymbol{Y}_0^{(0)} + \sum_{n\geq 1} \frac{\epsilon^n}{n!} \boldsymbol{Y}_0^{(n)}, \tag{4.15b}$$

where

$$\boldsymbol{y}_0^{(n)} = \frac{\partial \mathcal{W}_n}{\partial \boldsymbol{Y}} + \sum_{1\le j\le n-1} C_j^{n-1}\, G_j\, \boldsymbol{y}_0^{(n-j)}, \quad (n \ge 1) \tag{4.16a}$$

$$\boldsymbol{Y}_0^{(n)} = -\frac{\partial \mathcal{W}_n}{\partial \boldsymbol{y}} + \sum_{1\le j\le n-1} C_j^{n-1}\, G_j\, \boldsymbol{Y}_0^{(n-j)}, \quad (n \ge 1) \tag{4.16b}$$

and $\left(\boldsymbol{y}_0^{(0)},\, \boldsymbol{Y}_0^{(0)}\right)$ represent the secular variations, i.e., mean orbit. The inverse transformation, converting the space from the osculating to mean, is simply defined as

$$\boldsymbol{y} = \boldsymbol{x}_0^{(0)} + \sum_{n\ge 1} \frac{\epsilon^n}{n!} \mathcal{L}^n_{-\mathcal{W}}(\boldsymbol{x}) = \boldsymbol{x}_0^{(0)} + \sum_{n\ge 1} \frac{\epsilon^n}{n!} \boldsymbol{x}_0^{(n)}, \tag{4.17a}$$

$$\boldsymbol{Y} = \boldsymbol{X}_0^{(0)} + \sum_{n\ge 1} \frac{\epsilon^n}{n!} \mathcal{L}^n_{-\mathcal{W}}(\boldsymbol{X}) = \boldsymbol{X}_0^{(0)} + \sum_{n\ge 1} \frac{\epsilon^n}{n!} \boldsymbol{X}_0^{(n)}, \tag{4.17b}$$

where

$$\boldsymbol{x}_0^{(n)} = -\boldsymbol{y}_0^{(n)} + \sum_{1\le j\le n-1} C_j^{n}\, G_j\, \boldsymbol{y}_0^{(n-j)}, \quad (n \ge 1) \tag{4.18a}$$

$$\boldsymbol{X}_0^{(n)} = -\boldsymbol{Y}_0^{(n)} + \sum_{1\le j\le n-1} C_j^{n}\, G_j\, \boldsymbol{Y}_0^{(n-j)}. \quad (n \ge 1) \tag{4.18b}$$

Eq. (4.16) and (4.18) are simplified expressions defined by Kamel[41], where C_k^n represents the binomial coefficients and a function G_j is

$$G_j = \mathcal{L}_j - \sum_{0\le m\le j-2} C_m^{j-1} \mathcal{L}_{m+1} G_{j-m-1}. \qquad 1 \le j \le n \tag{4.19}$$

As seen in Equations (4.15) and (4.16), the periodic variations are defined with respect to the secular variations, i.e., mean orbit. Thus, an accurate conversion from osculating orbital elements into mean elements is one of the most critical part in applying the analytic solutions [60].

4.1.3 Analytic Algorithm for Space Conversion

As we demonstrate so far, the fundamental idea of the transformation is to eliminate periodic variations sequentially. An analytic conversion algorithm is based on Eq. (4.17). Basically, those equations indicate the eliminated variation with respect to the mean orbit (or trajectory); thus, if one wanted to have osculating elements at an arbitrary epoch t, the eliminated variation would be

recovered by Eq. (4.15) with respect to the mean orbit at that epoch. In this section, we address a more detailed procedure to apply the equations. Suppose that a given Hamiltonian is transformed twice, as seen in Figure 4.2, to eliminate two angular variables as

$$(l,\, g,\, h,\, L,\, G,\, H) \overset{STEP1}{\Longrightarrow} (l^*,\, g^*,\, h^*,\, L^*,\, G^*,\, H^*) \overset{STEP2}{\Longrightarrow} (l^{**},\, g^{**},\, h^{**},\, L^{**},\, G^{**},\, H^*), \quad (4.20)$$

and the corresponding Hamiltonians at each step are $\mathcal{F}$, $\mathcal{F}^*$, and $\mathcal{F}^{**}$, respectively.

4.1.3.1 Determination of the Mean Variables from the Osculating Variables

The secular variations are defined as

$$\begin{aligned} \frac{d}{dt}(l^{**},\, g^{**},\, h^{**})^{\mathrm{T}} &= \frac{\partial \mathcal{F}^{**}}{\partial (L^{**},\, G^{**},\, H^{**})} = \mathbb{C}, \\ \frac{d}{dt}(L^{**},\, G^{**},\, H^{**})^{\mathrm{T}} &= -\frac{\partial \mathcal{F}^{**}}{\partial (l^{**},\, g^{**},\, h^{**})} = \mathbf{0}, \end{aligned} \quad (4.21)$$

where $\mathbb{C}$ is an arbitrary 3×1 constant vector. Equation (4.21) is integrated to

$$\begin{aligned} (l^{**},\, g^{**},\, h^{**}) &= (l_0^{**},\, g_0^{**},\, h_0^{**}) + \mathbb{C} \cdot t, \\ (L^{**},\, G^{**},\, H^{**}) &= (L_0^{**},\, G_0^{**},\, H_0^{**}), \end{aligned} \quad (4.22)$$

where $(l_0^{**},\, g_0^{**},\, h_0^{**})$ and $(L^{**},\, G^{**},\, H^{**})$ represent the initial condition in the mean variables' space, which are constants and determined from a given initial conditions in the osculating variables' space. In order to obtain the mean initial conditions, we can apply Equation (4.17): the short-period variations and the long-period variations are removed sequentially. This procedure is defined as follows:

(1) STEP 1: elimination of the short-period variations, $(l^*,\, g^*,\, h^*,\, L^*,\, G^*,\, H^*)$

$$\begin{aligned} (l^*,\, g^*,\, h^*)^{\mathrm{T}} &= (l_0,\, g_0,\, h_0)^{\mathrm{T}} + \sum_{n \geq 1} \frac{\epsilon^n}{n!} \left(l_0^{(n)},\, g_0^{(n)},\, h_0^{(n)} \right)^{\mathrm{T}}, \\ (L^*,\, G^*,\, H^*)^{\mathrm{T}} &= (L_0,\, G_0,\, H_0)^{\mathrm{T}} + \sum_{n \geq 1} \frac{\epsilon^n}{n!} \left(L_0^{(n)},\, G_0^{(n)},\, H_0^{(n)} \right)^{\mathrm{T}}, \end{aligned} \quad (4.23)$$

where $(l_0,\, g_0,\, h_0,\, L_0,\, G_0,\, H_0)$ represents the initial conditions in the osculating variables' space.

(2) STEP 2: elimination of the long-period variations, (l^{**}, g^{**}, h^{**}, L^{**}, G^{**}, H^{**})

This step exactly repeats the calculation performed in the step 1 with the transformed variables, i.e., starred variables, as

$$\begin{aligned}(l^{**},\, g^{**},\, h^{**})^{\mathrm{T}} &= (l_0^*,\, g_0^*,\, h_0^*)^{\mathrm{T}} + \sum_{n\geq 1} \frac{\epsilon^n}{n!} \left(l_0^{*\,(n)},\, g_0^{*\,(n)},\, h_0^{*\,(n)}\right)^{\mathrm{T}}, \\ (L^{**},\, G^{**},\, H^{**})^{\mathrm{T}} &= (L_0^*,\, G_0^*,\, H_0^*)^{\mathrm{T}} + \sum_{n\geq 1} \frac{\epsilon^n}{n!} \left(L_0^{*\,(n)},\, G_0^{*\,(n)},\, H_0^{*\,(n)}\right)^{\mathrm{T}}.\end{aligned} \tag{4.24}$$

From the sequential computation, we can obtain the initial conditions in the mean variables' space for defining the secular variations in Equation (4.22).

4.1.3.2 Restoration of the Periodic Variations

This calculation is following the above procedure in reverse. At first, the long-period variations are added to the secular variations, i.e., the mean trajectory. After that, by considering the short-period variations with respect to the trajectory defined by the secular and long-period variations, the original trajectory in the osculating variables' space is recovered. We can carry out this procedure with Equation (4.17).

(1) Restore the long-period variations

By replacing $\boldsymbol{y}_0^{(0)}$ and $\boldsymbol{Y}_0$ (Equation (4.17)) with (l_0^{**}, g_0^{**}, h_0^{**}) and (L_0^{**}, G_0^{**}, H_0^{**}), respectively, we can recover an intermediate trajectory, i.e., including the secular and long-period variations.

(2) Restore the short-period variations

With the same procedure, the short-period variations are added to the intermediate trajectory.

Throughout the above procedure, the mean trajectory, i.e., defined only with the secular variations, is restored to the original trajectory includes all periodic variations.

4.2 The Symplecticity of the Transformation

In the case of Hamiltonian system, the Hamiltonian equations in Equation (2.24) can be rewritten with the symplectic unit matrix $\mathbf{J}$ as follows:

$$\dot{\boldsymbol{\mathcal{X}}} = \mathbf{J}\left(\frac{\partial \mathcal{H}}{\partial \boldsymbol{\mathcal{X}}}\right)^{\mathrm{T}}, \tag{4.25}$$

where $\boldsymbol{\mathcal{X}} = (\boldsymbol{x},\, \boldsymbol{X})$.

We would then absolutely keep this Hamiltonian character for a coordinate transformation $\boldsymbol{y}$ to $\boldsymbol{x}$, i.e., $(\boldsymbol{y},\, \boldsymbol{Y}\,;\, \epsilon) \longmapsto (\boldsymbol{x},\, \boldsymbol{X})$. From Equation (4.15), this coordinates transformation can be developed in series of power a "small" parameter ϵ. Then, a fundamental interpretation is obtained as [19]

$$\frac{d\boldsymbol{x}}{d\epsilon} = \frac{\partial}{\partial \boldsymbol{X}}\mathcal{W}(\boldsymbol{x},\, \boldsymbol{X}\,;\, \epsilon), \quad \frac{d\boldsymbol{X}}{d\epsilon} = -\frac{\partial}{\partial \boldsymbol{x}}\mathcal{W}(\boldsymbol{x},\, \boldsymbol{X}\,;\, \epsilon), \tag{4.26}$$

with a condition $(\boldsymbol{x},\, \boldsymbol{X}) = (\boldsymbol{y},\, \boldsymbol{Y}\,;\, 0)$. These relations can be rewritten with the symplectic unit matrix as follows:

$$\frac{d\boldsymbol{\mathcal{X}}}{d\epsilon} = \mathbf{J}\left(\frac{\partial \mathcal{W}}{\partial \boldsymbol{\mathcal{X}}}\right)^{\mathrm{T}}. \tag{4.27}$$

Thus, the Deprit-Lie transformation method can keep the symplecticity in the coordinates transformation as well.

4.3 Application of the Deprit-Lie Transformation

In 1969, Brouwer proposed analytic solutions for the problem of the artificial satellite theory, derived from the Von-Zeipel canonical transformation method [9, 10]. In the solutions, secular effects up to order two and periodic perturbations up to order first due to the zonal harmonics (J_2) is included. A procedure for deriving the solutions consists of two steps for eliminating each periodic variation as seen in Figure 4.2. Note that functions $\mathcal{W}$ and $\mathcal{W}^*$ are the generating functions, which corresponds to the deterministic functions S and S^* in [9]. For the sake of verifying feasibility and advantages of the new transformation method, we reproduce the analytic solutions with the Deprit-Lie transformation method. Equation (4.28) shows the solutions for the secular variations

with the same order to those by Brouwr [9] and is exactly equivalent to the original results.

$$\dot{l} = n - \frac{3\alpha^2 \mathrm{J}_2 \mu \left(3s^2-2\right)}{4a^5\eta^3 n} - \frac{\alpha^4 \mathrm{J}_2^2 n}{128a^4 e\eta^{11}} \Big[4e^5 \left(2-3s^2\right)^2 - 16e^4 \left(2-3s^2\right)^2 - 16e^2 \left(2\eta^2-1\right)\left(2-3s^2\right)^2$$
$$-e\Big\{48\eta^5\left(2-3s^2\right)^2 - 8\eta^2\left(2-3s^2\right)^2 + 4\left(2-3s^2\right)^2 + 15\eta^6\left(5s^4+8s^2-8\right) + \eta^4\left(351s^4-768s^2+376\right)\Big\}$$
$$-16\eta^2\left(\eta^2-1\right)\left(2-3s^2\right)^2\Big], \tag{4.28a}$$

$$\dot{g} = -\frac{3\alpha^2 \mathrm{J}_2 n \left(5s^2-4\right)}{4a^2\eta^4 n} + \frac{\alpha^4 \mathrm{J}_2^2 n}{128a^4 e\eta^{12}} \Big[4e^5 \left(135s^4-192s^2+68\right)$$
$$-16e^4\left(135s^4-192s^2+68\right) - 16e^2\left(3s^2-2\right)\left(-36\eta^2+\left(48\eta^2-45\right)s^2+34\right)$$
$$+e\left\{-8\left(21\eta^6-72\eta^5-131\eta^4-68\eta^2+34\right)+15\left(9\eta^6+72\eta^5+41\eta^4+72\eta^2-36\right)s^4\right.$$
$$\left.+12\left(9\eta^6-132\eta^5-151\eta^4-128\eta^2+64\right)s^2\right\} - 16\eta^2\left(\eta^2-1\right)\left(2-3s^2\right)^2\Big], \tag{4.28b}$$

$$\dot{h} = -\frac{3c\alpha^2 \mathrm{J}_2 n}{2a^2\eta^4} + \frac{3c\alpha^4 \mathrm{J}_2^2 n}{32a^4\eta^{12}} \Big[4e^4\left(3s^2-2\right) + e^3\left(32-48s^2\right) - 16e\left(\eta^2-1\right)\left(3s^2-2\right)$$
$$+4\left(\eta^6-6\eta^5-8\eta^4-4\eta^2+2\right)+\left(5\eta^6+36\eta^5+23\eta^4+24\eta^2-12\right)s^2\Big], \tag{4.28c}$$

$$\dot{L} = 0, \tag{4.28d}$$

$$\dot{G} = 0, \tag{4.28e}$$

$$\dot{H} = 0. \tag{4.28f}$$

In addition, the reproduced solutions are defined up to the third order for the secular variation and up to the second order for the periodic variations based on the advantages of the Deprit-Lie transformation method. The third-order analytic solutions and the generating functions for the problem are in Appendix E. The solutions are applied to propagate a state of a satellite in Low Earth Orbit (LEO) and in Medium Earth Orbit (MEO) under J_2 gravity field harmonics, i.e., J_2. The initial conditions for each example are as follows: For the both examples, the given initial conditions are propagated for 30 days. Table 4.2 shows the standard deviation of errors in each direction, i.e., position and velocity. Figure 4.3 depicts a time history of errors about the truth. The truth for each example is calculated from the TurboProp 4.0 [31]. As seen in the results, the higher-order solutions apparently improve the accuracy of the propagated state.

Table 4.1: Initial conditions for each example

Element	LEO	MEO
Semimajor axis, a, (km)	7028.136	26578.136
Eccentricity, e	0.01	0.01
Inclination, i, (deg)	55.0	55.0
Longitude of the ascending node, Ω, (deg)	45.0	45.0
Argument of periapsis, ω, (deg)	60.0	60.0
Mean anomaly, ν, (deg)	105.0	105.0

Table 4.2: Standard deviation errors of the second and third order solutions about the truth for each example under J_2 gravity field harmonics perturbation

	LEO		MEO	
	2^{nd}-order	3^{rd}-order	2^{nd}-order	3^{rd}-order
σ_x (km)	9.6715	1.5120	23.5714e-3	2.2191e-3
σ_y (km)	10.2287	1.5962	23.1487e-3	2.2430e-3
σ_z (km)	9.9689	1.5251	22.2099e-3	737.2663e-6
$\sigma_{\dot{x}}$ (km/s)	10.3769e-3	1.6224e-3	3.4413e-6	323.9452e-9
$\sigma_{\dot{y}}$ (km/s)	10.9698e-3	1.7111e-3	3.3962e-6	327.2676e-9
$\sigma_{\dot{z}}$ (km/s)	10.7015e-3	1.6372e-3	3.2164e-6	105.2836e-9

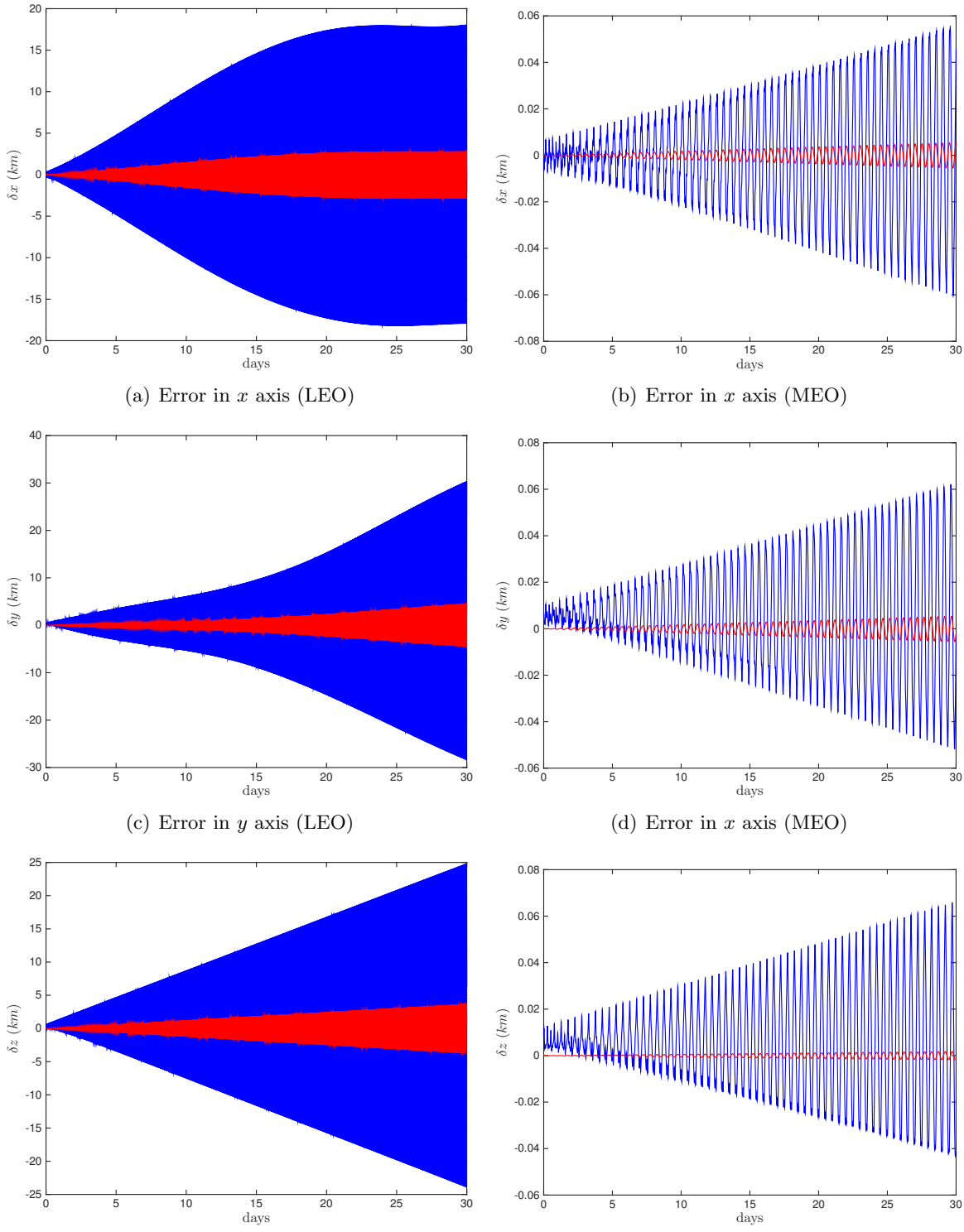

(a) Error in x axis (LEO)

(b) Error in x axis (MEO)

(c) Error in y axis (LEO)

(d) Error in x axis (MEO)

(e) Error in z axis (LEO)

(f) Error in x axis (MEO)

Figure 4.3: Time history of a position error on each direction in the Cartesian coordinate space for an object in Low Earth Orbit (LEO, left column) and in Medium Earth Orbit (MEO, right column): errors from the analytic solutions including the second-order secular+the first-order periodic effects and from those including the third-order secular+the second-order periodic effects are plotted in blue and red, respectively.

4.4 Conclusion

Throughout this chapter, we summarize the Lie transformation method by following Deprit's definition [19] and introduce the generalized expressions by Kamel [42]. Then, a procedure for deriving the (semi) analytic solutions for each variation is presented. We also demonstrate that the symplecticity of the Hamiltonian system is kept for the coordinates transformation. Finally, the feasibility and the improvement of accuracy of the Deprit-Lie transformation method are verified by revisiting the problem of the artificial satellite theory, originally proposed by Brouwer [9]. The semi-analytic solutions discussed in this chapter will be applied to more practical orbiting motions for verifying the dynamical realism and developing a new method.

Chapter 5

Dynamical Realism in Mapping Uncertainty

We focus on the role that the accuracy of the dynamical model plays in consistent uncertainty propagation, regardless of its representation. Simply put, we pose the question: how accurate must the mapped dynamics be in order to appropriately model the uncertainty distribution? This question is inspired by the discussion that the weak solution of the Stochastic Differential Equations (SDE) has the same distribution as sample path from the strong (actual) solution but does not depend on the particular noise realization [29]. The simplified models are called weak solutions of the stochastic dynamical model. More specifically, determination of weak solutions often suffices because the first few moments of the exact and weak solutions match to within the same order of magnitude. As these low-order moments are those that are required in many engineering tasks, it is possible to employ a simplified model which is computationally efficient [68, 69]. In this chapter, we compare distributions up to the fourth moment to verify our approach. We also test the veracity of our approximate PDFs with other tests that are independent of the moments. The main technical contribution of this paper is the statistical investigation of so called Simplified Dynamical System (SDS) for orbital motion, which is defined by removing the fast variable of a full dynamical system through averaging. Not only would such a simplified model lead to reduced computational burden, it could also shed insight into the dynamical driver of nonlinearity; e.g., secular, short-, or long-period variations.

The outline of this chapter is as follows. The SDSs, based on the Brouwer-Lyddane theory [9, 50] and averaged Lagrange Planetary Equations (LPEs), are defined for non-Keplerian motion

around the Earth. The former is applied to an object on the Low Earth Orbit (LEO) with J_2 gravity field harmonics and the latter to the Medium Earth Orbit (MEO) and a highly elliptic orbit (Molniya) cases with J_2 gravity field harmonics and a third-body perturbation. Then, for the sake of investigating the dynamical realism, we use Monte Carlo simulations with 10,000 samples. Finally, the accuracy and the improvement of the efficiency are verified through statistical methods and through a comparison of computational times.

5.1 Simplified Dynamical System

The SDS replaces the short-period terms included in the full dynamical system with constants by averaging. The constants are acquired from the initial offset correction, which play an important role for the SDS since the short-period terms are not cancelled out completely by averaging in general [67]. Using the SDS, we will investigate the relation between dynamical model precision and the propagated uncertainty accuracy, the importance of the short-period variations relative to the secular ones, and the enhancements in computational efficiency. In this section, we will discuss details about two types of SDSs: an analytic approach based on the SBT and an approximated numerical approach based on the LPEs.

5.1.1 Analytic Approach

In 1959, Brouwer had derived the analytic solutions (or solution flow) for the problem of the artificial satellite under J_2 perturbation via von Zeipel's method. The analytic solutions of the CBT are defined in terms of the classical orbital elements (COEs) at some given epoch. Equation (5.1) shows the mathematical definition of a solution flow [63], ϕ, with respect to the initial state, x_{OE}, and time, t_0.

$$\mathbf{x}_{\mathrm{OE}}(t) = \phi(t; \mathbf{x}_{\overline{\mathrm{OE}},0}, t_0), \tag{5.1}$$

where $\mathbf{x}_{\mathrm{OE}}(t)$ presents a propagated state at time t. SBT is a simplified form of the CBT, and can be derived by applying the usual averaging method to the original solution flow as seen in

Equation (5.2)

$$\overline{\mathbf{x}}(t) = \frac{1}{2\pi}\int_0^{2\pi} \phi(t; \mathbf{x}_{\overline{\mathrm{OE}},0}, t_0)\mathrm{d}M. \tag{5.2}$$

Equation (5.3) is also used in the integration [72]

$$\mathrm{d}M = \frac{(1-e^2)^{3/2}}{(1+e\cos f)^2}\mathrm{d}f \;\longmapsto\; \mathrm{d}f = \frac{a^2}{r^2}\sqrt{1-e^2}\mathrm{d}M, \tag{5.3}$$

which is derived from a relation between the mean and true anomalies for the two-body problem. After averaging the solutions [44], we get a new set of solutions required to define the SBT. Equations (5.4a) and (5.4b) show how the new solution flow can make the system simpler by comparing both the CBT and SBT.

$$\mathbf{x} = \mathbf{x}_0 + \mathbf{x}_{\mathrm{secular}} + \mathbf{x}_{\mathrm{short}} + \mathbf{x}_{\mathrm{long}} \tag{5.4a}$$

$$\overline{\mathbf{x}} = \mathbf{x}_0 + \mathbf{x}_{\mathrm{secular}} + \overline{\mathbf{x}_{\mathrm{short}}} + \mathbf{x}_{\mathrm{long}}, \tag{5.4b}$$

where $\overline{\mathbf{x}}$ indicates the solution flow of the SBT. The secular variations are not periodic; thus, the solutions are the same in both cases. Since the averaging is taken about the fast variable, the long-period terms are still functions of time; however, these terms are negligibly small for propagation intervals used in this study since they depend on a slow variable. On the other hand, the short-period term is converted into constants by the simplification. This means that the SBT requires at least nine less computations than the CBT: six for computing the short-period and three for the long-period terms. Therefore, if Monte Carlo simulations are used in this study, the use of the SBT should reduce computational burden compared to the CBT. Note that the initial offset correction is applied to Equation (5.4b) as a final step for the SBT.

5.1.2 Numerical Approximation Approach

The LPEs are a widely used general perturbation theory to compute the variation of parameters. We consider perturbations caused by J_2 gravity field harmonics and third-body, whose

perturbing potentials are shown in Equation (5.5a) and (5.5b) [72]

$$\mathcal{R}_{J_2} = \frac{\mu}{2r^3} R_{\oplus}^2 \mathrm{J}_2 \left[1 - 3\sin^2 i \, \sin^2(\omega + f) \right], \tag{5.5a}$$

$$\begin{aligned} \mathcal{R}_p &= \frac{\mu_p}{d} \sum_{i=2}^{\infty} \left(\frac{r}{d} \right)^i P_{i,0}(\boldsymbol{r} \cdot \boldsymbol{d}/rd) \\ &\approx \frac{1}{2} \frac{\mu_p}{d^3} \left[3 \left(\boldsymbol{r} \cdot \hat{\boldsymbol{d}} \right)^2 - r^2 \right]. \end{aligned} \tag{5.5b}$$

For the simplified LPEs, each perturbing potential, $\mathcal{R}$, has to be averaged with respect to the fast variable as in Equation (5.6)

$$\overline{\mathcal{R}} = \frac{1}{2\pi} \int_0^{2\pi} \mathcal{R} d\mathrm{M}. \tag{5.6}$$

Through averaging, the perturbing potential for J_2 gravity field harmonics can be redefined as

$$\overline{\mathcal{R}}_{\mathrm{J}_2} = -\frac{\mu \mathrm{J}_2 \mathrm{R}_{\oplus}^2}{(a\sqrt{1-e^2})^3} \left[\frac{3}{4} \sin i - \frac{1}{2} \right] \tag{5.7}$$

We set the moon to be the third-body and introduce one assumption applied in previous studies [23, 22, 73], which is to set the inclination of the third-body, i.e., the moon, as zero. Hence, the motion of the moon exists on the equatorial plane. Figure 5.1 shows the assumption conceptually:

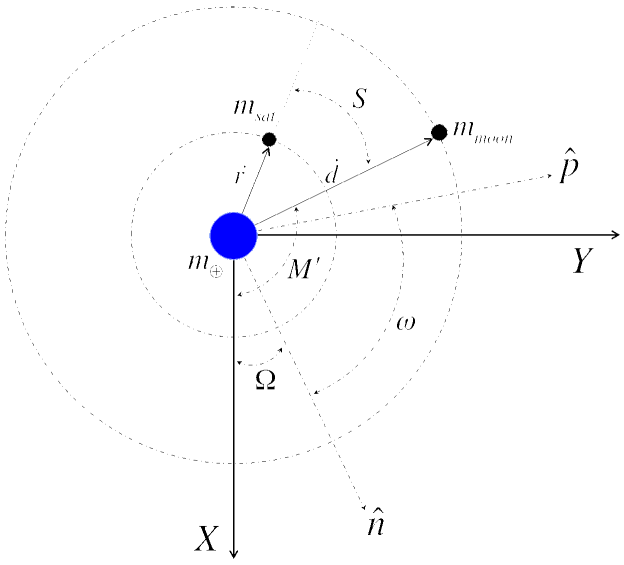

Figure 5.1: Illustration of the assumed dynamical system

the orbital plane of the artificial moon coincides with the equatorial plane ($I_M = 0°$). It helps us to

express Equation (5.5b) in a simpler form in terms of the classical orbital elements by eliminating $\sin I_M$ in the rotation matrix. Since the propagation interval in this study is relatively shorter than the period of the third-body, this assumption is applicable as well as beneficial to make the derivation more manageable. Based on these assumptions, it is possible to rewrite Equation (5.5b) as shown below

$$\begin{aligned}\mathcal{R}_p &= \frac{1}{2}\frac{\mu_p\, r^2}{d^3}\left[3\cos^2(S)-1\right] \\ &= \frac{1}{2}\frac{\mu_p\, r^2}{d^3}\left[3(\alpha\cos f+\beta\sin f)^2-1\right],\end{aligned} \tag{5.8}$$

where

$$\begin{aligned}\alpha &= \cos\omega\,\cos(\Omega-\mathrm{M}') - \cos i\,\sin\omega\,\sin(\Omega-\mathrm{M}') \\ \beta &= -\sin\omega\,\cos(\Omega-\mathrm{M}') - \cos i\,\cos\omega\,\sin(\Omega-\mathrm{M}').\end{aligned} \tag{5.9}$$

Thus, the perturbing potential due to the moon can be rewritten as

$$\mathcal{R}_p = \frac{1}{2}\frac{\mu_p\, r^2}{d^3}\left[3(\alpha^2\cos^2 f+2\alpha\beta\cos f\sin f+\beta^2\sin^2 f)-1\right]. \tag{5.10}$$

Equation (5.10) can be averaged by using Equation (5.6), then,

$$\overline{\mathcal{R}}_p = \frac{\mu_p a^2 n_p^2}{2}\left(\frac{a_p}{d}\right)^3\left\{\left(1+\frac{3}{2}e^2\right)\left[\frac{3}{2}(\alpha^2+\beta^2)-1\right]+\frac{15}{4}(\alpha^2-\beta^2)e^2\right\}. \tag{5.11}$$

Therefore, the total averaged perturbing potential, $\overline{\mathcal{R}}$, can be acquired by a simple linear summation as

$$\overline{\mathcal{R}} = \overline{\mathcal{R}}_{\mathrm{J}_2} + \overline{\mathcal{R}}_p. \tag{5.12}$$

Based on the basic definition of the LPEs [72] and the averaged perturbing potentials, the simplified LPEs can be presented as below in terms of the classical orbital elements.

$$\dot{a} = \frac{2}{na}\frac{\partial\overline{\mathcal{R}}}{\partial\sigma} \tag{5.13a}$$

$$\dot{e} = \frac{1}{na^2 e}\left[(1-e^2)\frac{\partial\overline{\mathcal{R}}}{\partial\sigma}-\sqrt{1-e^2}\,\frac{\partial\overline{\mathcal{R}}}{\partial\omega}\right] \tag{5.13b}$$

$$\dot{i} = \frac{1}{na^2\sqrt{1-e^2}}\left[\cot i\frac{\partial\overline{\mathcal{R}}}{\partial\omega}-\csc i\frac{\partial\overline{\mathcal{R}}}{\partial\Omega}\right] \tag{5.13c}$$

$$\dot{\Omega} = \frac{\csc i}{na^2\sqrt{1-e^2}}\frac{\partial\overline{\mathcal{R}}}{\partial i} \tag{5.13d}$$

$$\dot{\omega} = \frac{\sqrt{1-e^2}}{na^2e}\frac{\partial \overline{\mathcal{R}}}{\partial e} - \frac{\cot i}{na^2\sqrt{1-e^2}}\frac{\partial \overline{\mathcal{R}}}{\partial i} \tag{5.13e}$$

$$\dot{\sigma} = -\frac{1-e^2}{na^2e}\frac{\partial \overline{\mathcal{R}}}{\partial e} - \frac{2}{na}\frac{\partial \overline{\mathcal{R}}}{\partial a}. \tag{5.13f}$$

The analytic solutions for the second SDS can be derived simply through integrating Equations (5.13a)- (5.13f) [67]. As with the SBT, an initial offset correction has to be introduced to map the uncertainty more accurately.

5.2 Correction of Offset due to Periodic Terms

Even though the first-order solution, i.e., secular variation, assumes a mean motion by averaging, it strongly depends on the initial conditions since the periodic parts usually have a non-zero value after the averaging. Hence, we consider the initial offset belonging to the initial conditions. In this section, we show general description how this initial offset correction can be calculated briefly, and then discuss how the initial offset correction is acquired for the SBT. Let us consider

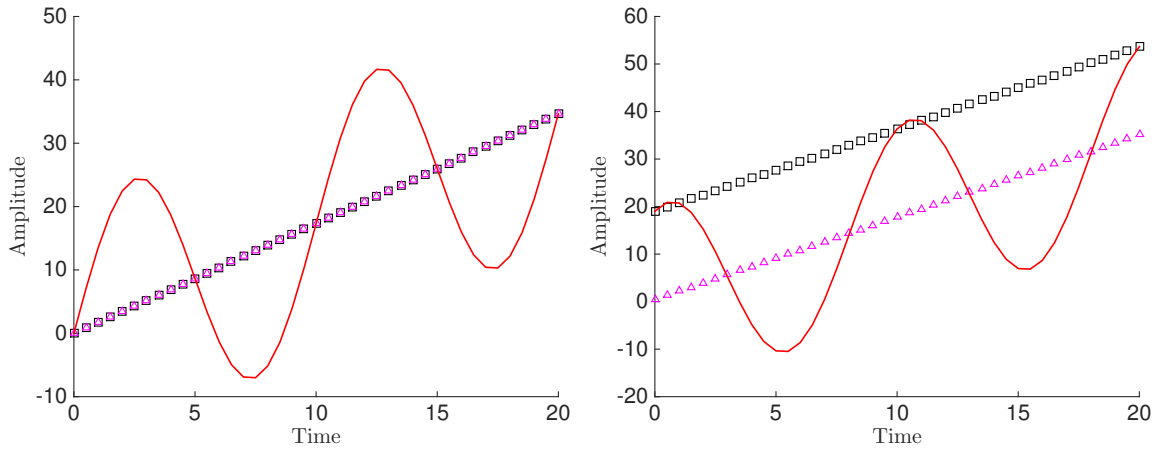

(a) Zero offset (general)

(b) Non-zero offset (general)

Figure 5.2: Dependency of the first-order solution on the initial conditions.

the solution over one orbital period. An orbital element, α, at any time can be expressed as a sum of the initial conditions, the secular term (or averaged) term, which varies linearly with time over

one period, and the periodic term for $0 \leq t \leq \mathrm{T}$ as

$$\alpha(t) = \alpha_0 + \overline{\dot{\alpha}} \cdot t + \alpha_{\mathrm{p}}, \tag{5.14}$$

where α_0, $\overline{\dot{\alpha}}$, α_{p}, and T represent a given initial condition, secular rate, and the periodic term, and the orbital period respectively. Note that one orbital period is a relatively short interval compared to the time scale of long-periodic effects; thus, it is possible to assume that the periodic term is only short-period. The averaged value of the orbital element over one orbital period becomes

$$\overline{\alpha} = \alpha_0 + \overline{\dot{\alpha}} \cdot \frac{\mathrm{T}}{2} + \overline{\alpha}_{\mathrm{p}}. \tag{5.15}$$

In Equation (5.15), $\overline{\alpha}_{\mathrm{p}}$ is the average value of the periodic term. Although the averaging theory assumes that this term is zero, it will have some non-zero value in most cases as seen in Figure 5.2. A mean value from the averaging theory (squares) and that from the assumption (triangles) are plotted in the figure: the ideal case is shown in Figure 5.2(a) and more general case is in Figure 5.2(b). The time derivative of Equation (5.14) can be rearranged as a differential equation for the periodic term as below [67, 72]

$$\dot{\alpha}_{\mathrm{p}} = f(\boldsymbol{x}, t) - \overline{\dot{\alpha}}(\boldsymbol{x}). \tag{5.16}$$

where $f(\boldsymbol{x}, t)$ is the full dynamical system for the orbital elements, i.e., $\dot{\alpha}(\boldsymbol{x}, t)$, and $\boldsymbol{x}$ represents a set of orbital elements. Integrating the above equation for an arbitrary interval, t, and taking an average, the average value of $\overline{\alpha}_{\mathrm{p}}$ is given as

$$\overline{\alpha}_{\mathrm{p}} = \frac{1}{2\pi} \int_0^{2\pi} \left[\int_0^t f(\boldsymbol{x}(\tau), \tau) d\tau - \overline{\dot{\alpha}}(\boldsymbol{x}_0) \cdot t \right] d\mathrm{M}. \tag{5.17}$$

If the ideal initial conditions were used, Equation (5.17) should become zero (Figure 5.2(a)) and the initial offset correction is unnecessary. By applying the averaged value acquired through Equation (5.17), the corrected initial conditions can be expressed as

$$\overline{\alpha}(t_0) = \alpha_0 + \overline{\alpha}_{\mathrm{p}}. \tag{5.18}$$

An advantage of the analytic approach is that the computation of the initial offset correction is simplified. The analytic solutions are defined with respect to the mean orbit, which is a characteristic of the perturbation theory. More specifically, as shown in Equation (5.1), the propagated

state at any epoch, t_i, can be computed based on the mean orbital element at the initial epoch, $\mathbf{x}_{\overline{\mathrm{OE}},0}$. Thus, the mean orbital elements at the initial epoch can be directly acquired by iterating Equation (5.1) with $t = 0$ [12]. This conversion algorithm may be replaced with a completely analytic method by using a generating function from a canonical transformation, e.g., von Zeipel, Lie transformation, and so on.

For the numerical approximation approach, the periodic offset in Equation (5.14) is solved by integrating the full nonlinear dynamics including the disturbing forces shown in Equation (5.19) for one orbit, then, subtracting the initial conditions and the secular change acquired from the simplified LPEs. Finally, the result is inserted into Equation (5.18) to determine the corrected initial conditions.

$$\boldsymbol{a}_{\mathrm{J2}} = -\frac{3\mu \mathrm{J}_2 \mathrm{R}_{\oplus}^2}{2|\boldsymbol{r}|^4} \left\{ \left[1 - 5(\hat{\boldsymbol{r}} \cdot \hat{\boldsymbol{z}})^2 \right] \hat{\boldsymbol{r}} + 2(\hat{\boldsymbol{r}} \cdot \hat{\boldsymbol{z}})\hat{\boldsymbol{z}} \right\} \tag{5.19a}$$

$$\boldsymbol{a}_{\mathrm{3rd}} = -\mu_{\mathrm{3rd}} \left[\frac{(\boldsymbol{r} - \boldsymbol{d})}{|\boldsymbol{r} - \boldsymbol{d}|^3} + \frac{\boldsymbol{d}}{|\boldsymbol{d}|^3} \right] \tag{5.19b}$$

5.3 Verification of the Simplified Dynamical System

The accuracy of the SDS is verified through Monte Carlo simulations for two scenarios: a Low Earth Orbit (LEO) satellite and Medium Earth Orbit (MEO) satellite. The altitude of the LEO satellite is approximately 602 km, which allows the dynamical system to be highly nonlinear due to gravitation. The MEO satellite has a similar altitude with classical global navigation satellite systems (GNSS) such as GPS, Galileo, or Glonass; this case demonstrates the capabilities of the proposed method when propagating the state uncertainty including the perturbation due to a third-body. Table 5.1 provides the initial orbit elements for these scenarios. The initial conditions are chosen to avoid singularity problems, e.g., zero eccentricity, zero inclination, and critical inclination, because the current SDSs are defined in terms of the Delaunay variables. For the Monte Carlo simulations, 10,000 samples, normally distributed within some specified 3-σ region, are generated with respect to the initial Keplerian elements. We are using a large covariance so as to push

Table 5.1: Initial Keplerian elements and propagation method for the test orbits

Element	LEO	MEO	Molniya
Semimajor axis, a, (km)	6980.041	26578.140	26600.000
Eccentricity, e	0.1	0.01	0.74
Inclination, i, (deg)	30	55	62.8
Longitude of the ascending node, Ω, (deg)	45	45	45
Argument of periapsis, ω, (deg)	60	60	270
Mean anomaly, ν, (deg)	105	105	105
Propagation method	SBT	simplified LPEs	

the algorithm into the highly nonlinear regime. The selected number of samples is the minimum number of samples that ensure consistent mean and variance as shown in Figure 5.3. In the figure, the propagated mean and variance from five iterations are represented by different symbols. After 10,000 samples, the change in the mean value is less than 1% with respect to the mean of 25,000 samples. The convergence test shows that the mean and variance do not have any significant change over 10,000 samples. The numerical integration result with the full dynamical system is assumed

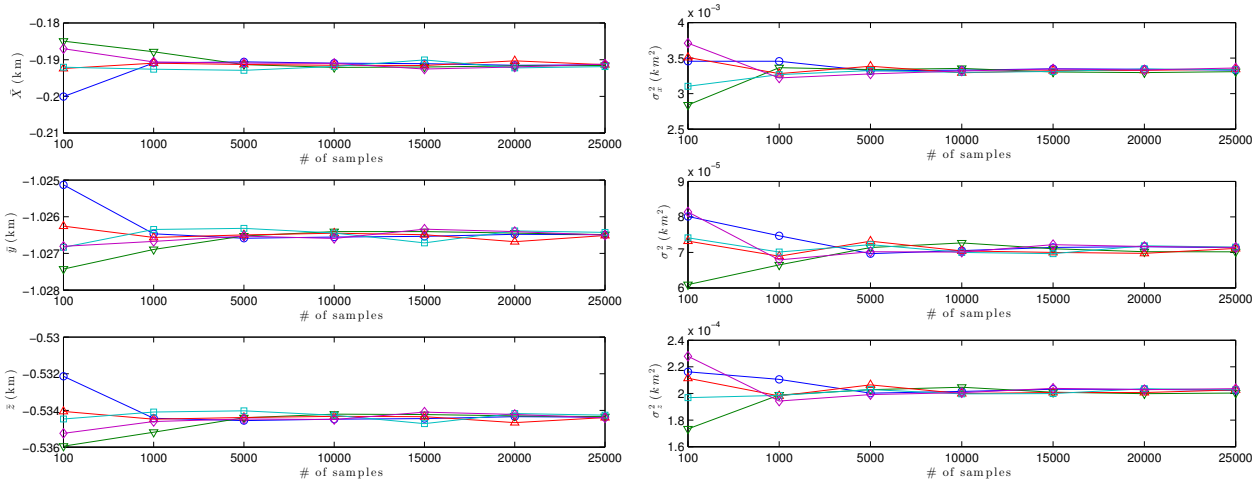

(a) Mean from the Monte Carlo simulations

(b) Variance from the Monte Carlo simulations

Figure 5.3: Mean and variance after 50-orbital periods of propagation with different size of samples

as the truth. The full dynamical system includes the same perturbations as each test case, i.e., LEO with J_2 and MEO with J_2+moon, and the results from it include short periodic variations.

The initial state is integrated with the *ode45* function in MATLAB. In this section, we compare the propagated distributions from two different SDSs and verify the accuracy statistically.

5.3.1 Result I: The Accuracy of the SDS for LEO

A Gaussian error centered at the initial Keplerian elements of the LEO object is assumed with standard deviations of 20 km in the semi-major axis, 0.005 in eccentricity, and 0.01° in the inclination, longitude of ascending node, the argument of the pericenter, and the mean anomaly directions. The LEO satellite case is propagated for 50-orbital periods, which is approximately three days.

5.3.1.1 Verification of the Accuracy

For the sake of demonstration of statistical comparison, we plot the propagated distributions for both the full dynamical model and SDS on the δx-$\delta \dot{x}$ phase-space and the histograms of the PDFs in each direction in Figure 5.4: histogram of the conditional PDF on the $\delta \dot{x}$(ER/s) axis (top-left), that on δx(ER) axis (bottom-right), and the distributions of the samples on the δx-$\delta \dot{x}$ phase space (top-right) from two different methods. Since results on the δy-$\delta \dot{y}$ and δy-$\delta \dot{y}$ phase spaces have similar shapes to Figure 5.4, we do not attach figures on those spaces. Even though the distribution at the initial epoch is Gaussian, the propagated uncertainty does not have a normal distribution because of the nonlinearity in dynamics. We verify how well the SDS captures the nonlinear effect by comparing the moments of the PDF. Table 5.2 is a summary for all coordinate directions of the moments of the propagated distribution with the SDS and relative errors of them with respect to the truth in percentage. All values are normalized with respect to Earth radius. The first-order central moment, μ_1, is defined to be zero, so we use actual mean values instead of the central moment. The third and fourth-order moments are defined with the standardized moments. The table shows that the relative errors are less than 0.5% from the truth. These values describe the shape of the PDFs shown in Figure 5.4. For instance, a positive skewness, or third-order standardized moment indicates that the PDF in the x direction (bottom-right) has a long tail

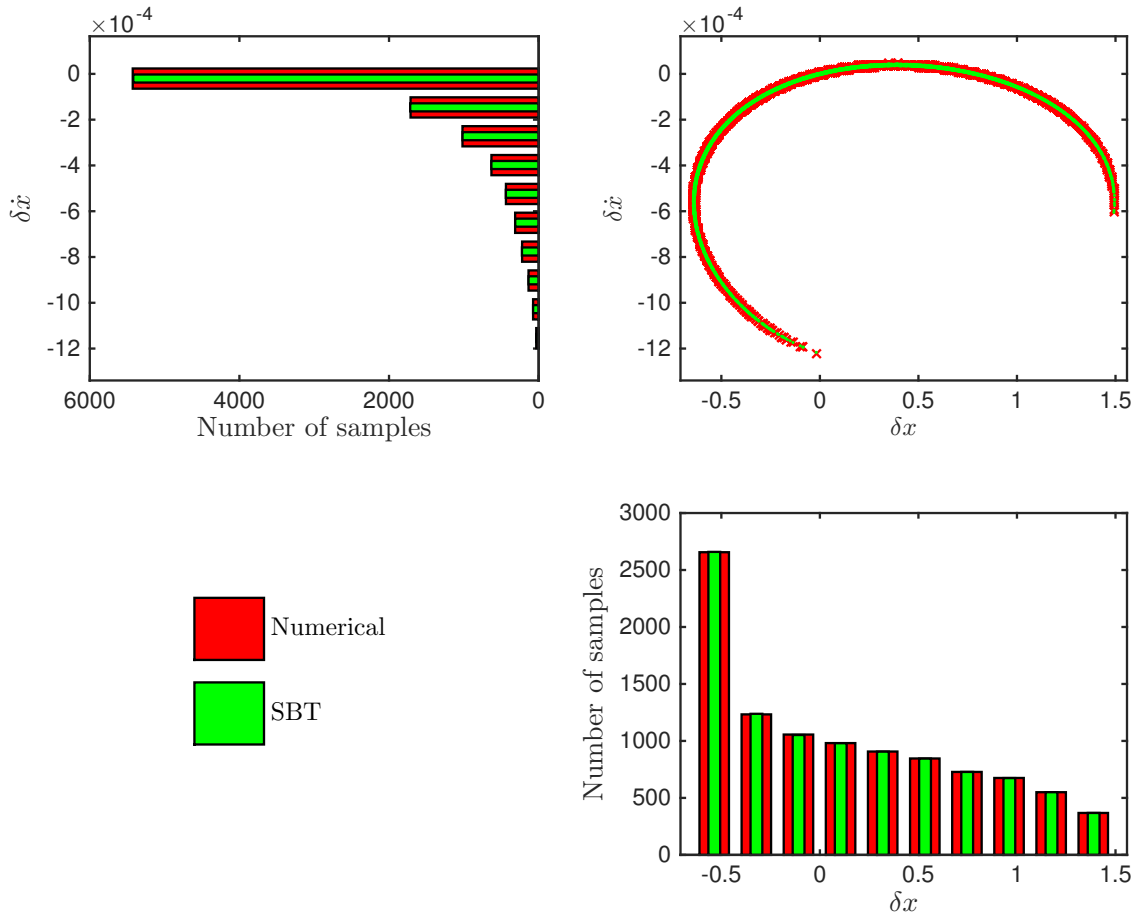

Figure 5.4: Sample point distribution on the $\delta\dot{x}$ (ER/s, top-left) and δx (ER, bottom-right) direction, and its conditional histograms after 50-orbital periods of propagation in LEO.

Table 5.2: Central moments and relative errors after 50-orbital periods of propagation (J_2 only)

	1st order		2nd order		3rd order		4th order	
	μ_1	Δ (%)	μ_2	Δ (%)	$\overline{\mu}_3$	Δ (%)	$\overline{\mu}_4$	Δ (%)
δx	0.1146	0.3312	0.3722	0.1392	0.4765	0.2222	2.0311	0.5313e-1
δy	0.2571	0.7574e-1	0.1218	0.2467	1.5184	0.3868e-1	4.8877	0.5524e-1
δz	0.1105	0.7904e-1	0.7482e-1	0.3944	1.0339	0.1509	3.0474	0.1357
$\delta \dot{x}$	-0.1594e-3	0.8730e-1	0.5752e-7	0.4756e-1	-1.6568	0.9476e-1	5.3795	0.1229
$\delta \dot{y}$	0.2871e-4	0.5567	0.1174e-6	0.1514	0.2461	0.4639	1.8794	0.2171e-1
$\delta \dot{z}$	0.5208e-4	0.1674	0.2451e-7	0.3037	0.8252	0.2252	2.6823	0.1176

on the right-hand side. On the other hand, that in the $\dot{x}$ direction has a long tail on the opposite side, which corresponds to the negative value of $\overline{\mu}_3$.

We apply the statistical energy test to the distributions propagated with the full dynamical system and the SDS at five orbital epochs and within one period. The significance probability, i.e., p-value, for the hypothesis test is plotted in Figure 5.5 for every 5 orbital periods from 0 to 50 orbital periods of propagation, Figure 5.5(a), and within 49-50 orbital periods of propagation, Figure 5.5(b). As seen in the figure, the significance probability is always larger than the designated significance level of $\alpha = 5\%$. This result represents that the distribution propagated with the SBT is equal to that from the full dynamical system with a 95% confidence level.

5.3.1.2 Periodic Effects Within One Period

Since the short-period variations are replaced with constants, a periodic offset exists between the distributions computed using the full dynamical system and the SDS. Figure 5.6 shows an oscillation in the offset on the g-G phase-space between 49 and 50 orbital periods. In the figure, the distributions of the deviation about the mean computed with the numerical integration (black crosses) and those with the SBT (gray circles) reflect the difference between the full and constant short-period terms. To investigate the impact in the accuracy of the propagated uncertainty due to the offset, we compare the skewness and kurtosis of PDFs in the ECI coordinate frame, which is shown in Figure 5.7: time history of the moment from the truth is represented with triangles and that from the SDS squares. As seen the figure, both statistical values from two dynamical systems

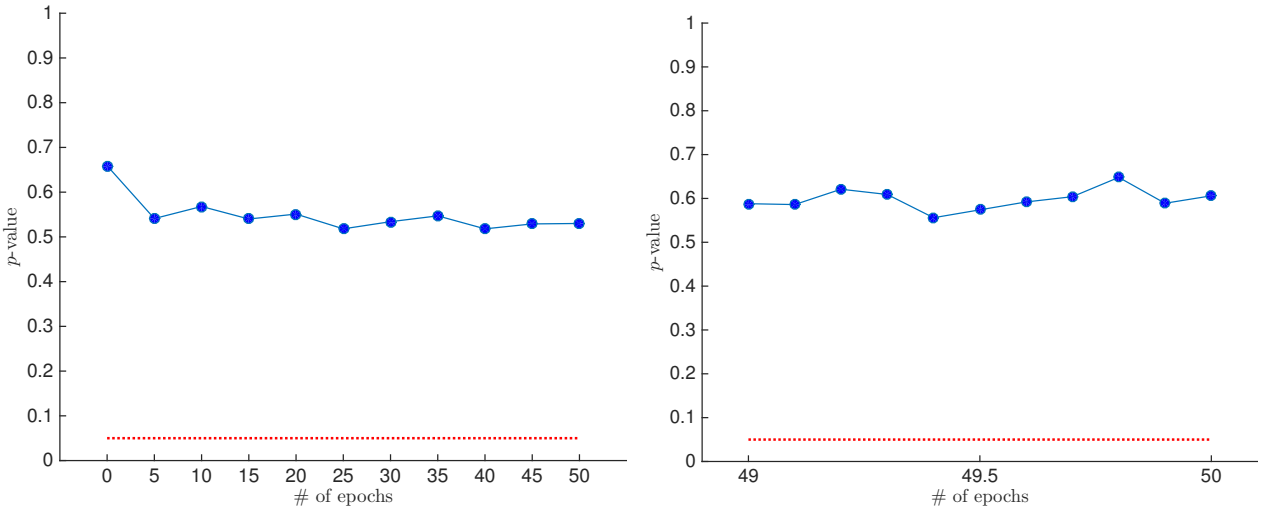

(a) Time history of the p-value every 5 orbital periods (b) Time history of the p-value within the one period

Figure 5.5: Time history of the p-value (solid line) with the SBT and the designated significance level, α (dotted line).

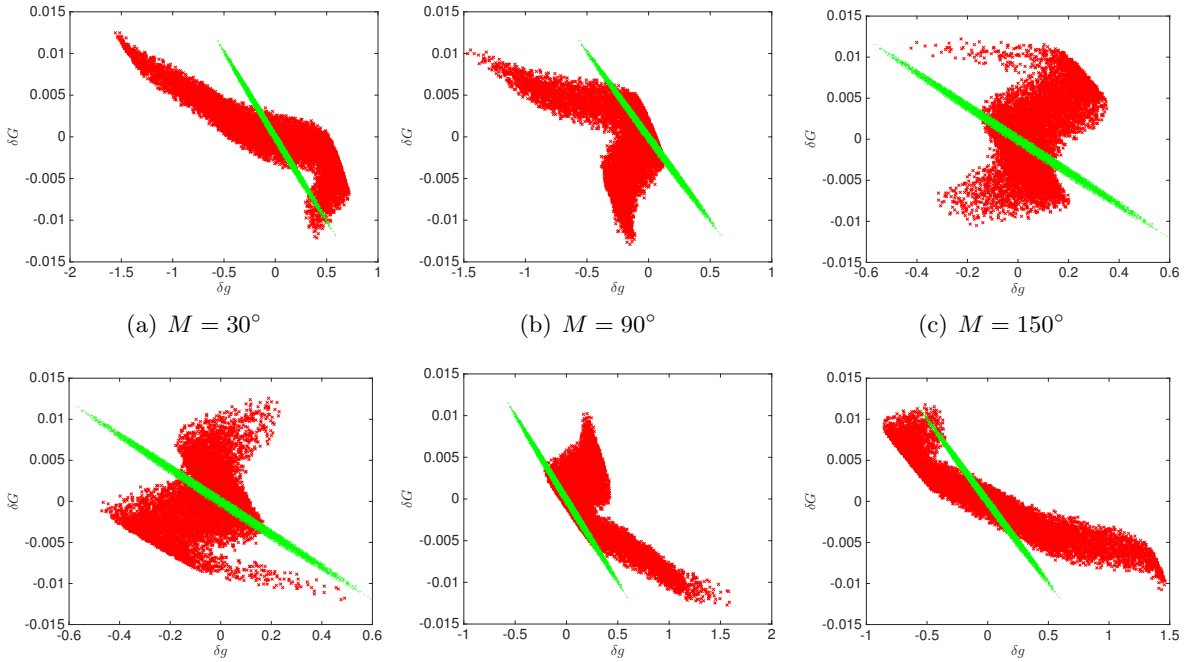

(a) $M = 30°$ (b) $M = 90°$ (c) $M = 150°$

(d) $M = 210°$ (e) $M = 270°$ (f) $M = 330°$

Figure 5.6: The effects from the short-period terms inside one orbital period on the g-G phase space.

match each other. Therefore, the short-period variations are a negligible factor in the propagation of uncertainty in ECI coordinates.

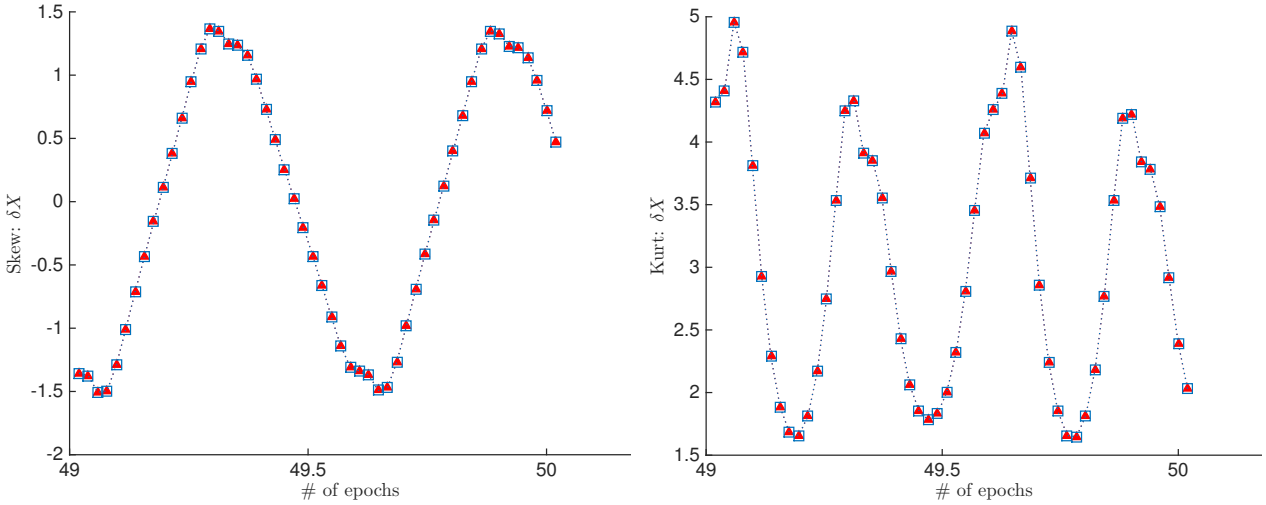

(a) Skewness on δx direction

(b) Kurtosis on δx direction

Figure 5.7: Time history of the skewness and kurtosis in the δx direction within one period plotted over time.

5.3.1.3 Consistency of the SBT in Uncertainty Propagation

The L_2-norm of the STD for the true distribution (squares) and that for the error (triangles), $\Delta\delta\mathbf{x}$, increase in time as shown in Figure 5.8(a). The time history of the normalized STD of each position component is plotted in Figure 5.8(b): x (squares), y (circles), and z (triangles). The figure shows that the normalized STD varies less than 0.3% for a propagation of approximately one week. Therefore, it is possible to see that the propagated uncertainty with the SDS follows the truth consistently.

5.3.2 Result II: The Accuracy of the SDS for MEO

The initial distribution at the initial epoch for the MEO is generated with the same initial error, 1-σ, to the LEO case. This MEO satellite is propagated for 30 orbit periods, which is about 15 days.

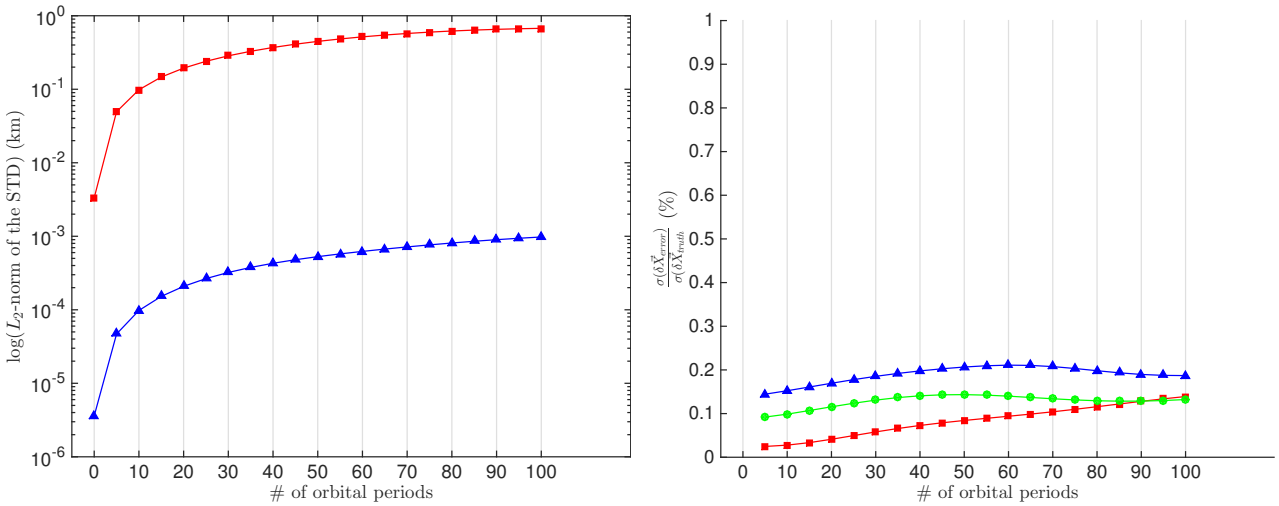

(a) Time history of L_2-norm between the STD

(b) Normalized STD on each direction

Figure 5.8: Time history of L_2-norm and normalized STD for LEO.

5.3.2.1 Verification of the Accuracy

Figure 7.2 shows the distributions on the δx-$\delta \dot{x}$ phase-space and the histograms of the PDFs belonging to each direction: the conditional PDF on the $\delta \dot{x}$(ER/s) axis (top-left), that on δx(ER) axis (bottom-right), and the distributions of the samples on the δx-$\delta \dot{x}$ phase space (top-right) from two different methods. To verify the results statistically, we summarize the moments of the PDFs and relative errors in Table 5.3. The PDF in the $\delta \dot{x}$ direction, at top-left in Figure 7.2,

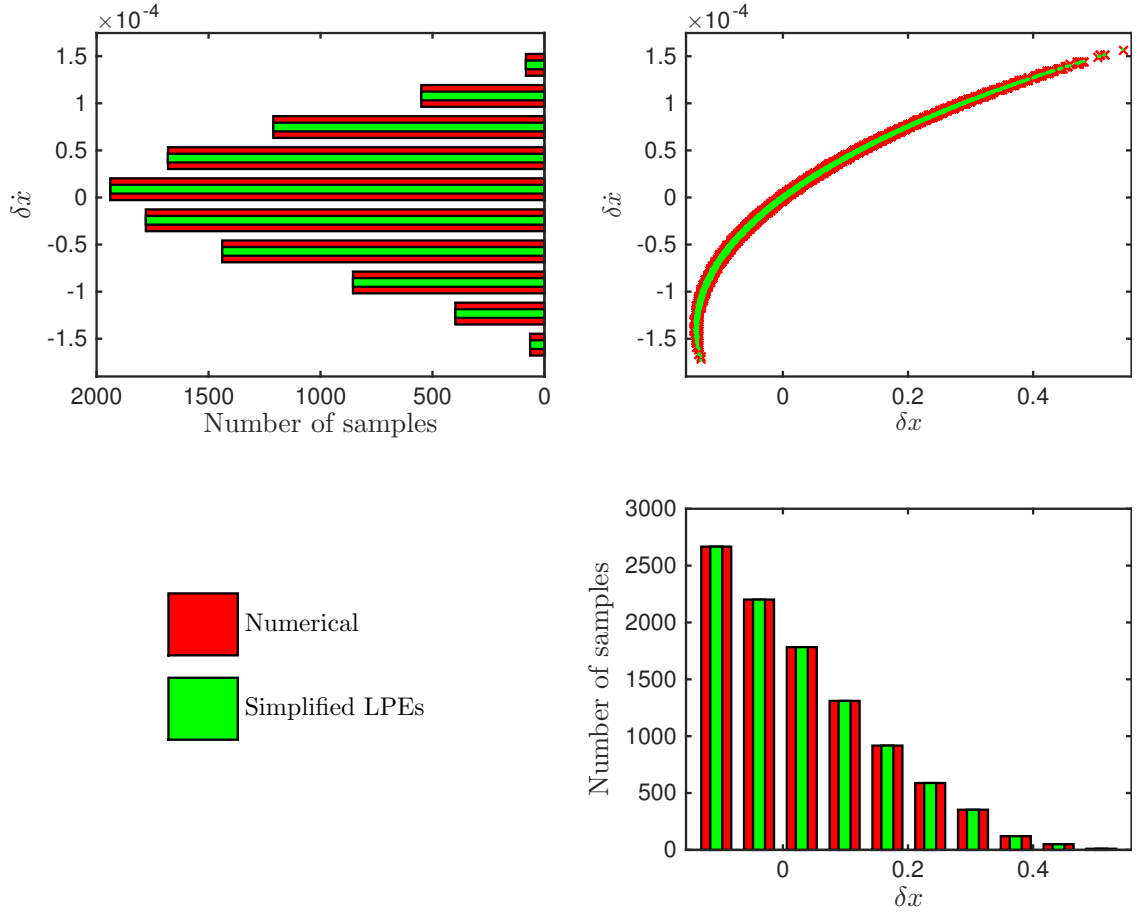

Figure 5.9: Sample point distribution on the $\delta \dot{x}$ (ER/s, top-left) and δx (ER, bottom-right) direction, and its conditional histograms after 30-orbital periods of propagation in MEO.

has a slightly asymmetric shape, which corresponds to the small skewness $\overline{\mu}_3$. Relative errors of the moments with respect to the truth are less than 0.1%; thus, the SDS in this scenario, which includes the multiple perturbations, captures the nonlinearity and maps the uncertainty accurately.

The gravitational force of the two-body problem, which is inversely proportional to the square of

Table 5.3: Central moments and relative errors after 30-orbital periods of propagation (MEO, J_2+moon)

	1st order		2nd order		3rd order		4th order	
	μ_1	Δ (%)	μ_2	Δ (%)	$\overline{\mu}_3$	Δ (%)	$\overline{\mu}_4$	Δ (%)
δx	0.2684e-1	0.2990e-1	0.1610e-1	0.2520e-1	0.8429	0.1592e-1	3.1445	0.7941e-2
δy	0.2153e-1	0.2377e-1	0.8941e-1	0.3712e-1	0.2993	0.4522e-2	2.4681	0.1848e-3
δz	-0.4725e-2	0.6861e-1	0.1822	0.2194e-1	-0.4414e-1	0.5888e-1	2.3731	0.3081e-3
$\delta \dot{x}$	-0.1417e-5	0.9387e-3	0.3730e-8	0.3781e-1	-0.9819e-1	0.2023e-1	2.3822	0.1126e-2
$\delta \dot{y}$	0.2596e-5	0.6200e-1	0.2122e-8	0.3193e-1	0.2309	0.4495e-1	2.4272	0.1520e-2
$\delta \dot{z}$	0.4070e-5	0.4401e-1	0.2221e-9	0.9406e-1	1.0773	0.4937e-2	3.6383	0.4653e-2

the distance, causes the largest nonlinearity in the dynamical system with a given altitude for this case. Thus, the relative error becomes smaller than that in the previous test.

The accuracy of the uncertainty propagated with the simplified LPEs is also verified through the energy test. A time history of the significance probability is computed for two cases, over several orbital epochs and within one period, as before. As seen in Figure 5.10, the significance probabilities are larger than the significance level in both cases: every 1 orbital period from 0 to 50 orbital periods of propagation, Figure 5.10(a), and within $29 \sim 30$ orbital periods of propagation, Figure 5.10(b). Therefore, the propagated uncertainty including both the effects of J_2 gravity field harmonics and the moon's perturbation is equal to the truth with a 95% confidence level.

5.3.2.2 Periodic Effects Within One Period

The periodic offset on the Delaunay element space and the time history of moments in the ECI coordinates frame are also investigated to verify the accuracy of the SDS under the multiple perturbations The distributions on the g-G phase-space within 29-30 orbital periods are compared in Figure 5.11. In the figure, the distributions of the deviation about the mean computed with the numerical integration (black crosses) and those with the simplified LPEs (gray circles) reflect the difference between the full and constant short-period terms. Similar to the LEO case, there exists an oscillating offset in element space. However, this offset does not have a critical effect when the

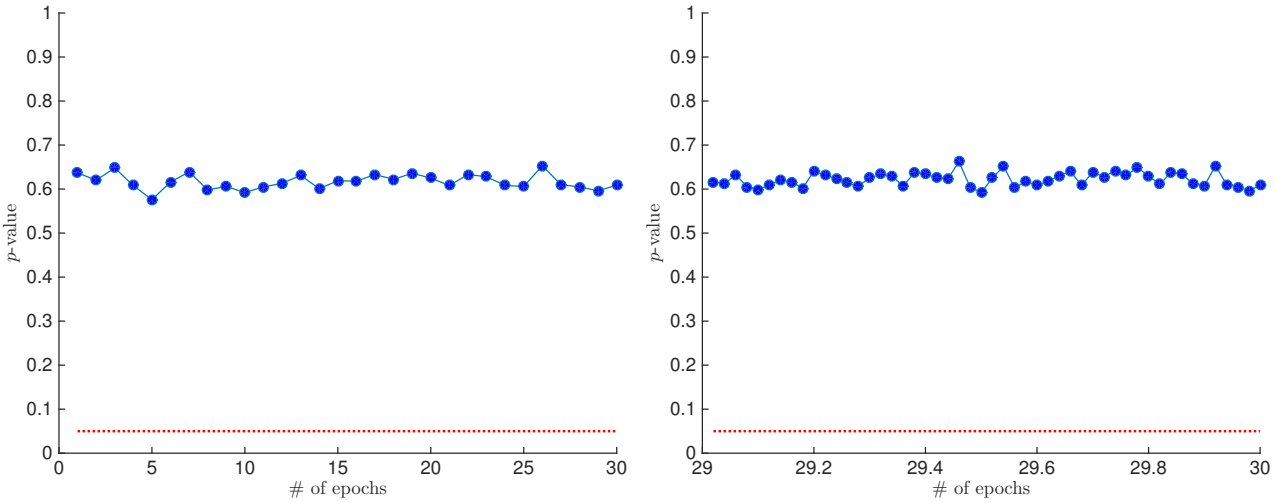

(a) Time history of the p-value every one orbital period

(b) Time history of the p-value within the one period

Figure 5.10: Time history of the p-value (solid line) with the simplified LPEs and the designated significance level, α (dotted line).

distributions are considered in the Cartesian space. The time history of the skewness and kurtosis in the Cartesian space in the x direction are plotted in Figure 5.12: the history from the truth is plotted with triangles and that from the SDS squares. As seen in the figures, even though there exists an offset in element space, it does not influence uncertainty propagation in ECI coordinates.

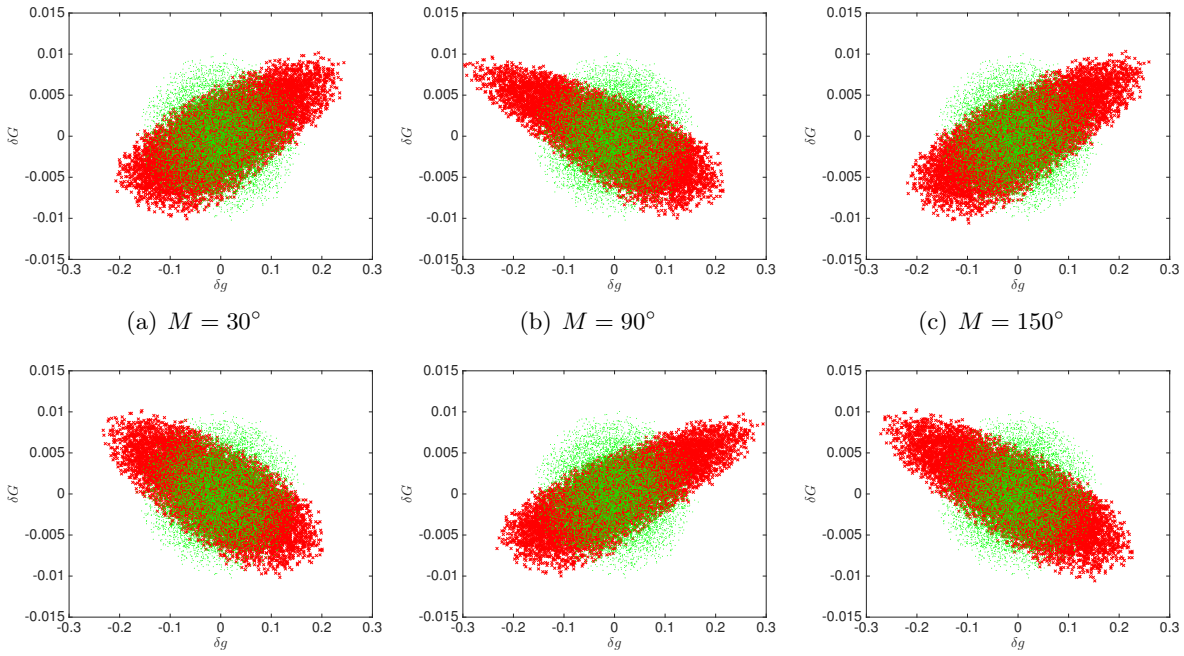

(a) $M = 30°$ (b) $M = 90°$ (c) $M = 150°$

(d) $M = 210°$ (e) $M = 270°$ (f) $M = 330°$

Figure 5.11: The effects from the short-period terms inside one orbital period on the g-G phase space.

5.3.2.3 Consistency of the Simplified LPEs in Uncertainty Propagation

Figure 5.13 shows that the time history of the L_2-norm of the STD for the true distribution (squares) and that for the error (triangles), $\Delta\delta\mathbf{x}$, (Figure 5.13(a)) as well as the normalized STD of each component (Figure 5.13(b)) for 0 to 30 orbital periods of propagation. Similar to the previous case, the normalized STD varies within a small region, less than 0.1%, for each component. Hence, the propagated uncertainty with the SDS for the MEO case also maintains consistency.

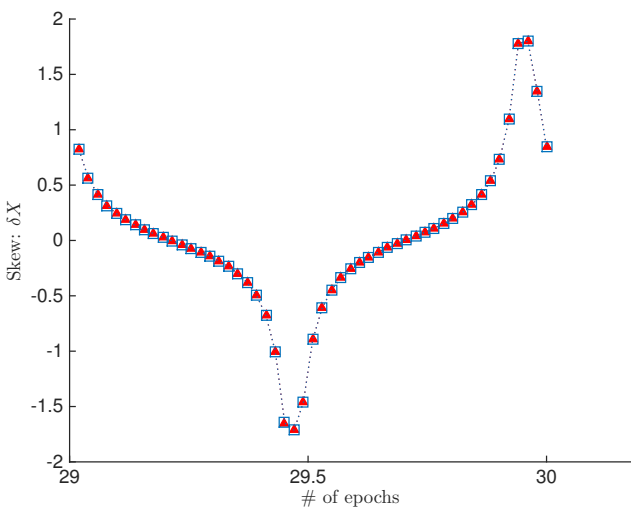

(a) Skewness on δx direction

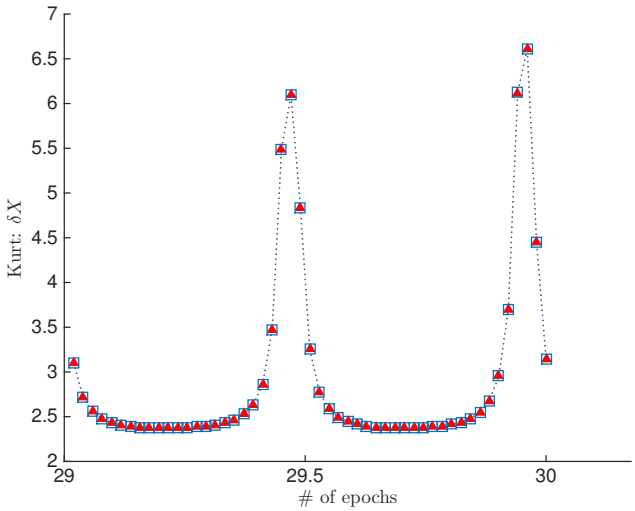

(b) Kurtosis on δx direction

Figure 5.12: Time history of the skewness and kurtosis in the δx direction within one period plotted over time.

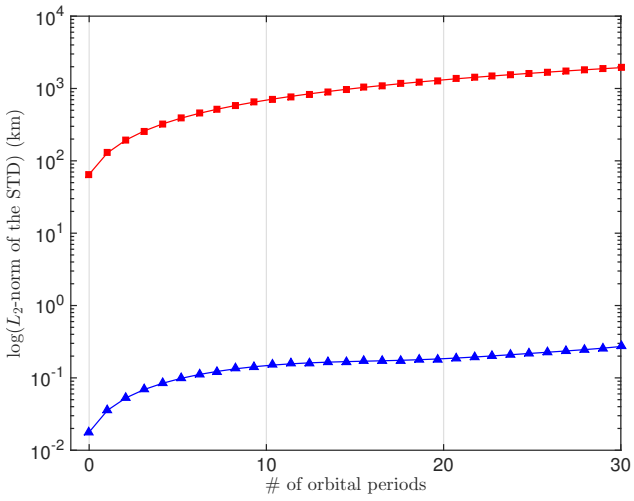

(a) Time history of L_2-norm between the STD

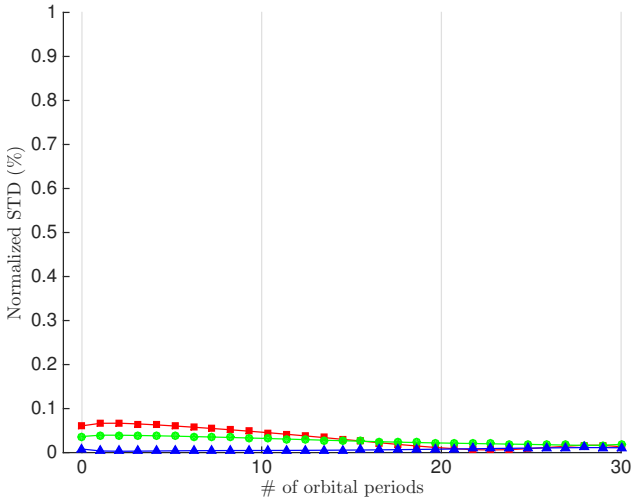

(b) Normalized STD on each direction

Figure 5.13: Time history of L_2-norm and normalized STD for MEO.

5.3.3 Result III: The Accuracy of the SDS for Highly Elliptical Orbit

As a particular case, we apply the SDS to propagate uncertainty of objects in the highly elliptical orbit, i.e., Molniya. Table 5.4 is a summary of the moments of the propagated uncertainty with the SDS and relative errors of them about the truth in percentage. Each value on each direction is normalized with respect to Earth radius. As seen in the table, the relative errors of the moments about the truth are less than 1.3%.

Table 5.4: Central moments and relative errors after 30-orbital periods of propagation (Molniya, J_2+moon)

	1st order		2nd order		3rd order		4th order	
	μ_1	Δ (%)	μ_2	Δ (%)	$\overline{\mu}_3$	Δ (%)	$\overline{\mu}_4$	Δ (%)
δx	-0.1238e-3	0.5668	0.4108e-1	0.2238	0.1820e-1	4.8874	2.3879	0.6740e-2
δy	-0.8298e-2	0.4336	0.1052e-2	1.2248	-0.9647	0.9431	3.3395	0.5936
δz	-0.1175e-1	0.1304e-1	0.5023e-1	0.6947	-0.2403	0.3446	2.4664	0.2749e-1
$\delta \dot{x}$	4.7262e-07	1.1428	4.7478e-12	0.4250	0.8108	0.8444	3.0177	0.4020
$\delta \dot{y}$	7.8976e-07	0.8233	3.3971e-10	1.8018	0.2025	0.7714e-1	2.4665	0.5631e-2
$\delta \dot{z}$	5.0601e-07	0.2438	8.4819e-10	1.6981	0.9417e-1	0.48664	2.4158	0.7443e-2

The propagated distribution on the δx-$\delta \dot{x}$ and the histograms of the PDFs belonging to each direction is shown in Figure 7.5: the conditional PDF on the $\delta \dot{x}$(ER/s) axis (top-left), that on δx(ER) axis (bottom-right), and the distribution of the samples on the phase-space (top-right) from the SDS and truth. Since the comparison of the distributions and histograms on another phase-spaces, i.e., δy-$\delta \dot{y}$ and δz-$\delta \dot{z}$, are analogous to them on the δx-$\delta \dot{x}$ phase-space, we skip the figures on those phase-spaces.

Figure 5.15 presents a history of the p-value over time: each orbit period and within one orbit period. As seen in the figure, the SDS is verified to be applicable to the highly elliptic orbit case. A wedge-shaped curve at the right-hand side in the figure is appeared around the perigee: in case of the Molniya orbit, orbital elements are rapidly changed in passing the perigee.

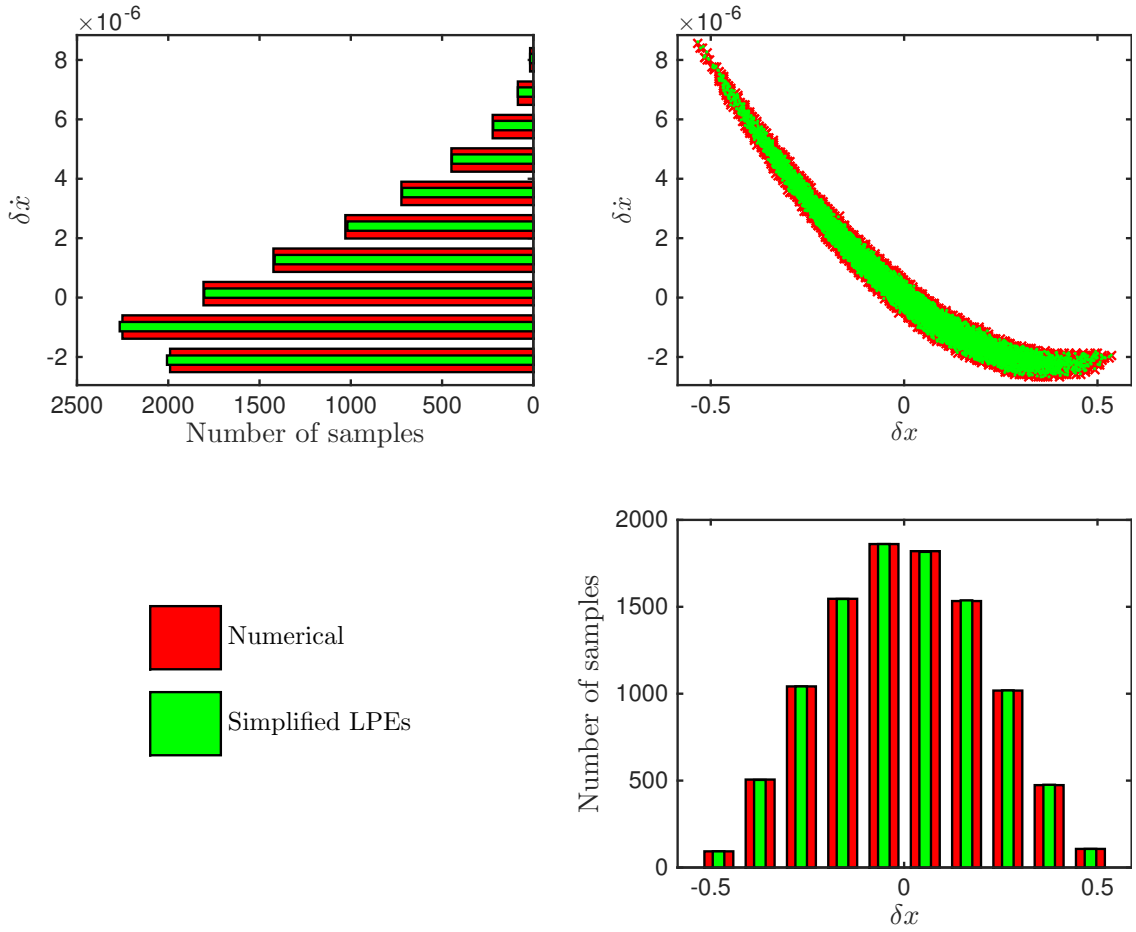

Figure 5.14: Sample point distribution on the $\delta\dot{x}$ (ER/s, top-left) and δx (ER, bottom-right) direction, and its conditional histograms after 30-orbital periods of propagation in Molniya.

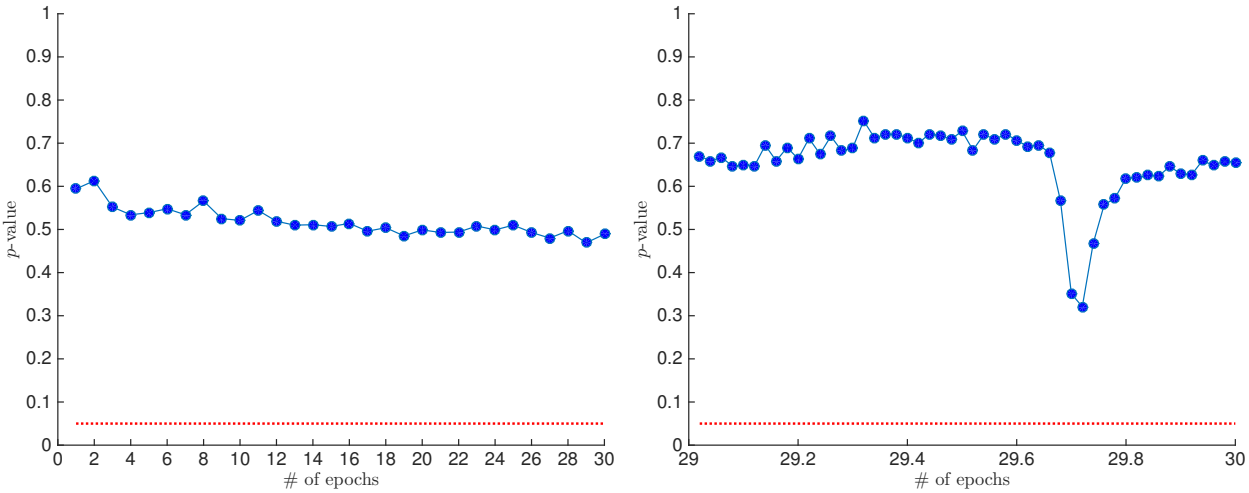

(a) Time history of the p-value every one orbital period (b) Time history of the p-value within the one period

Figure 5.15: Time history of the p-value (solid line) with the simplified LPEs and the designated significance level, α (dotted line).

5.4 Performance Improvement of the Simplified Dynamical System

The SDS has lower nonlinearity relative to the full dynamical system since it replaces the short period variations with constants, which allows us to use a wider integration step for state propagation. Therefore, there exists an additional advantage, an improvement in the computational efficiency, following this simplification. We compare the number of dynamical equation function calls and total elapsed time for the integration to quantify this improvement. All computations for these test results are performed on a laptop, 2.8 GHz Intel® Core i7 and 4 GB 1067 MHz DDR3. Total elapsed times from the full dynamical system and the simplified LPEs are about 32815.7 seconds and about 2371.9 seconds respectively; thus, total elapsed time shows remarkable enhancement, about 13.8 times faster. The elapsed time is an average of measurements acquired from 10 runs. A comparison of the number of dynamical equation function calls is shown in Figure 5.16. There are 65,623 required function calls to propagate one sample for 50 orbital periods for the full dynamical system, whereas this number is reduced to just 85 for the SDS. This result is a clear indication of the advantage of SDS's lower nonlinearity.

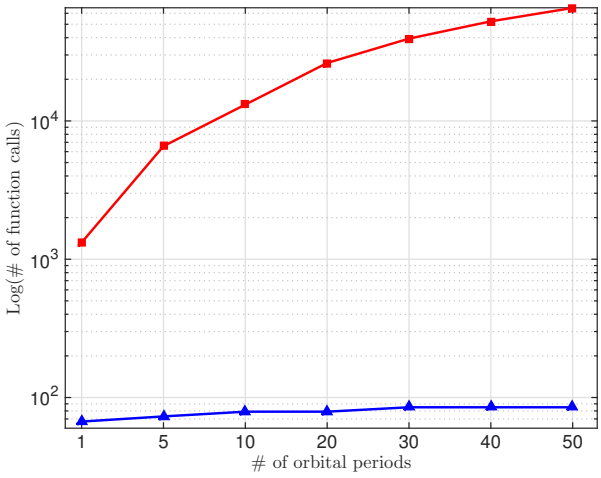

Figure 5.16: Comparison of the number of function calls in the full dynamical system (squares) and the SDS (triangles)

Since the approximated numerical approach is still using a numerical integrator for state propaga-

tion, it is possible to further improve the computational efficiency by reformulating this approach analytically. This motivates the future implementation of a new analytic SDS. Moreover, deriving an expanded analytic solution including more perturbations, e.g., the Sun or Solar Radiation Pressure (SRP), or that with the non-singular variables are also of interest.

5.5 Conclusion

The idea of the weak solution for stochastic partial differential equations [29] motivates us to identify a dominant variation and explore the Simplified Dynamical System (SDS) for uncertainty propagation. The main goals of this section is to verify the accuracy and performance improvement of the SDS, as well as to identify the dominant variation in uncertainty propagation.

Throughout this chapter, we show that the SDS is capable of propagating the initial PDF while maintaining accuracy even though the short-period variations are regarded as constants. It is worth mentioning that we also discuss how much the short-period variations influence the mapping of uncertainty is also tested by comparing distributions within one period. The replacement of periodic variations apparently make an offset in the orbit element space; however, it is verified that there is a negligible effect in mapping uncertainty in the Cartesian space. Figure 5.17 represents a ratio of a magnitude of the short-period variations with respect to the semi-major axis in percentage. This result could be meaningful in that most of the applications of the space situational awareness, such as a collision assessment, are usually described based on the Cartesian space. Therefore, we can conclude that the most dominant variation for the accurate propagation of uncertainty is the secular variation of the dynamical system of the orbiting bodies.

We also introduce a new statistical method, called the statistical energy test, for comparing multivariate PDFs more rigorously [2, 3]. Based on this test, we conclude that the propagated uncertainty with the SDS is verified that it describes the true uncertainty accurately with 95% of confidence level for every test scenarios.

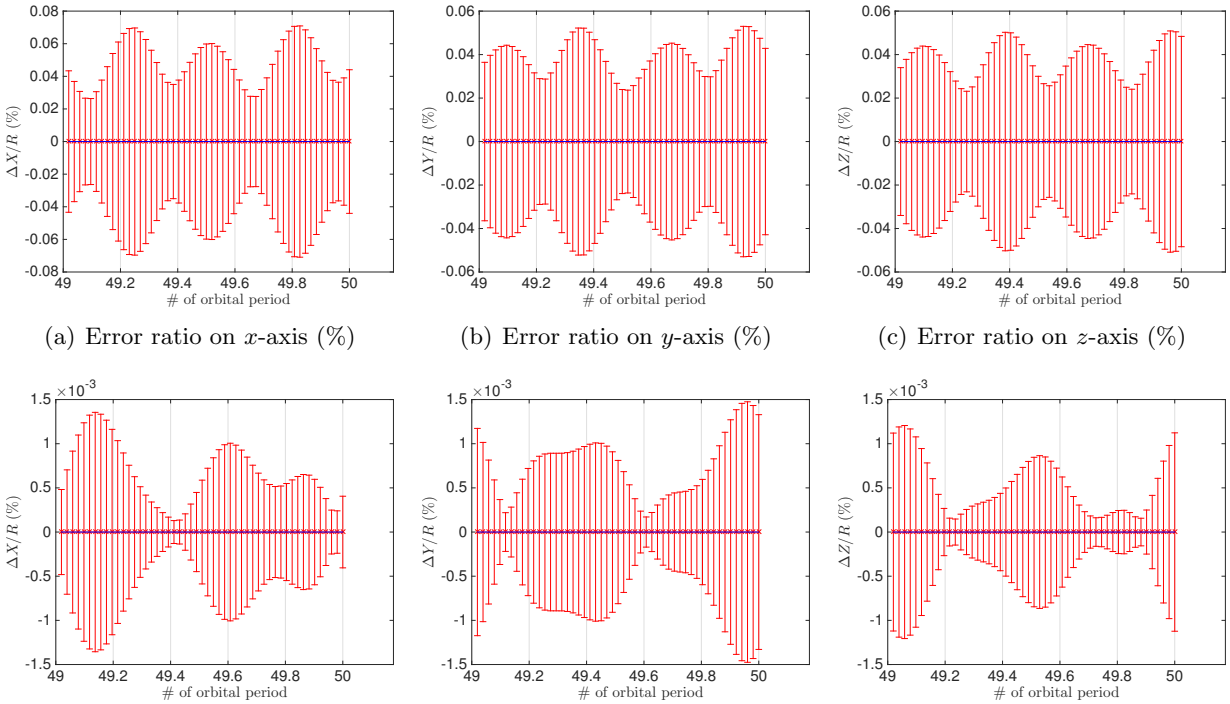

(a) Error ratio on x-axis (%) (b) Error ratio on y-axis (%) (c) Error ratio on z-axis (%)

(d) Error ratio on x-axis (%) (e) Error ratio on y-axis (%) (f) Error ratio on z-axis (%)

Figure 5.17: The ratio of short-period variation in the Cartesian coordinate frame: time history of the ratio for the LEO case on each axis is at the top, and that for the MEO case on each axis is at the bottom.

Chapter 6

Expansion of the Simplified Dynamical System through the Deprit-Lie Transformation

In Chapter 5, we have verified that the Simplified Dynamical System (SDS) improves the computational efficiency while maintaining the accuracy and concluded that the secular variations are the most dominant factor in mapping uncertainty. The goal of this chapter is to expand the previous discussion by introducing higher-order secular dynamics to the SDS and by considering additional perturbations exerting on orbiting objects. The Deprit-Lie transformation method is applied to define the SDS for this expanded system since it provides a systematic way to compute the higher-order averaged dynamics, as well as to include additional perturbations. In this chapter, we define the SDS includes the second-order, i.e., $\mathcal{O}(\epsilon^2)$, secular dynamics, called the expanded SDS, through the Deprit-Lie transformation method. The expanded SDS considers multiple perturbations, such as J_2 gravity field harmonics, a gravitational attraction due to the moon, and a direct Solar Radiation Pressure (SRP). The ephemerides of the Sun and moon are calculated from the JPL ephemeris file (DE405) from January 19, 2008 00:00:00 UCT to February 2, 2008, 23:59:59 UCT (15 days). In particular, the assumption considered in the averaged LPEs, i.e., a planar motion, is released by introducing a distance angle. The cannonball model with the two different area-to-mass ratios is realized to describe a disturbance due to the SRP.

The outline of this chapter is as follows. Each Hamiltonian of the perturbations is presented, and then is grouped with respect to the magnitude of the small parameter, J_2. In order to magnify effects of the third-body attraction and a SRP, an object on the Medium Earth Orbit (MEO) is

considered. In particular, we propagate uncertainty of low area-to-mass ratio and high area-to-mass ratio (HAMR) objects with the expanded SDS. Then, a new initial offset correction method is suggested for the expanded SDS based on the property of the Deprit-Lie transformation. Investigation of the accuracy and the computational enhancement are also carried out with the Monte Carlo simulations. Finally, the accuracy of the propagated uncertainty with the expanded SDS are verified throughout the statistical approaches.

6.1 Simplified Dynamical System from the Deprit-Lie Transformation

For any given deterministic Hamiltonian, we can systematically derive the analytic solutions up to any desired order through the Deprit-Lie transformation method. The analytic solutions can be presented as

$$\mathbf{X}(t) = \mathbf{X}_{\text{secular}}(\overline{\mathbf{X}}_0,\, t) + \mathbf{X}_{\text{LP}}(\mathbf{X}_{\text{secular}}) + \mathbf{X}_{\text{SP}}(\mathbf{X}_{\text{secular}}), \tag{6.1}$$

where $\mathbf{X}_{\text{secular}}$, $\mathbf{X}_{\text{LP}}$, and $\mathbf{X}_{\text{SP}}$ represent the analytic solution for the secular variations, long-period variations, and short-period variations. Note that the solution for the secular variations is the only time-dependent function. The others are defined with respect to the solution of the secular variations; thus, the both periodic variations are varied about the mean trajectory.

By definition, the SDS is simply defined from Equation (6.1) by considering only first two terms on the right-hand side; thus

$$\mathbf{X}(t) = \mathbf{X}_{\text{secular}}(\overline{\mathbf{X}}_0,\, t) + \mathbf{X}_{\text{LP}}(\mathbf{X}_{\text{secular}}), \tag{6.2}$$

which is also called as the semi-analytic solutions. In a practice implementation, the semi-analytic solutions, i.e., SDS, is obtained by performing only the first two steps in Figure 4.2.

6.2 Expansion of the Dynamical System through the Transformation

For the sake of testing the expanded SDS, we consider the non-Keplerian motion under multiple perturbations: J_2 gravity field harmonics, the gravitational attraction due to the moon,

and the SRP. Since the motions of the sun and the moon make the Hamiltonian time-variant, the extended variables has to be considered for applying the Deprit-Lie transformation method, that is

$$(l,\, g,\, h,\, L,\, G,\, H) \;\rightarrow\; \left(l,\, g,\, h,\, k_{\leftmoon},\, k_{\odot},\, L,\, G,\, H,\, H_{\leftmoon},\, H_{\odot}\right). \tag{6.3}$$

The Delaunay variables are introduced for the canonical transformation since this set of variables are canonical, i.e., satisfies Equation (2.24). The original definition of the Delaunay variables are

$$\begin{aligned} l &= M, \qquad L = \sqrt{\mu a}, \\ g &= \omega, \qquad G = L\sqrt{1-e^2}, \\ h &= \Omega, \qquad H = G\cos I, \end{aligned} \tag{6.4}$$

where a, e, I, Ω, ω, and M represent a semi-major axis, eccentricity, inclination, longitude of ascending node, argument of periapsis, and the mean anomaly, i.e., the classical orbital elements. The extended angular variables, $k_{\leftmoon}$ and $k_{\odot}$, represent the mean longitude of the moon and that of the Sun: these variables are

$$\begin{aligned} k_{\leftmoon} &= \nu_{\leftmoon} \cdot t + \mathcal{C}_{\leftmoon}, \\ k_{\odot} &= \nu_{\odot} \cdot t + \mathcal{C}_{\odot}, \end{aligned} \tag{6.5}$$

where $\nu_{\leftmoon}$ and $\nu_{\odot}$ are the mean motion of the moon and the Sun, respectively. The conjugate momenta corresponding to each angular variable are $H_{\leftmoon}$ and $H_{\odot}$. The Hamiltonians corresponding to the extended variables can be defined by Equation (2.40) as follows:

$$\begin{aligned} \mathcal{H}_{\leftmoon} &= -\nu_{\leftmoon}\, H_{\leftmoon}, \\ \mathcal{H}_{\odot} &= -\nu_{\odot} H_{\odot}. \end{aligned} \tag{6.6}$$

Then, the Hamiltonians for each perturbation have to be grouped with respect to their magnitudes. We use the mean motion of the moon, $\nu_{\leftmoon}$, as the small parameter in order to define the Hamiltonian of the non-Keplerian motion.

$$\mathcal{H} = \sum_{n=0}^{4} \frac{\epsilon^n}{n!}\mathcal{H}_n = \mathcal{H}_0 + \frac{\nu_{\leftmoon}}{1!}\mathcal{H}_1 + \frac{\nu_{\leftmoon}^2}{2!}\mathcal{H}_2 + \frac{\nu_{\leftmoon}^3}{3!}\mathcal{H}_3 + \frac{\nu_{\leftmoon}^4}{4!}\mathcal{H}_4. \tag{6.7}$$

Each Hamiltonian in Equation (6.7) corresponds to the perturbing terms included in the non-Keplerian motion as given below.

$$\begin{aligned}
&\mathcal{O}(\epsilon^0):\ \mathcal{H}_0 = \mathcal{H}_k = -\frac{\mu}{2a},\\
&\mathcal{O}(\epsilon^1):\ \mathcal{H}_1 = \frac{1}{\nu_{\mathbb{C}}}\mathcal{H}_{\mathbb{C}}\ ,\\
&\mathcal{O}(\epsilon^2):\ \mathcal{H}_2 = \frac{2!}{\nu_{\mathbb{C}}^2}\left(\mathcal{H}_o + \mathcal{H}_{3b} + \mathcal{H}_{\odot}\right),\\
&\mathcal{O}(\epsilon^3):\ \mathcal{H}_3 = 0,\\
&\mathcal{O}(\epsilon^4):\ \mathcal{H}_4 = \frac{4!}{\nu_{\mathbb{C}}^4}\mathcal{H}_s,
\end{aligned} \tag{6.8}$$

where $\mathcal{H}_k$, $\mathcal{H}_o$, $\mathcal{H}_{3b}$, and $\mathcal{H}_s$ indicate the Hamiltonians for the Keplerian motion, J_2 gravity field harmonics, gravitational attraction due to the moon, and SRP. A detailed description about the Hamiltonian for each perturbation is presented here.

6.2.1 Keplerian Motion with J_2 Gravity Field Harmonics

We consider the Earth as a point mass including the effect of J_2 gravity field harmonics, then the disturbing function can be written in the form:

$$\mathcal{U} = -\frac{\mu}{2a} + \frac{\mu}{r_1}\sum_{n=2} \mathrm{J}_n \left(\frac{\alpha}{r_1}\right)^n \mathrm{P}_n(\sin\delta), \tag{6.9}$$

where μ, r_1, α, δ, and $\mathrm{P}_n(x)$ denote the gravitational parameter of the Earth, radial distance of the orbiting body, earth radius, declination of the satellite, and the Legendre polynomial [72]. By using an expression by Brouwer [9], $\sin\delta$ is defined in terms of the orbital elements.

$$\sin\delta = \sin i \sin(g+f)$$

In the verification of the SDS, we include only the second-order zonal harmonics; thus, the Hamiltonians for the Keplerian motion and J_2 gravity field harmonics perturbation can be defined by

$$\begin{aligned}
\mathcal{H}_k &= -\frac{\mu}{2a},\\
\mathcal{H}_o &= \frac{1}{2}\frac{\mu}{r_1}\left(\frac{\alpha}{r_1}\right)^2 \mathrm{J}_2\left[\frac{3}{2}s^2 - \frac{3}{2}s^2\cos(2f+2g) - 1\right].
\end{aligned} \tag{6.10}$$

6.2.2 Gravitational Attraction due to the Moon

For the sake of releasing the assumption applied in Chapter 5, the disturbance due to a perturbing body is revisited based on a spatial distribution depicted in Figure 6.1. A gravitational

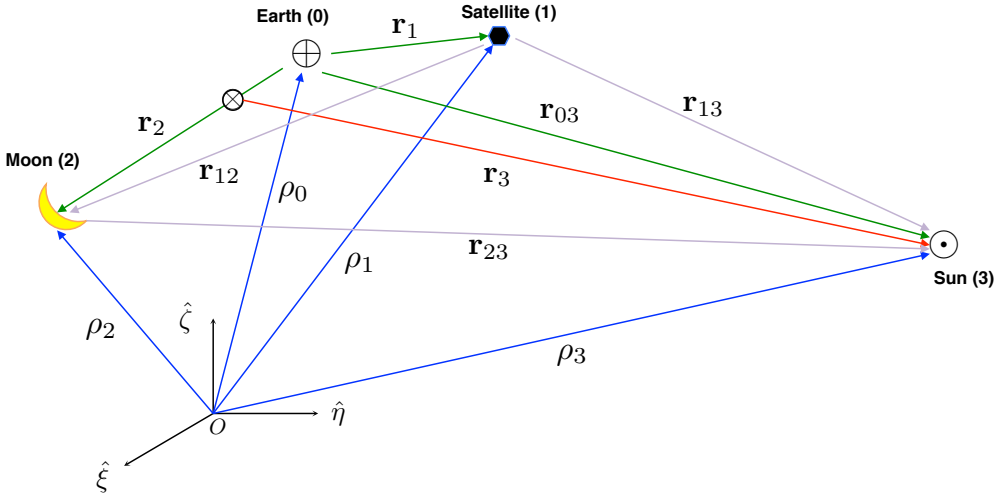

Figure 6.1: Relative positions of the Earth, satellite, moon, and Sun: the inertial coordinates frame is expressed in unit vectors ($\hat{\xi}$, $\hat{\eta}$, $\hat{\zeta}$) and $\otimes$ indicates the barycenter between the Earth and moon.

potential due to N objects is simply defined in Equation (6.11) in terms of the relative position vector [67].

$$\mathcal{U}_{3b} = \frac{1}{2}\sum_{i=0}^{N}\sum_{\substack{j=0 \\ j\neq i}}^{N}\frac{G\,m_i m_j}{|\boldsymbol{r}_{ij}|}, \tag{6.11}$$

where G, m_i, and $\boldsymbol{r}_{ij}$ represent the universal gravitational constant, mass of i-th body, and a relative position vector between i and j bodies, respectively. By assuming $r_1 \ll r_{03}$, Equation (6.11) can be rewritten in a form of polynomial series expansion [72], and then we truncate terms higher than the second-order. As a result of this procedure, the Hamiltonian for the moon's attraction becomes as follows:

$$\mathcal{U}_{3b} = \frac{\mu_2 r_1^2}{2r_2^3}(3\cos^2\theta_{12} - 1), \tag{6.12}$$

where μ_2 and μ_3 represent the gravitational parameters of the moon and the Sun, respectively. A more detailed description for rewriting Equation (6.11) to (6.12) can be found in [67]. An angle θ_{12} in Equation (6.12) is the included angle between the position vectors $\boldsymbol{r}_1$ and $\boldsymbol{r}_2$, called an angular

distance. Figure 6.2 shows a geometric relations between relative vectors.

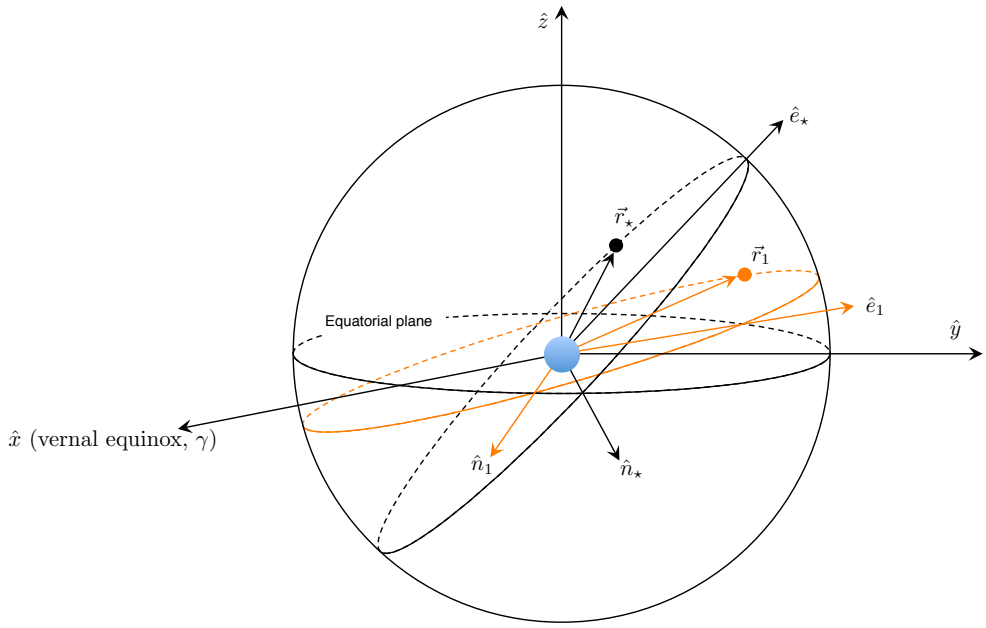

Figure 6.2: Geometric relation between two orbiting bodies with respect to a central body: direction cosines for defining the potential due to perturbing bodies and SRP are derived from this geometry.

The angular distance θ_{1m} can be obtained by a dot product as

$$\cos\theta_{1m} = \frac{\boldsymbol{r}_1 \cdot \boldsymbol{r}_m}{r_1\, r_m} = \hat{\boldsymbol{r}}_1 \cdot \hat{\boldsymbol{r}}_m, \tag{6.13}$$

where θ_{1m} denotes the angular distance between the position vectors of the satellite and m-th perturbing body. The next step is to express Equation (6.13) in terms of the extended variables presented in Equation (6.3). This conversion can be carried out by rotations based on Figure 6.2,

$$\hat{\boldsymbol{r}}_i(a,\, e,\, I,\, \Omega\,\omega,\, M) = \mathfrak{R}_3(-\Omega)\mathfrak{R}_1(-I)\mathfrak{R}_3(-\omega - M) \begin{pmatrix} 1 \\ 0 \\ 0 \end{pmatrix}, \tag{6.14}$$

The classical orbital elements, (Ω, ω, M), can be rewritten with the Delaunay variables, (h, g, l). As a result, the unit position vectors for the satellite and m-th body are

$$\begin{aligned}\hat{\boldsymbol{r}}_1 &= \begin{pmatrix} \cos h_1 \cos(f_1+g_1) - \cos I_1 \sin h_1 \sin(f_1+g_1) \\ \cos I_1 \cos h_1 \sin(f_1+g_1) + \sin h_1 \cos(f_1+g_1) \\ \sin I_1 \sin(f_1+g_1) \end{pmatrix} \\ \hat{\boldsymbol{r}}_m &= \begin{pmatrix} \cos h_m \cos u_m - \cos I_m \sin h_m \sin u_m \\ \cos I_m \cos h_m \sin u_m + \sin h_m \cos u_m \\ \sin I_m \sin u_m \end{pmatrix},\end{aligned} \tag{6.15}$$

where $u_m = f_m + g_m$ represents the mean longitude. Finally, by substituting Equation (6.15) into (6.13), we can rewrite Equation (6.13) in terms of the Delaunay variables as

$$\cos\theta_{1m} = \mathrm{T}_{c,m}\cos f_1 + \mathrm{T}_{s,m}\sin f_1, \tag{6.16}$$

where

$$\begin{aligned}\mathrm{T}_{c,m} =& \frac{1}{4}\{(c_1+1)(c_m+1)\cos(g+h-h_m-u_m) + (c_1-1)(c_m-1)\cos(g-h+h_m-u_m) \\ & -(c_1+1)(c_m-1)\cos(g+h-h_m+u_m) - (c_1-1)(c_m+1)\cos(g-h+h_m+u_m)\} \\ & + s\, s_m \sin g \sin(u_m) \\ \mathrm{T}_{s,m} =& \frac{1}{4}\{(c_1-1)(c_m+1)\sin(g-h+h_m+u_m) - (c_1+1)(c_m+1)\sin(g+h-h_m-u_m) \\ & -(c_1-1)(c_m-1)\sin(g-h+h_m-u_m) + (c_1+1)(c_m-1)\sin(g+h-h_m+u_m)\} \\ & + s\, s_m \cos g \sin(u_m).\end{aligned}$$

By Equations (6.16), a potential for the gravitational attraction in Equation (6.12) can be redefined in terms of the Delaunay variables. Since the potential is identical to the Hamiltonian, we can define the Hamiltonian for the gravitational attraction as

$$\mathcal{H}_{\mathbb{C}} = \mathcal{U}_{3b} = \frac{\mu_2 r_1^2}{2r_2^3}\{3(\mathrm{T}_{c,2}\cos f_1 + \mathrm{T}_{s,2}\sin f_1)^2 - 1\}. \tag{6.17}$$

6.2.3 Solar Radiation Pressure

The Hamiltonian due to the SRP perturbation of the cannonball model [32] is simply defined

$$\mathcal{H}_s = -\beta \frac{r}{r_{\odot,sat}^2} \cos\theta_{13}, \tag{6.18}$$

where β and θ_{13} represent the solar perturbation strength and the angular distance between the satellite and the Sun. The solar perturbation strength is defined by

$$\beta = (1+\rho)\frac{\mathrm{A}_{sat}}{m_{sat}}\mathrm{P}_\Phi,$$

where the solar constant, P_Φ, is approximately $1 \times 10^8\, kg\, km^3/s^2/m^2$ [72]. As similar to the gravitational attraction, this Hamiltonian is also rewritten by Equation (6.16) as follows:

$$\mathcal{H}_s = -\beta \frac{r_1}{r_{13}^2} \left(\mathrm{T}_{c,3} \cos f_1 + \mathrm{T}_{s,3} \sin f_1\right). \tag{6.19}$$

6.3 Analytic Algorithm for the Offset Correction

The Deprit-Lie transformation method provides a systematic way to recover or extract the short-period variations from the full dynamical system as discussed in Section 4.1.3. A new analytic initial offset correction algorithm is proposed based on this property of the transformation method. From the homological equations, the generating functions are obtained sequentially. In order to convert the initial conditions from the osculating to the mean spaces, we can use the inverse transformation given in Equation (4.17), which is

$$\boldsymbol{y} = \boldsymbol{x}_0^{(0)} + \sum_{n\geq 1} \frac{\epsilon^n}{n!} \left[-\boldsymbol{y}_0^{(n)} + \sum_{1\leq j\leq n-1} C_j^n\, G_j\, \boldsymbol{y}_0^{(n-j)} \right], \quad (n \geq 1)$$

$$\boldsymbol{Y} = \boldsymbol{X}_0^{(0)} + \sum_{n\geq 1} \frac{\epsilon^n}{n!} \left[-\boldsymbol{Y}_0^{(n)} + \sum_{1\leq j\leq n-1} C_j^n\, G_j\, \boldsymbol{Y}_0^{(n-j)} \right], \quad (n \geq 1)$$

where $(\boldsymbol{x}_0,\, \boldsymbol{X}_0)$ represents a given initial conditions in the osculating space. The second terms on the right-hand side of the above equations stand for the corrections in order to convert the given initial condition from the osculating to the mean spaces precisely. It is worth noting again that these corrections are very sensitive to the order of semi-analytic solutions. Because an additional

order of solutions shifts the mean orbit, even though even though a magnitude is tiny; thus, one has to calculate the generating function up to necessary orders. In particular, the SDS is defined by eliminating the short-period variations; thus, the given original Hamiltonian is transformed only once. Therefore, we can define the analytic conversion algorithm by considering Equation (4.23) only.

6.4 Verification of the Expanded Simplified Dynamical System

We focus on verifying the expanded SDS with two aspects: 1) if the SDS is applicable to propagate uncertainty with additional perturbations, and 2) if the analytic initial correction algorithm works properly. The SDS is tested with two scenarios with the different SRP effect in

Table 6.1: Initial Keplerian elements and parameters for the test orbits

Element	MEO	MEO (HAMR)
Semimajor axis, a, (km)	26578.140	26578.140
Eccentricity, e	0.01	0.01
Inclination, i, (deg)	55.0	55.0
Longitude of the ascending node, Ω, (deg)	45.0	45.0
Argument of periapsis, ω, (deg)	60.0	60.0
Mean anomaly, ν, (deg)	105.0	105.0
Reflectivity, ρ	0.2	0.2
A/m, (m^2/kg)	2.0	20.0

MEO; one has a small area-to-mass ratio, 2.0 m^2/kg, and the other is assumed as a high area-to-mass ratio (HAMR) object with 20 m^2/kg as the area-to-mass ratio. Table 6.1 shows an initial state for the centered object in the orbital elements space. Through the tests, we verify the capabilities of the SDS when propagating the state uncertainty with the multiple perturbations, as well as show the analytic correction algorithm plays the expected role properly. The verification of the SDS is performed through Monte Carlo simulations. For the simulation, normally distributed 10,000 samples are generated within 3-σ region. An 1-σ Gaussian error centered at the initial Keplerian elements of the MEO object is assumed with standard deviations of 20 km in the semi-major axis,

0.005 in eccentricity, and 0.01° in the inclination, longitude of ascending node, the argument of the pericenter, and the mean anomaly directions. The ephemerides of the Sun and moon have been obtained from the JPL ephemeris file (DE405) from January 19, 2008 00:00:00 UCT to February 2, 2008, 23:59:59 UCT (15 days), which covers the period studied. We note that the effect due

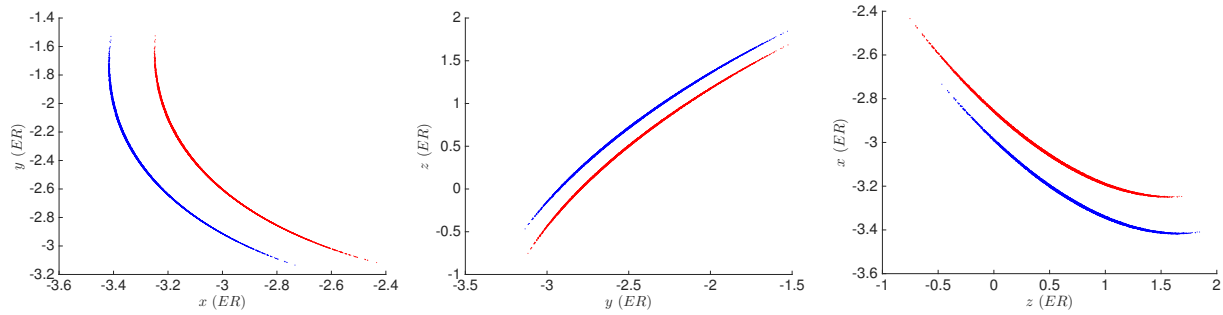

(a) x-y phase-space (b) y-z phase-space (c) z-x phase-space

Figure 6.3: Propagated uncertainty due to different area-to-mass ratios (after 15 days): the first case, $A/m = 2.0$, is plotted with blue circles, and the other, $A/m = 20$, is plotted with red crosses.

to the difference in the area-to-mass ratio in the evolution of uncertainty. Figure 6.3 shows the propagated uncertainty with the given initial conditions after 15 days. As seen in the figure, both distributions have an almost identical shape, but there exists an offset on every phase-space. The standard deviation of the offset between the distributions is

$$\sigma_{\text{offset}} = \big(165.872\,km,\ 27.642\,km,\ 155.761\,km,\ 0.0302\,km/s,\ 0.0463\,km/s,\ 0.0192\,km/s\big).$$

6.4.1 Result I: The Accuracy of the Expanded SDS for MEO

We present results from the first scenario, i.e., $A/m = 2.0$ m^2/kg, and verify the accuracy of the propagated uncertainty through the statistical approaches.

6.4.1.1 Moments Comparison

As the first statistical verification, we compare the central and standardized moments of the PDFs quantitatively and graphically : 1) Table 6.2 presents quantities of the moments of the PDFs and relative errors, and 2) Figure 6.4 shows the distributions on the δy-$\delta \dot{y}$ phase-space

and the histograms of the PDFs belonging to each direction for a graphical interpretation: the density distribution on the $\delta\dot{y}$ (ER/s) axis (top-left), on the δy (ER) axis (bottom-right), and the distributions of the samples on the δy-$\delta\dot{y}$ phase space (top-right). As seen in the density distribution on δy axis (bottom-right) in Figure 6.4, the distribution is strongly skewed. This is apparently described with the third-order standardized moment, i.e., the skewness, on the δy direction in Table 6.2; the negative skewness describes that the PDF has a long left tail. Every value in the table is normalized with respect to Earth radius. Results on other phase-spaces are summarized in the Appendix. Figure 6.5 shows time-histories of the skewness and kurtosis calculated by the SDS (blue squares) and the full dynamical system (red triangles) within one orbital period in the ECI coordinate frame. From the time-histories, we conclude that the short-period variations are negligible in an evolution of uncertainty within one orbital period.

Table 6.2: Higher-order central moments and relative errors after 15 days with A/m=2.0(m^2/kg)

	1st order		2nd order		3rd order		4th order	
	μ_1	Δ (%)	μ_2	Δ (%)	$\overline{\mu}_3$	Δ (%)	$\overline{\mu}_4$	Δ (%)
δx	-0.01672	0.04432	0.1163	0.01223	-0.2000	0.05017	2.4143	0.2088e-2
δy	-0.02759	0.3290e-2	0.4950e-2	0.1617	-1.4515	0.06098	4.7376	0.01161
δz	-0.01157	0.06028	0.1632	0.01162	-0.1210	0.06424	2.3863	0.1063e-2
$\delta\dot{x}$	3.2538e-06	0.05319	1.6593e-09	0.05021	0.3314	0.07711	2.4863	0.7935e-2
$\delta\dot{y}$	-5.5847e-07	0.3615	3.8851e-09	0.02311	-0.03463	0.3972	2.3724	0.6109e-3
$\delta\dot{z}$	-3.8145e-06	0.01414	5.5176e-10	0.1408	-0.6566	0.08328	2.8402	0.02922

6.4.1.2 Statistical Energy Test

The statistical energy test is applied to compare the PDFs at every orbital period and those within one orbital period. For both comparisons, we assume that the significance level, α, for the statistical energy test is set as 5%. Figure 6.6 plots a time-history of the p-value (blue circled line) with respect to the significance level (red dotted line). As a result of the tests, we can conclude that the propagated uncertainty by the SDS is identical to the truth with a 95% confidence level in both comparisons. In particular, the result shown in Figure 6.6(b) more robustly supports the conclusion that the short-period variations are negligible.

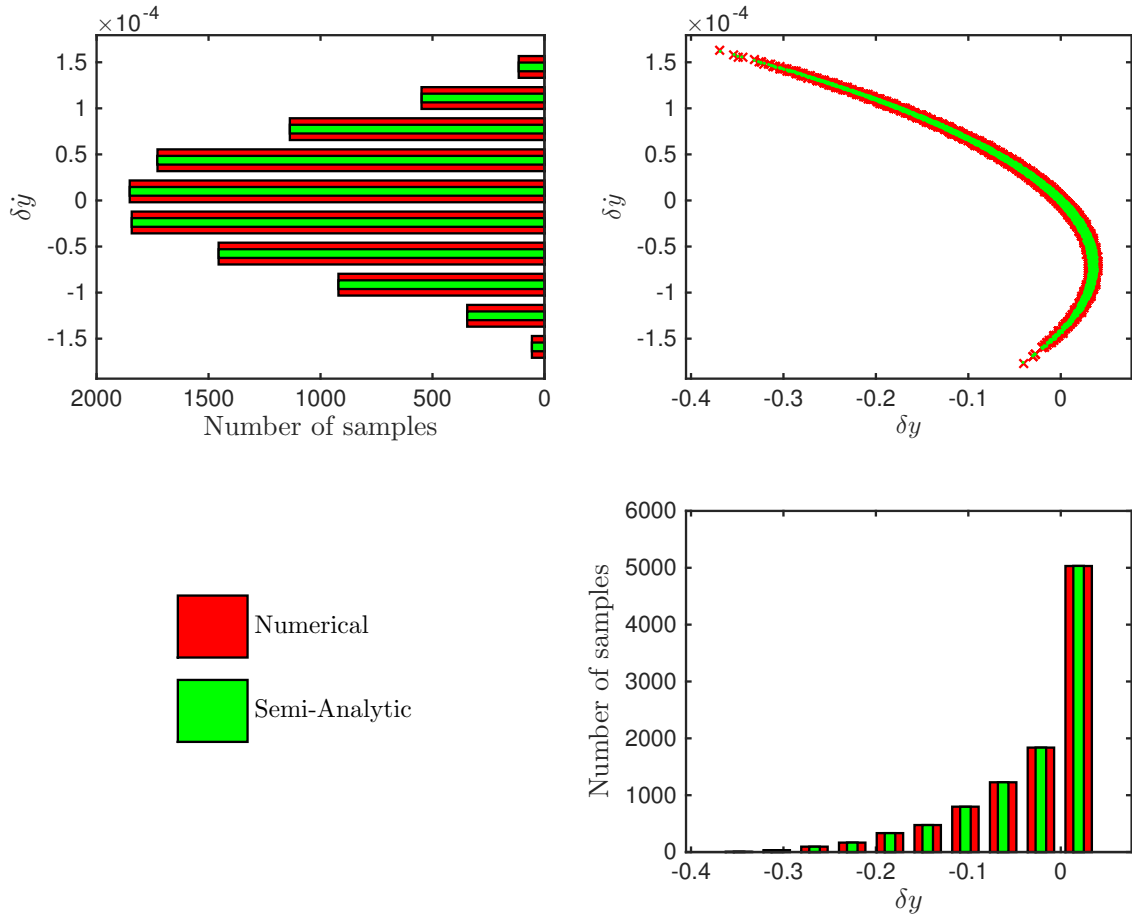

Figure 6.4: Sample point distribution on the $\delta\dot{x}$ (ER/s, top-left) and δx (ER, bottom-right) direction, and its density distribution after 30-orbital periods of propagation in MEO.

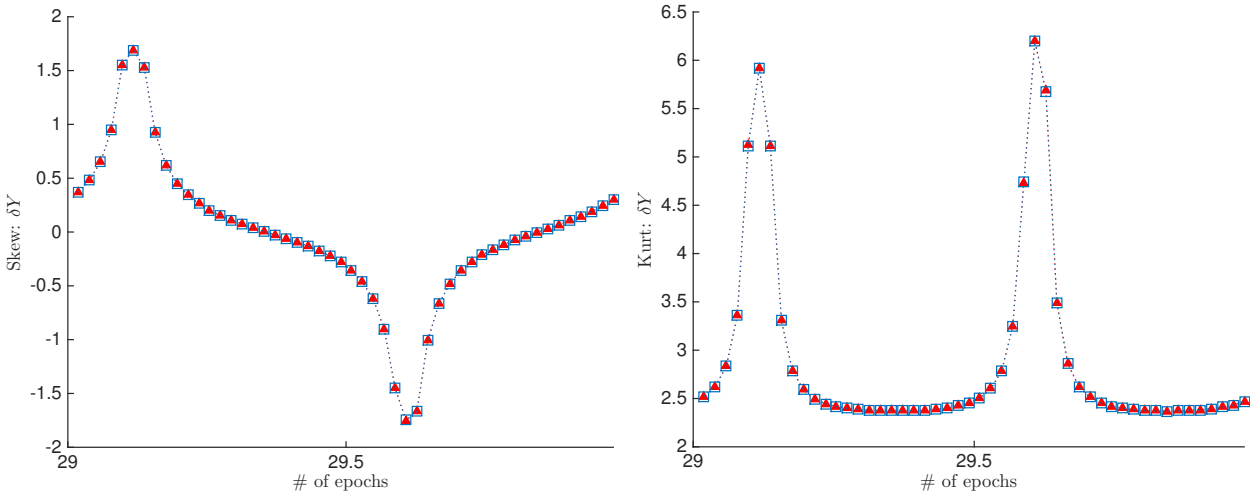

(a) Skewness on δy direction

(b) Kurtosis on δy direction

Figure 6.5: Time history of the skewness and kurtosis in the δy direction within one period plotted over time.

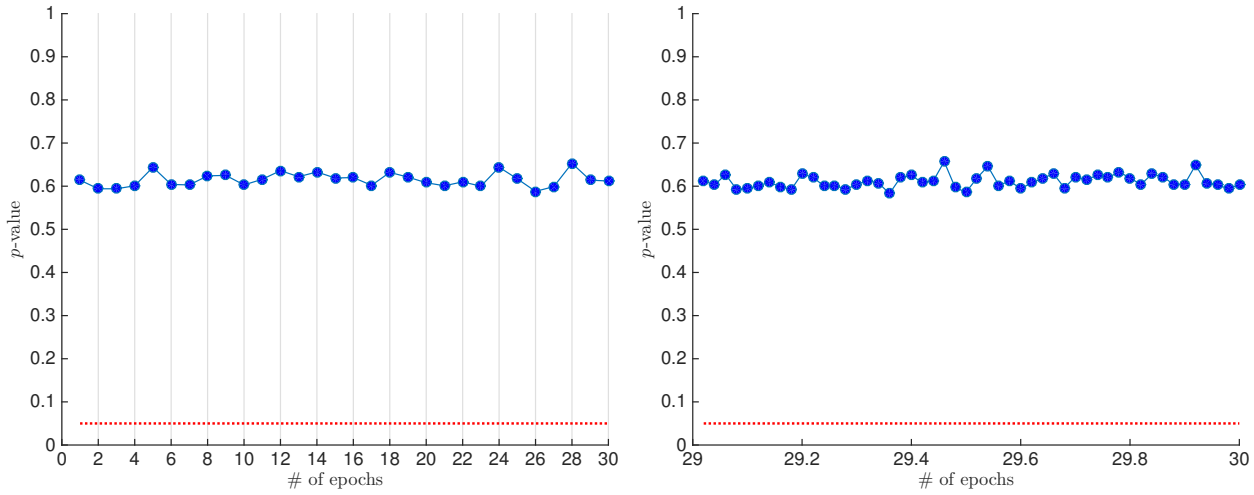

(a) Time history of the p-value every orbital period

(b) Time history of the p-value within the one period

Figure 6.6: Time history of the p-value (solid line) with the SDS and the designated significance level, α (dotted line).

6.4.1.3 Normalized Standard Deviation

We plot a time history of the normalized STD in Figure 6.7. Figure 6.7(a) shows the standard deviation from the full dynamical system (red squares) and that of errors in the propagated states, i.e., the STD of $(\boldsymbol{X}_{SDS} - \boldsymbol{X}_{Num})$, in time. As seen in the figure, the standard deviation increases in time; thus, it is not suitable to check the consistency of the SDS with it. On the other hand, the normalized STD, shown in Figure 6.7(b), varies less than 0.1% in time. Therefore, the SDS can propagate the initial distribution consistently in time.

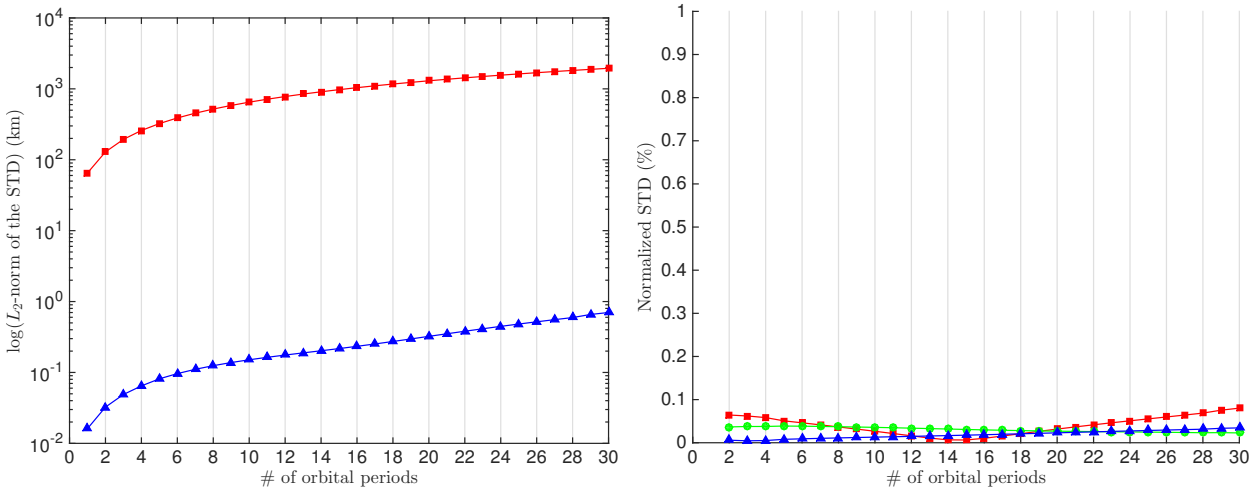

(a) Time history of L_2-norm between the STD

(b) Time history of normalized STD on each direction

Figure 6.7: Time history of L_2-norm and normalized STD for 15 days ($A/m = 2.0$).

6.4.2 Result II: The Accuracy of the Expanded SDS for the HAMR Objects

In this simulation, we assume a area-to-mass ratio as 20 m^2/kg, i.e., high area-to-mass ratio (HAMR) objects. As seen in Figure 6.3, the enlarged SRP effect makes difference in the propagated uncertainty with hundreds of kilometers in distance, but the propagated distributions of the samples have similar shapes.

6.4.2.1 Moments Comparison

As the same way to the first simulation, the results are compared quantitatively and graphically in Table 6.3 and Figure 6.8. The table shows that a maximum relative error in the first-order moment is about 2.5 %. As seen in Figure 6.8 (top-right), the propagated uncertainty on the δy-$\delta \dot{y}$ phase-space has a similar distribution to the previous test. The time-history of the skewness and

Table 6.3: Higher-order central moments and relative errors after 15 days with A/m=20.0(m^2/kg)

	1st order		2nd order		3rd order		4th order	
	μ_1	Δ (%)	μ_2	Δ (%)	$\overline{\mu}_3$	Δ (%)	$\overline{\mu}_4$	Δ (%)
δx	-0.01648	0.3290	0.1098	0.3915	-0.2033	0.5325	2.4195	0.02597
δy	-0.02594	0.1795	0.4680e-2	1.6879	-1.4096	0.8170	4.5914	0.8486
δz	-0.01016	0.9858	0.1546	0.01554	-0.1096	0.9636	2.3847	0.9780e-2
$\delta \dot{x}$	2.6840e-06	0.9742	1.6054e-09	0.4348	0.2791	1.1723	2.4521	0.08030
$\delta \dot{y}$	-8.3935e-07	2.4861	3.4399e-09	0.4614	-0.05675	2.8265	2.3796	0.01655
$\delta \dot{z}$	-3.5334e-06	0.1035	4.1710e-10	2.1652	-0.7022	0.9565	2.9232	0.3863

kurtosis on each axis is plotted in Figure 6.9: results from the SDS (blue squares) and from the full dynamical system (red triangles). As seen in the time-histories, even though the short-period variations are ignored, the propagated uncertainty with the SDS is describing the true distribution accurately.

6.4.2.2 Statistical Energy Test

Figure 6.10 presents the time-history of the p-value for the propagated HAMR objects. The significance level, α, is also assumed as 5 %; thus, we can conclude that the SDS propagates the uncertainty of the HAMR objects accurately with 95 % confidence level.

6.4.2.3 Normalized Standard Deviation

As seen in Figure 6.11, the normalized STD varies less than 0.6 % at most. From this result, we can conclude that consistency loss in mapping the uncertainty of the HAMR for 15 days is less than 1%. This result, however, motivates us to expand the analytic solution for SRP effect up to

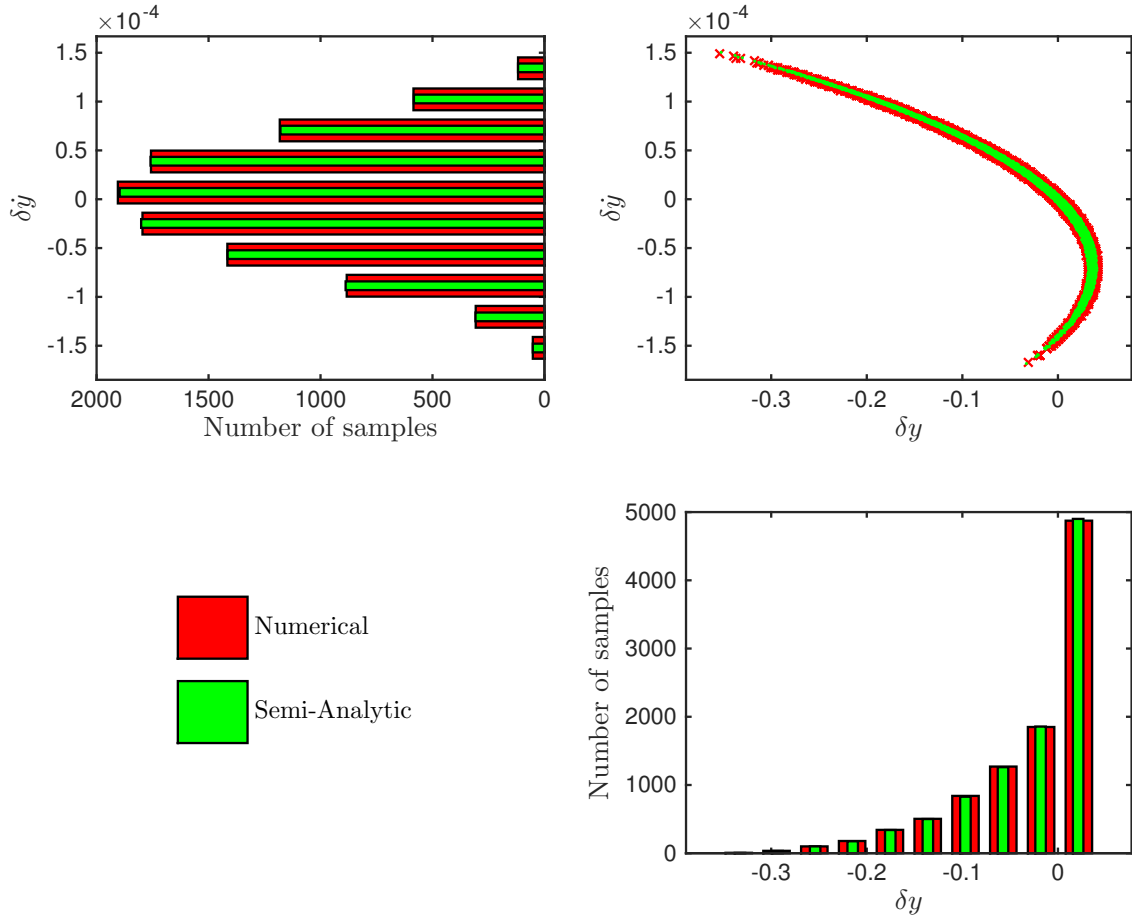

Figure 6.8: Sample point distribution on the $\delta\dot{x}$ (ER/s, top-left) and δx (ER, bottom-right) direction, and its density distribution after 30-orbital periods of propagation in MEO.

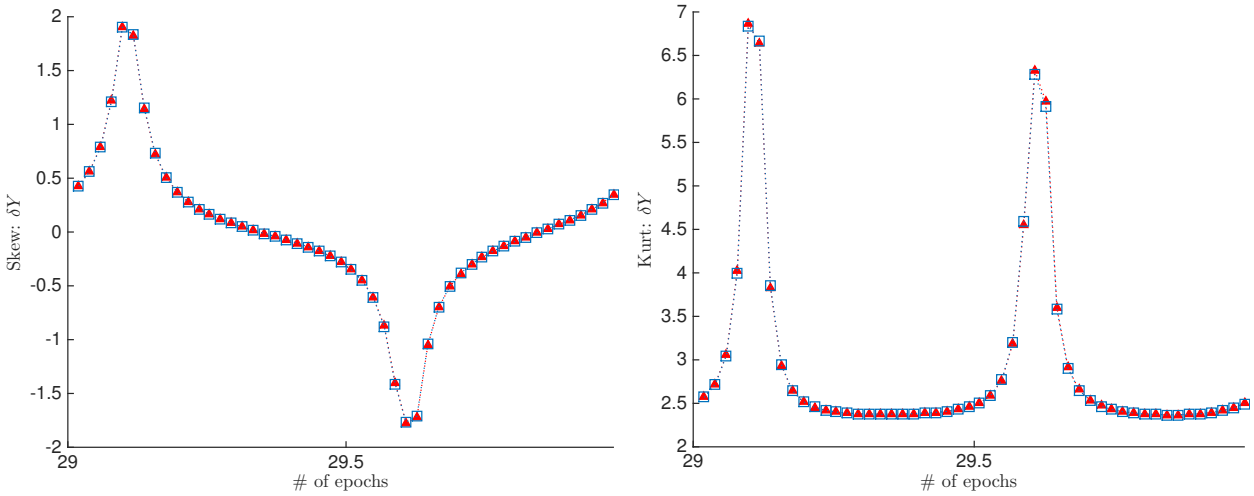

(a) Skewness on δy direction

(b) Kurtosis on δy direction

Figure 6.9: Time history of the skewness and kurtosis in the δy direction within one period plotted over time.

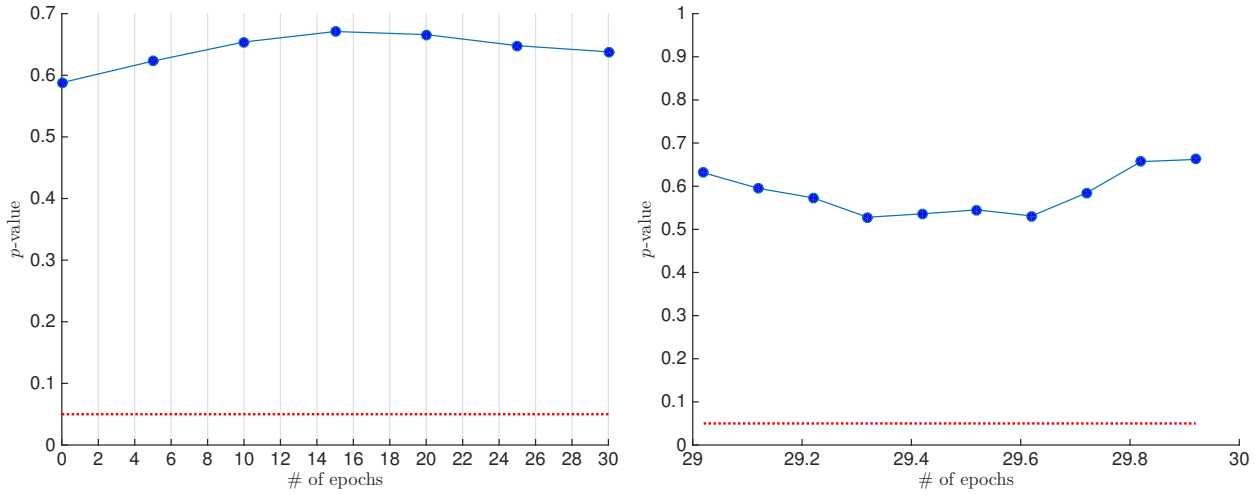

(a) Time history of the p-value every orbital period

(b) Time history of the p-value within the one period

Figure 6.10: Time history of the p-value (solid line) with the SDS and the designated significance level, α (dotted line).

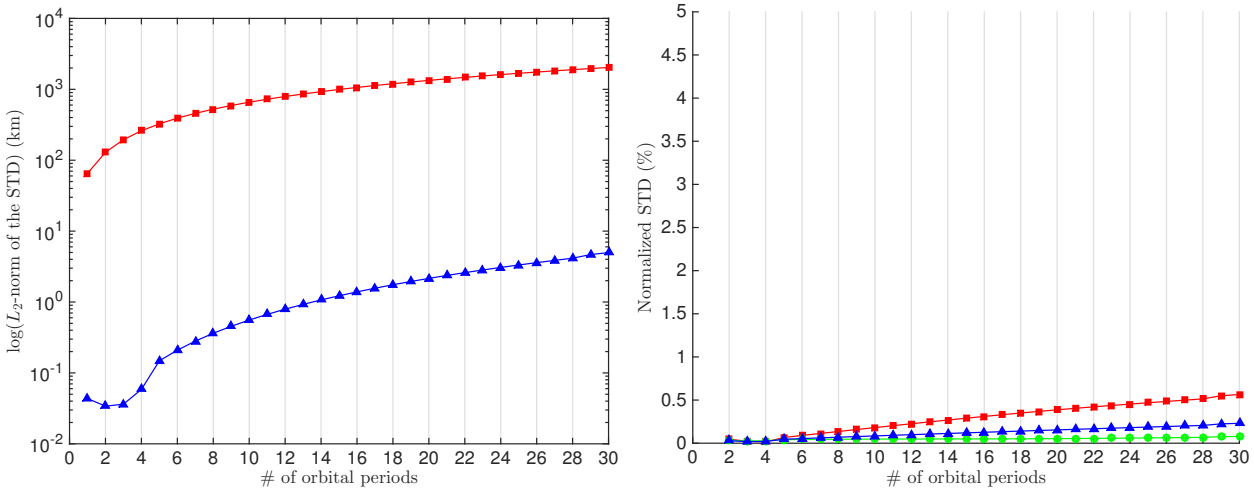

(a) Time history of L_2-norm between the STD

(b) Time history of normalized STD on each direction

Figure 6.11: Time history of L_2-norm and normalized STD for 15 days ($A/m = 20.0$).

second- or higher-order since the result shows that the normalized STD linearly increases.

6.5 Performance Improvement of the Expanded SDS

All computations for discussed test results are performed on a laptop, 2.8 GHz Intel® Core i7 and 4 GB 1067 MHz DDR3. Total elapsed times from the full dynamical system and the SDS are about 1.5360e6 seconds and about 3.3431e4 seconds, respectively; thus, total elapsed time shows remarkable enhancement, about 46 times faster. Figure 6.12 shows the elapsed time to propagate the initial uncertainty from one to 30 orbital periods. The number of dynamical equation function calls per points is about 2.2216e4 times for the full dynamical system and 300 times for the SDS. One of the aspects we are focusing on is the analytic initial offset correction algorithm. So far, we

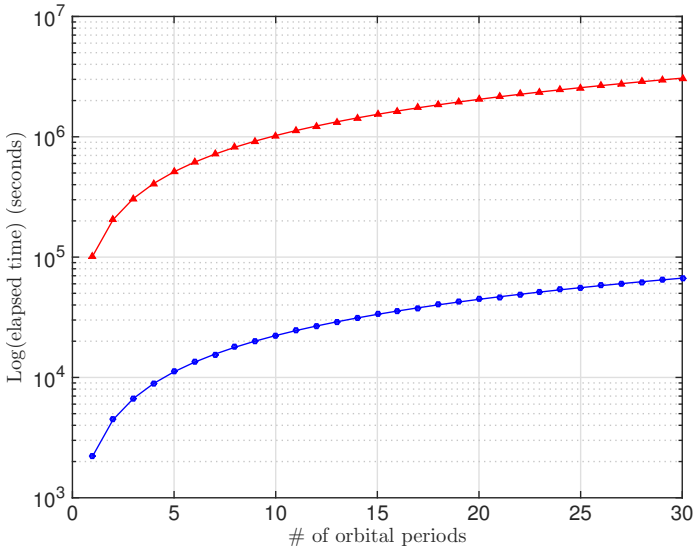

Figure 6.12: Elapsed time for propagating the samples from 1 to 30-orbital periods with the full dynamical system(red triangles) and the SDS (blue circles)

verify the accuracy of the SDS, which means that the new correction algorithm provides an accurate mean orbit. In the computational efficiency point of view, this new algorithm has an advantage over the aforementioned methods since it computes the corrections with no integrations.

6.6 Conclusion

The property of the Deprit-Lie transformation method [19] inspires us to expand the Simplified Dynamical System (SDS) and to replace the initial offset correction algorithm with a fully analytic one. The expanded SDS, based on the second-order secular (averaged) dynamics, considers multiple perturbations, such as J_2 gravity field harmonics, gravitational attraction of the moon, and a direct Solar Radiation Pressure (SRP). And the analytic initial correction algorithm is implemented by using the generating functions. Thus, the main goal of this chapter is to verify the capability of the expanded SDS in two aspects, i.e., accuracy and efficiency.

Throughout this chapter, we describe how the Deprit-Lie transformation method is applied to define the expanded SDS and the analytic initial offset correction algorithm; and we verify how accurately and efficiently the expanded SDS propagates the initial uncertainty. The three statistical methods show that the SDS is, with even better computational efficiency, capable of propagating uncertainty while maintaining accuracy, even though an evolution of uncertainty is disturbed by multiple perturbations. In particular, an evolution of uncertainty of high area-to-mass ratio (HAMR) objects is tested since these objects are one of the most interesting targets in a field of the Space Situational Awareness (SSA). Through this test, we also verify that the expanded SDS is applicable to map uncertainty for this special cases. One interesting result of this test is that the propagated uncertainty has a similar shape, Figures 6.5 and 6.9, to that of the objects with low area-to-mass ratio, even though their absolute spatial distributions have a few hundreds kilometers offset in distance shown in Figure 6.3.

Lastly, we define the new initial offset correction algorithm based on the generating function and show that it successfully replaces with the previous ones. As seen in Equation (6.3), the analytic initial offset correction algorithm calculates the corrections straightforwardly; thus, this may be another advantage of an application of the Deprit-Lie transformation method.

Chapter 7

Development and Application of the Hybrid Method

As we have discussed so far, the efficient and accurate representation of uncertainty for orbiting objects under nonlinear dynamics is a topic of great interest for space situational awareness. Throughout Chapter 5 and 6, we show that the Simplified Dynamical System (SDS) is capable of mapping uncertainty efficiently while maintaining the accuracy. In this chapter, we propose a new method, called a hybrid method, to map PDFs directly to any desired epochs without applying Monte Carlo simulations. This new method is defined by combining two ideas. First, we derive the second-order semi-analytic solutions based on a Deprit-Lie transformation to describe an orbiting motion under multiple perturbations. From the semi-analytic solutions, the SDS is defined by eliminating the short-period variation. Next, this SDS will be rewritten in a form of the State Transition Tensors (STTs), which can analytically map uncertainty while capturing the nonlinearity of higher-order dynamics. Verification of the method is performed statistically by comparing the moments and statistical energy test.

The hybrid method presented here is developed under multiple perturbations, including J_2 gravity field harmonics, a direct Solar Radiation Pressure (SRP), and gravitational attractions due to the Sun and moon. We generate a set of combinations with the second-order secular dynamics and the STT up to third-order to investigate differences in accuracy and processing time.

The outline of this chapter is as follows. A new Hamiltonian that includes an additional perturbation, i.e., Sun's attraction, is presented, which is more deliberate than that considered in Chapter 6. Then, we present detailed descriptions about a procedure to combine the SDS and

STTs. The hybrid method can be designed to have different levels of accuracy by adjusting the expansion level of the Deprit-Lie theory and the order of expansion in the STTs. Lastly, the hybrid method is verified by applying it to practical orbital problems. In order to increase the effects of the non-gravitational perturbations, medium earth orbit (MEO) and highly eccentric orbit (Molniya) are chosen as examples.

7.1 Hamiltonian Dynamics for Non-Keplerian Motion

The Hamiltonian is redefined by introducing the gravitational attraction due to the Sun. Similar to Chapter 6, the mean motion of the moon is used as the small parameter (i.e., $\epsilon = n_2$) to group the Hamiltonian in expandable form as

$$\mathcal{H} = \sum_{n=0}^{4} \frac{\epsilon^n}{n!} \mathcal{H}_n. \tag{7.1}$$

Each Hamiltonian in Equation (7.1) corresponds to the perturbing terms included in the non-Keplerian motion as given below.

$$\begin{aligned}
\mathcal{H}_0 &= \mathcal{H}_k = -\frac{\mu}{2a}, \\
\mathcal{H}_1 &= \mathcal{H}_{\leftmoon} \ , \\
\mathcal{H}_2 &= \mathcal{H}_o + \mathcal{F}_{1,\leftmoon} + \mathcal{F}_{\odot} + \mathcal{H}_{\odot}, \\
\mathcal{H}_3 &= 0, \\
\mathcal{H}_4 &= \mathcal{H}_s + \mathcal{F}_{2,\leftmoon} \ ,
\end{aligned} \tag{7.2}$$

where $\mathcal{H}_k$, $\mathcal{H}_o$, and $\mathcal{H}_s$ indicate the Hamiltonians for the Keplerian motion, J_2 gravity field harmonics, and SRP. Newly defined Hamiltonian $\mathcal{F}_{\odot}$ represents the gravitational attraction due to the Sun; and $\mathcal{F}_{1,\leftmoon}$ and $\mathcal{F}_{2,\leftmoon}$ represent the second and third order terms of the Legendre polynomial of the gravitational attractions due to the moon, respectively. Lastly, $\mathcal{H}_{\leftmoon}$ and $\mathcal{H}_{\odot}$ are conjugates of the extended variables for describing the motion of the Sun and moon [32, 70]. A detailed description about each Hamiltonian will be presented in this section.

From series expansion of Equation (6.11), the new Hamiltonians for describing the gravita-

tional attractions are simply defined as

$$\mathcal{U}_{3b} = \frac{\mu_2 r_1^2}{2r_2^3}(3\cos^2\theta_{12} - 1) + \frac{\mu_3 r_1^2}{2r_3^3}(3\cos^2\theta_{13} - 1) + \frac{\mu_2 r_1^3}{2r_2^4}\left(5\cos^3\theta_{12} - 3\cos\theta_{12}\right), \tag{7.3}$$

where μ_2 and μ_3 represent the gravitational parameters of the moon and the Sun, respectively. Replacing the trigonometric functions with Equation (6.16), then

$$\begin{aligned}\mathcal{U}_{3b} =& \frac{\mu_2 r_1^2}{2r_2^3}\{3(\mathrm{T}_{c,2}\cos f_1 + \mathrm{T}_{s,2}\sin f_1)^2 - 1\} + \frac{\mu_3 r_1^2}{2r_3^3}\{3(\mathrm{T}_{c,3}\cos f_1 + \mathrm{T}_{s,3}\sin f_1)^2 - 1\} \\ &+ \frac{\mu_2 r_1^3}{2r_2^4}\left\{5(\mathrm{T}_{c,2}\cos f_1 + \mathrm{T}_{s,2}\sin f_1)^3 - 3(\mathrm{T}_{c,2}\cos f_1 + \mathrm{T}_{s,2}\sin f_1)\right\}.\end{aligned} \tag{7.4}$$

Each term in the above equation can be defined the Hamiltonians $\mathcal{F}_{odot}$, $\mathcal{F}_{1,\mathbb{C}}$, and $\mathcal{F}_{2,\mathbb{C}}$, respectively, as follows:

$$\begin{aligned}\mathcal{F}_{\odot} &= \frac{\mu_3 r_1^2}{2r_3^3}\{3(\mathrm{T}_{c,3}\cos f_1 + \mathrm{T}_{s,3}\sin f_1)^2 - 1\}, \\ \mathcal{F}_{1,\mathbb{C}} &= \frac{\mu_2 r_1^2}{2r_2^3}\{3(\mathrm{T}_{c,2}\cos f_1 + \mathrm{T}_{s,2}\sin f_1)^2 - 1\}, \\ \mathcal{F}_{2,\mathbb{C}} &= \frac{\mu_2 r_1^3}{2r_2^4}\left\{5(\mathrm{T}_{c,2}\cos f_1 + \mathrm{T}_{s,2}\sin f_1)^3 - 3(\mathrm{T}_{c,2}\cos f_1 + \mathrm{T}_{s,2}\sin f_1)\right\}.\end{aligned} \tag{7.5}$$

As a result, the expanded form of Equation (7.2) is given below:

$$\begin{aligned}&\mathcal{O}(\epsilon^0):\ \mathcal{H}_0 = \mathcal{H}_k = -\frac{\mu}{2a}, \\ &\mathcal{O}(\epsilon^1):\ \mathcal{H}_1 = \frac{1}{\nu_{\mathbb{C}}}\mathcal{H}_{\mathbb{C}}\,, \\ &\mathcal{O}(\epsilon^2):\ \mathcal{H}_2 = \frac{2!}{\nu_{\mathbb{C}}^2}\left(\mathcal{H}_o + \mathcal{F}_{\odot} + \mathcal{F}_{1,\mathbb{C}} + \mathcal{H}_{\odot}\right), \\ &\mathcal{O}(\epsilon^3):\ \mathcal{H}_3 = 0, \\ &\mathcal{O}(\epsilon^4):\ \mathcal{H}_4 = \frac{4!}{\nu_{\mathbb{C}}^4}\left(\mathcal{H}_s + \mathcal{F}_{2,\mathbb{C}}\right).\end{aligned} \tag{7.6}$$

7.2 The Hybrid Method

7.2.1 Combination of the Two Concepts

In Chapters 5 and 6, the Monte Carlo simulations are applied to propagate uncertainty. A motivation of a hybrid method is to find a way to avoid using this computationally expensive

procedure. The salient idea of the hybrid method is a combination of advantages of the SDS and the STT. As described in Chapter 3, the STT is generated from an expanded dynamical system by taking higher-order terms to capture nonlinearity. Even though the SDS has lower nonlinearity, it is still nonlinear dynamical system. Thus, the combination consists of two steps: expanding the STT as a form of the Taylor series expansion, and then generating the STT by taking terms from the expanded SDS. Through this procedure, the hybrid method can have the advantages of each idea. In summary, Figure 7.1 presents the advantages of each idea and the hybrid method.

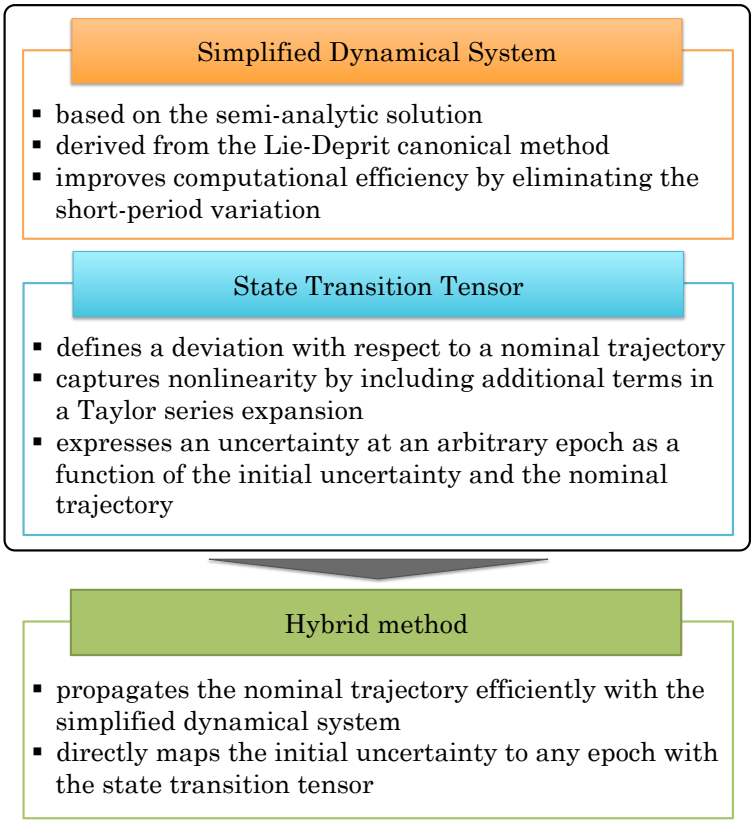

Figure 7.1: The combination of the advantages of the SDS and STT

The semi-analytic solutions are derived from Equation (7.6) through the Deprit-Lie transformation method. Suppose that the semi-analytic solutions (SDS), $\dot{\mathbf{X}}_{\text{sds}}$, is

$$\dot{\mathbf{X}}_{\text{sds}} = \left[\dot{l},\, \dot{g},\, \dot{h},\, \dot{k}_{\mathbb{C}} ,\, \dot{k}_{\odot},\, \dot{L},\, \dot{G},\, \dot{H},\, \dot{H}_{\mathbb{C}} ,\, \dot{H}_{\odot} \right]. \tag{7.7}$$

For the sake of deriving the LDT, Equation (7.7) can be rewritten as follows:

$$\begin{aligned}\boldsymbol{f} = \dot{\mathbf{X}}_{\text{sds}} &= \left[\, \dot{l},\, \dot{g},\, \dot{h},\, \dot{k}_{\text{☾}} ,\, \dot{k}_{\odot},\, \dot{L},\, \dot{G},\, \dot{H},\, \dot{H}_{\text{☾}} ,\, \dot{H}_{\odot} \,\right]^{\mathrm{T}} \\ &= \left[\, \frac{\partial \mathcal{K}}{\partial L}, \frac{\partial \mathcal{K}}{\partial G}, \frac{\partial \mathcal{K}}{\partial H}, \frac{\partial \mathcal{K}}{\partial H_{\text{☾}}}, \frac{\partial \mathcal{K}}{\partial H_{\odot}}, -\frac{\partial \mathcal{K}}{\partial l}, -\frac{\partial \mathcal{K}}{\partial g}, -\frac{\partial \mathcal{K}}{\partial h}, -\frac{\partial \mathcal{K}}{\partial k_{\text{☾}}}, -\frac{\partial \mathcal{K}}{\partial k_{\odot}} \,\right]^{\mathrm{T}},\end{aligned} \tag{7.8}$$

where $\mathcal{K}$ represents the transformed Hamiltonian, i.e., complete the elimination of the short-period variations. From Equation (3.10), the LDTs can be calculated by taking the partial derivative recursively with respect to the state vector. Since we use the extended variables, the state vector is

$$\mathbf{X}_{\text{ext}} = \left[\, l,\, g,\, h,\, k_{\text{☾}} ,\, k_{\odot},\, L,\, G,\, H,\, H_{\text{☾}} ,\, H_{\odot} \,\right]. \tag{7.9}$$

For instance, the LDTs up to third-order are obtained as Equation (7.10).

$$\mathrm{A}_{1\text{st}} = \frac{\partial \boldsymbol{f}}{\partial \mathbf{X}_{\text{ext}}},\ \mathrm{A}_{2\text{nd}} = \frac{\partial \mathrm{A}_{1\text{st}}}{\partial \mathbf{X}_{\text{ext}}},\ \mathrm{A}_{3\text{rd}} = \frac{\partial \mathrm{A}_{2\text{nd}}}{\partial \mathbf{X}_{\text{ext}}}\ \ldots \tag{7.10}$$

It is worth noting that the first-order LDT, A_{1st}, is a Jacobian matrix whose dimension is 10×10 as follows:

$$\mathrm{A}_{1st} = \left[\begin{array}{ccccc:ccccc}
\mathcal{K}_{6,1} & \mathcal{K}_{6,2} & \mathcal{K}_{6,3} & \mathcal{K}_{6,4} & \mathcal{K}_{6,5} & \mathcal{K}_{6,6} & \mathcal{K}_{6,7} & \mathcal{K}_{6,8} & \mathcal{K}_{6,9} & \mathcal{K}_{6,10} \\
\mathcal{K}_{7,1} & \mathcal{K}_{7,2} & \mathcal{K}_{7,3} & \mathcal{K}_{7,4} & \mathcal{K}_{7,5} & \mathcal{K}_{7,6} & \mathcal{K}_{7,7} & \mathcal{K}_{7,8} & \mathcal{K}_{7,9} & \mathcal{K}_{7,10} \\
\mathcal{K}_{8,1} & \mathcal{K}_{8,2} & \mathcal{K}_{8,3} & \mathcal{K}_{8,4} & \mathcal{K}_{8,5} & \mathcal{K}_{8,6} & \mathcal{K}_{8,7} & \mathcal{K}_{8,8} & \mathcal{K}_{8,9} & \mathcal{K}_{8,10} \\
\mathcal{K}_{9,1} & \mathcal{K}_{9,2} & \mathcal{K}_{9,3} & \mathcal{K}_{9,4} & \mathcal{K}_{9,5} & \mathcal{K}_{9,6} & \mathcal{K}_{9,7} & \mathcal{K}_{9,8} & \mathcal{K}_{9,9} & \mathcal{K}_{9,10} \\
\mathcal{K}_{10,1} & \mathcal{K}_{10,2} & \mathcal{K}_{10,3} & \mathcal{K}_{10,4} & \mathcal{K}_{10,5} & \mathcal{K}_{10,6} & \mathcal{K}_{10,7} & \mathcal{K}_{10,8} & \mathcal{K}_{10,9} & \mathcal{K}_{10,10} \\
\hdashline
-\mathcal{K}_{1,1} & -\mathcal{K}_{1,2} & -\mathcal{K}_{1,3} & -\mathcal{K}_{1,4} & -\mathcal{K}_{1,5} & -\mathcal{K}_{1,6} & -\mathcal{K}_{1,7} & -\mathcal{K}_{1,8} & -\mathcal{K}_{1,9} & -\mathcal{K}_{1,10} \\
-\mathcal{K}_{2,1} & -\mathcal{K}_{2,2} & -\mathcal{K}_{2,3} & -\mathcal{K}_{2,4} & -\mathcal{K}_{2,5} & -\mathcal{K}_{2,6} & -\mathcal{K}_{2,7} & -\mathcal{K}_{2,8} & -\mathcal{K}_{2,9} & -\mathcal{K}_{2,10} \\
-\mathcal{K}_{3,1} & -\mathcal{K}_{3,2} & -\mathcal{K}_{3,3} & -\mathcal{K}_{3,4} & -\mathcal{K}_{3,5} & -\mathcal{K}_{3,6} & -\mathcal{K}_{3,7} & -\mathcal{K}_{3,8} & -\mathcal{K}_{3,9} & -\mathcal{K}_{3,10} \\
-\mathcal{K}_{4,1} & -\mathcal{K}_{4,2} & -\mathcal{K}_{4,3} & -\mathcal{K}_{4,4} & -\mathcal{K}_{4,5} & -\mathcal{K}_{4,6} & -\mathcal{K}_{4,7} & -\mathcal{K}_{4,8} & -\mathcal{K}_{4,9} & -\mathcal{K}_{4,10} \\
-\mathcal{K}_{5,1} & -\mathcal{K}_{5,2} & -\mathcal{K}_{5,3} & -\mathcal{K}_{5,4} & -\mathcal{K}_{5,5} & -\mathcal{K}_{5,6} & -\mathcal{K}_{5,7} & -\mathcal{K}_{5,8} & -\mathcal{K}_{5,9} & -\mathcal{K}_{5,10}
\end{array}\right], \tag{7.11}$$

where $\mathcal{K}_{i,j} = \partial^2 \mathcal{K} / (\partial \mathbf{X}_{\text{ext,i}} \partial \mathbf{X}_{\text{ext,j}})$. In order to compute higher-order LDTs, we have to compute elements included in tensors obtained by substituting Equation (7.8) into (7.10), then, the number

of elements in tensors exponentially increases. For instance, if the second-order LDT is defined based on the given extended variables, then,

$$\mathrm{A}_{\mathrm{2nd,i}} = \frac{\partial}{\partial \mathrm{X}_{\mathrm{ext,i}}} \mathrm{A}_{1st} \tag{7.12}$$

where i represents an i-th element of the state vector, e.g., $\mathrm{X}_{\mathrm{ext},4} = k_{\mathbb{Q}}$. Therefore, we have to compute 1,000 elements to obtain the second-order LDT because its dimension becomes $10 \times 10 \times 10$.

7.2.2 Simplified Computation based on the Symplecticity

Complexity of higher-order LDTs grows exponentially as the order increases: specifically, the number of elements evolves m^2, m^3, ..., m^p, where m and p means a dimension of a state vector and a desired order of STT, respectively. This cumbersome computation could be reduced by considering the symplecticity, shown in Equation (2.25), of the Hamiltonian dynamics.

In order to find a general expression easier, we temporarily define LDTs based on 6-dimensional state space $\boldsymbol{\mathcal{X}}$. A first order LDT is the Jacobian matrix $\mathrm{A}_{\mathrm{1st}}$, then second and third order LDTs are as follows:

$$\mathrm{A}_{\mathrm{2nd}}(:,:,n) = \frac{\partial \mathrm{A}_{\mathrm{1st}}}{\partial \mathbf{X}_n} = \left[\begin{array}{ccc:ccc} \mathcal{K}_{4,1,n} & \mathcal{K}_{4,2,n} & \mathcal{K}_{4,3,n} & \mathcal{K}_{4,4,n} & \mathcal{K}_{4,5,n} & \mathcal{K}_{4,6,n} \\ \mathcal{K}_{5,1,n} & \mathcal{K}_{5,2,n} & \mathcal{K}_{5,3,n} & \mathcal{K}_{5,4,n} & \mathcal{K}_{5,5,n} & \mathcal{K}_{5,6,n} \\ \mathcal{K}_{6,1,n} & \mathcal{K}_{6,2,n} & \mathcal{K}_{6,3,n} & \mathcal{K}_{6,4,n} & \mathcal{K}_{6,5,n} & \mathcal{K}_{6,6,n} \\ \hdashline -\mathcal{K}_{1,1,n} & -\mathcal{K}_{1,2,n} & -\mathcal{K}_{1,3,n} & -\mathcal{K}_{1,4,n} & -\mathcal{K}_{1,5,n} & -\mathcal{K}_{1,6,n} \\ -\mathcal{K}_{2,1,n} & -\mathcal{K}_{2,2,n} & -\mathcal{K}_{2,3,n} & -\mathcal{K}_{2,4,n} & -\mathcal{K}_{2,5,n} & -\mathcal{K}_{2,6,n} \\ -\mathcal{K}_{3,1,n} & -\mathcal{K}_{3,2,n} & -\mathcal{K}_{3,3,n} & -\mathcal{K}_{3,4,n} & -\mathcal{K}_{3,5,n} & -\mathcal{K}_{3,6,n} \end{array}\right], \tag{7.13}$$

and the third order LDT is obtained by taking partial derivatives to $\mathrm{A}_{\mathrm{2nd}}$, *i.e.*, $\partial \mathrm{A}_{\mathrm{2nd}} / \partial \mathbf{X}_m$, with

respect to the state vector.

$$\mathrm{A}_{3\mathrm{rd}}(:,:,m,n) = \left[\begin{array}{ccc:ccc} \mathcal{K}_{4,1,m,n} & \mathcal{K}_{4,2,m,n} & \mathcal{K}_{4,3,m,n} & \mathcal{K}_{4,4,m,n} & \mathcal{K}_{4,5,m,n} & \mathcal{K}_{4,6,m,n} \\ \mathcal{K}_{5,1,m,n} & \mathcal{K}_{5,2,m,n} & \mathcal{K}_{5,3,m,n} & \mathcal{K}_{5,4,m,n} & \mathcal{K}_{5,5,m,n} & \mathcal{K}_{5,6,m,n} \\ \mathcal{K}_{6,1,m,n} & \mathcal{K}_{6,2,m,n} & \mathcal{K}_{6,3,m,n} & \mathcal{K}_{6,4,m,n} & \mathcal{K}_{6,5,m,n} & \mathcal{K}_{6,6,m,n} \\ \hdashline -\mathcal{K}_{1,1,m,n} & -\mathcal{K}_{1,2,m,n} & -\mathcal{K}_{1,3,m,n} & -\mathcal{K}_{1,4,m,n} & -\mathcal{K}_{1,5,m,n} & -\mathcal{K}_{1,6,m,n} \\ -\mathcal{K}_{2,1,m,n} & -\mathcal{K}_{2,2,m,n} & -\mathcal{K}_{2,3,m,n} & -\mathcal{K}_{2,4,m,n} & -\mathcal{K}_{2,5,m,n} & -\mathcal{K}_{2,6,m,n} \\ -\mathcal{K}_{3,1,m,n} & -\mathcal{K}_{3,2,m,n} & -\mathcal{K}_{3,3,m,n} & -\mathcal{K}_{3,4,m,n} & -\mathcal{K}_{3,5,m,n} & -\mathcal{K}_{3,6,m,n} \end{array}\right], \tag{7.14}$$

where m and n indicate m-th and n-th elements in the state vector $\boldsymbol{\mathcal{X}}$, respectively ($0 \leq m,\, n \leq 6$). Subscripts of elements in a tensor means

$$\mathcal{K}_{i,\,m,\,n} = \left(\frac{\partial}{\partial \mathcal{X}_n}\right)\left(\frac{\partial}{\partial \mathcal{X}_m}\right)\left(\frac{\partial \mathcal{K}}{\partial \mathcal{X}_i}\right). \tag{7.15}$$

Equations (7.13) and (7.14) can be simply expressed in

$$\mathrm{A_k} = \left[\begin{array}{c:c} \mathcal{A}_{11} & \mathcal{A}_{12} \\ \hdashline \mathcal{A}_{21} & \mathcal{A}_{22} \end{array}\right], \tag{7.16}$$

where

$$\mathcal{A}_{22} = -\mathcal{A}_{11}^{T}, \tag{7.17a}$$

$$\mathcal{A}_{12},\, \mathcal{A}_{21} :\ \text{Symmetric matrices} \tag{7.17b}$$

As a result of Equation (7.17), the number of elements for generating the STT is reduced to half. The above symplectic relation can generalize each element to vectorize tensors as follows:

$$\mathrm{A_k}(i,j,m,n,\ldots) = \begin{cases} \mathcal{K}_{i+N/2,j,m,n,\ldots} & i = 1,\,\ldots,\,N/2 \\ -\mathcal{K}_{i-N/2,j,m,n,\ldots} & i = N/2+1,\,\ldots,\,N, \end{cases} \tag{7.18}$$

where k and N represent the order of the dimension of a state vector, respectively. A range of each index, i.e., $j, m, n, \ldots$, is between 1 and N. An element in tensors is relocated in a vector based on

the regulation in Equation (7.18); and the relocation of an elements from tensors to the vector is expressed generally by

$$\mathrm{A}_k(i_1, i_2, \ldots, i_k) = \mathrm{A}_k(i_1 + (i_2 - 1)N + (i_3 - 1)N^2 + \ldots + (i_k - 1)N^\alpha), \tag{7.19}$$

where N and α are the number of state vectors and order of the STT, respectively.

In summary, the primary advantage of the hybrid method is two-fold: the SDS propagates the nominal trajectory, basis of the STTs, more rapidly, and the STTs directly maps the initial deviation to any desired epoch instead of using the Monte Carlo simulations.

7.3 Verification of the Hybrid Method

The accuracy and improved efficiency of the hybrid method are investigated through two simulations: a Medium Earth Orbit (MEO) and a highly elliptical orbit (Molniya). Table 7.1 provides the initial orbit conditions for each scenario. The JPL ephemeris file (DE405) has been

Table 7.1: Initial Keplerian elements and parameters for the test orbits

Element	MEO	Molniya
Semimajor axis, a, (km)	26578.140	26578.140
Eccentricity, e	0.01	0.74
Inclination, i, (deg)	55.0	63.0
Longitude of the ascending node, Ω, (deg)	45.0	45.0
Argument of periapsis, ω, (deg)	60.0	270.0
Mean anomaly, ν, (deg)	105.0	105.0
Reflectivity, ρ	0.2	0.2
A/m, (m^2/kg)	2.0	2.0

applied to calculate the positions of the Sun and the moon from January 19, 2008 00:00:00 UCT to February 2, 2008, 23:59:59 UCT. For the sake of generating the truth, Monte Carlo simulations are used with 300,000 samples. The samples, normally distributed within some specified 3-σ region, are generated with respect to the initial condition. A Gaussian error centered at the initial Keplerian elements of the both object is assumed with standard deviations of 10 km in the semi-major axis, 0.05 in eccentricity, and 0.01° in the inclination, longitude of ascending node, the argument of

the pericenter, and the mean anomaly directions. A propagation interval is 30-orbital periods ($\approx$ 15 days.) A propagated distribution of the samples from Monte Carlo simulations with the full dynamical system is assumed as the truth. The full dynamical system, include short periodic variations, uses the same perturbations as each test case, i.e., J_2 gravity field harmonics, SRP, and gravitational attractions from perturbing bodies. The *ode45* function in MATLAB is applied to integrate the initial state. The accuracy and the improvement of the efficiency are verified through statistical approaches and through a comparison of computational times, respectively.

7.3.1 Result I: The Accuracy of the Hybrid Method for MEO

7.3.1.1 Moments Comparison

We verify how well the hybrid method captures the nonlinear effect graphically and quantitatively by comparing the moments of the PDF. The uncertainties from the numerical integration and hybrid method are plotted on the δx-$\delta\dot{x}$ phase-space, and the histograms of the PDFs in each direction in Figure 7.2 in order to demonstrate a statistical comparison. The histogram of the conditional PDF on the $\delta\dot{x}$(ER/s) axis (top-left), that on δx(ER) axis (bottom-right), and the distributions of the samples on the δx-$\delta\dot{x}$ phase space (top-right) are from two different methods. Since results on the δy-$\delta\dot{y}$ and δy-$\delta\dot{y}$ phase spaces have similar shapes to Figure 7.2, we do not include figures on those spaces. First of all, we can see that the propagated uncertainty with the hybrid method describes the truth accurately from a plot on the δx-$\delta\dot{x}$ phase space. Moreover, it is intuitively observed that the initial distribution loses its Gaussianity because of the nonlinear effects of the dynamical system, seen in the PDF on δx axis (bottom-right); the PDF has a right long tail, which is compatible to a positive skewness in Table 7.2. This table shows the moments of the propagated distribution with the hybrid method and relative errors with respect to the truth for δx axis. All values are normalized with respect to Earth radius. The table shows that the relative errors are less than 0.02% from the truth at most.

The STM has similar accuracy in the mean and variance, but, for the higher-order moments, the

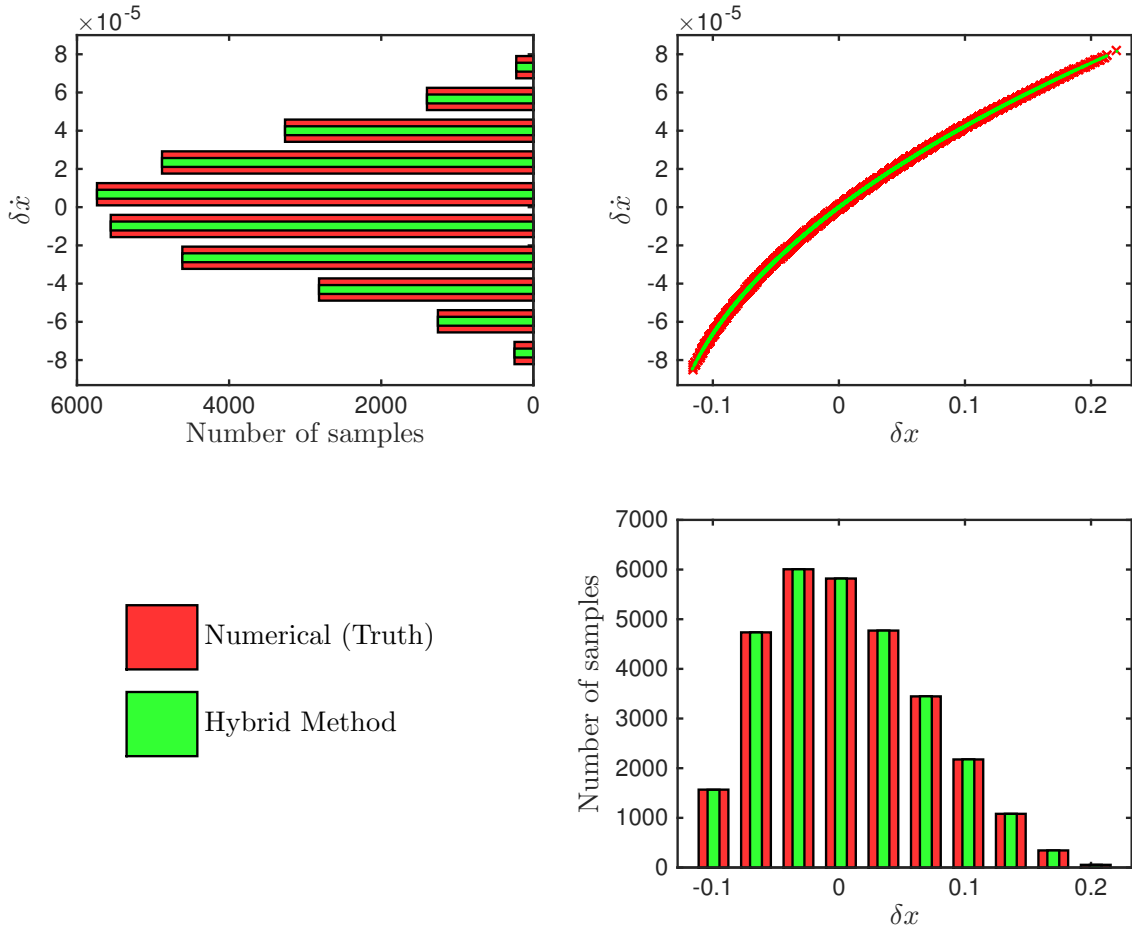

Figure 7.2: Sample point distribution on the $\delta\dot{x}$ (ER/s, top-left) and δx (ER, bottom-right) direction, and its conditional histograms after 30-orbital periods of propagation in MEO.

Table 7.2: Central moments and relative errors on x-axis after 30-orbital periods of propagation (MEO)

	Mean		Variance		Skewness		Kurtosis	
	μ_1	Δ (%)	μ_2	Δ (%)	$\overline{\mu}_3$	Δ (%)	$\overline{\mu}_4$	Δ (%)
STM	4.3307e1	1.1262e-2	1.5851e5	3.5856e-2	4.5546e-1	2.5119e-1	2.6102	5.9306e-2
2^{nd} STT	4.3316e1	9.9390e-3	1.5861e5	2.7296e-2	4.5660e-1	2.9677e-3	2.6117	6.5514e-4
3^{rd} STT	4.3317e1	1.1706e-2	1.5861e5	2.7325e-2	4.5660e-1	3.3154e-3	2.6117	6.8701e-4

relative error gets larger, i.e., less accurate, than the STTs; thus, the combination with the STT should be necessary to get a more accurate result. Moreover, an advantage of the STT in the accuracy point of view is also appeared when we directly map the initial mean and the initial covariance. As demonstrated in Equation (3.26), the current mean and covariance can be directly calculated from the initial mean and covariance. Table 7.3 presents the directly mapped mean with the STM and the STTs in the Delaunay variables space. This table shows that the STTs provide a higher

Table 7.3: Errors in the analytically propagated mean with respect to the truth (MEO)

	STM	STT (2nd order)	STT (3rd order)
$\Delta\delta l$	-386.9584e-6	-52.5691e-6	-53.3358e-6
$\Delta\delta g$	371.7383e-6	52.3290e-6	53.0957e-6
$\Delta\delta h$	-105.0857e-9	-124.8589e-9	-124.8321e-9
$\Delta\delta L$	17.0751e-3	17.0751e-3	17.0751e-3
$\Delta\delta G$	30.6445e-3	30.6445e-3	30.6445e-3
$\Delta\delta H$	2.8398e-3	2.6646e-3	2.6633e-3

accuracy than the STM more apparently. One more thing worth mentioning is that the accuracy of the propagated uncertainty with the second and third order STTs is identical. This infers that there may exist an optimal combination between the order of semi-analytic solutions and that of STTs.

7.3.1.2 Optimal Combination for the Hybrid Method

As seen in Tables 7.2 and 7.3, the accuracy of the hybrid method based on second and third order STTs is similar, but it is different from a result that the higher order STT has the higher

accuracy demonstrated in Fujimoto el al. [27] or Park et al. [64]. This, however, could be explained with a dynamical accuracy of the SDS, i.e., errors due to the ignored short-period variation. As seen in Figure 7.3, the correction values from the third-order STT are less than 0.1% with respect to a magnitude of the short-period variation in time; thus, it could be negligible even if the accuracy is improved. On the other hand, the values from the second-order STT are worth considering because of their magnitude and growing effect in time. Therefore, for the given non-Keplerian

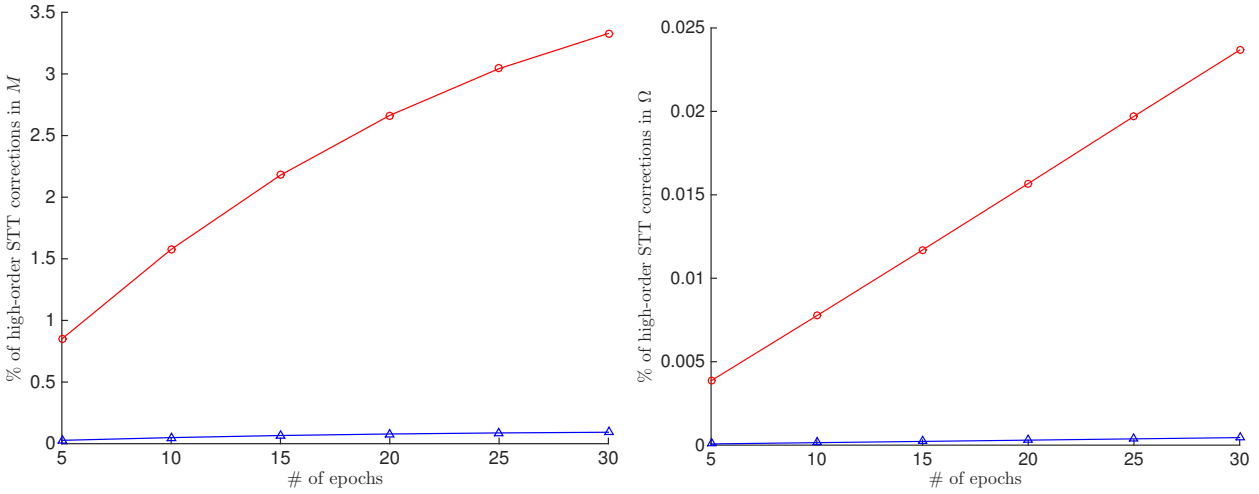

(a) Corrections of the mean anomaly in time (b) Corrections of longitude of the ascending node in time

Figure 7.3: Time history of a ratio of correction values from the second and third-order STTs with respect to the short-period variation. Figure 7.6(a) shows the corrections in the mean anomaly in time. As seen in the figure, the correction of the mean anomaly from the third-order STT is negligible. Figure 7.6(b) depicts an evolution of longitude of the ascending node, and it represents that the corrections from the STTs are less than 0.03%. This angle changes slowly, i.e., almost the constant, in time in the given dynamical system, i.e., almost linear evolution; thus, the high order STTs are meaningless for this angle.

motion, we may be able to suggest an optimal combination of the hybrid method in propagating the uncertainty from this comparison.

7.3.1.3 Statistical Energy Test

As more rigorous statistical verification, the statistical energy test is introduced. The significance level(α) for the hypothesis test is set at 5%. The test is applied to uncertainties based

on the STM and the second order STT at every five orbital periods of propagation. As seen in Figure 7.4, the calculated p-value for every case is larger than the designated significance level, which represents that the propagated uncertainties are equal to the truth with a 95% confidence level.

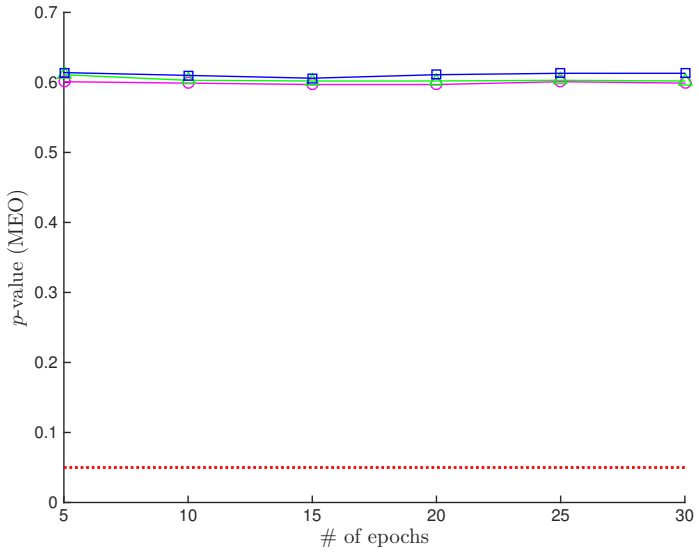

Figure 7.4: Time histories of the p-value from the STM (circles in magenta), the second (triangles in green), and third (squares in blue) order STT with the SDS and the designated significance level, α (dottedline)

7.3.2 Result II: The Accuracy of the Hybrid Method for Highly Elliptical Orbit

7.3.2.1 Moments Comparison

The verification of accuracy for the highly elliptic orbit case is carried out in the same manner. Figure 7.5 shows the distributions on the δx-$\delta \dot{x}$ phase-space and the histograms of the PDFs belonging to each direction: the conditional PDF on the $\delta \dot{x}$(ER/s) axis (top-left), that on δx(ER) axis (bottom-right), and the distributions of the samples on the δx-$\delta \dot{x}$ phase space (top-right) from two different methods. Table 7.4 shows the moments of the PDFs and relative errors up to fourth order in the Cartesian coordinate space for the statistical verification. There exists a difference in accuracy, but the hybrid method captures nonlinearity and maps the uncertainty

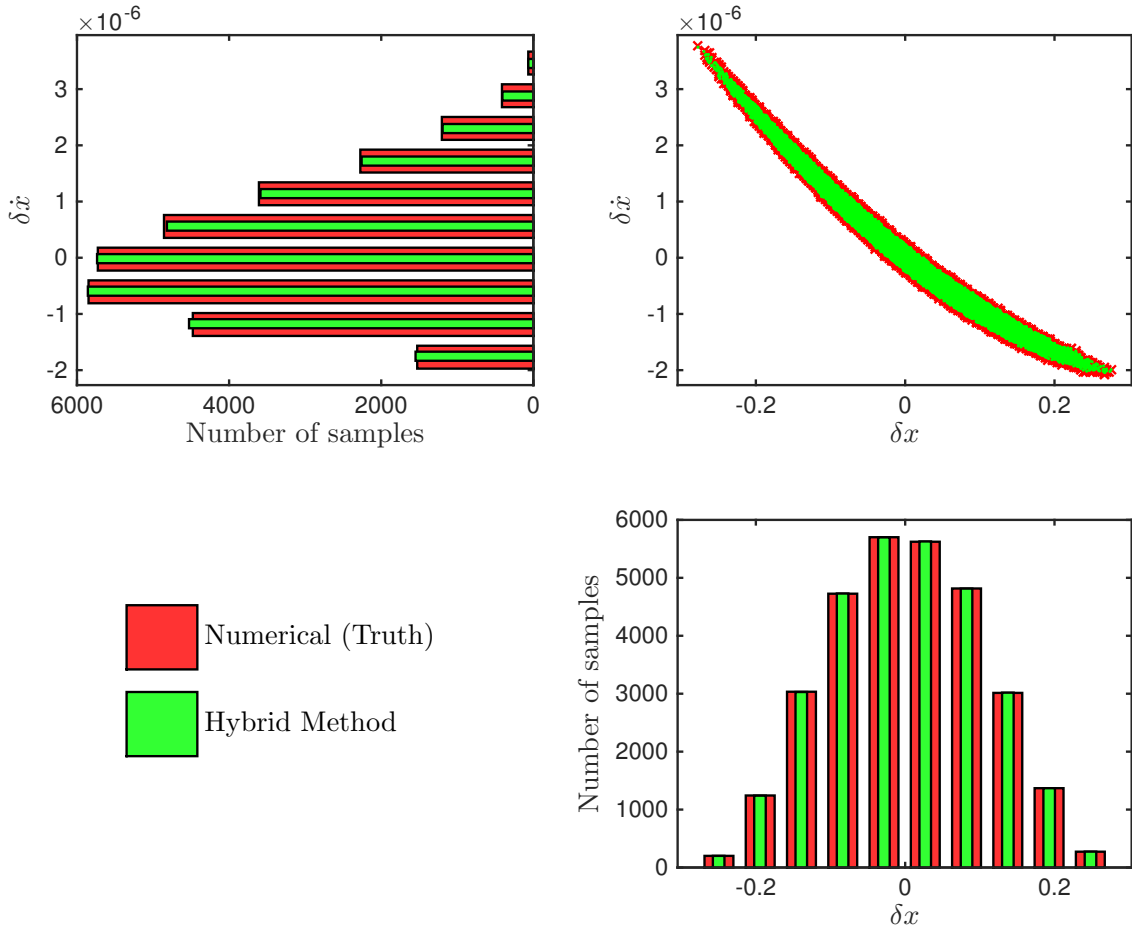

Figure 7.5: Sample point distribution on the $\delta\dot{x}$ (ER/s, top-left) and δx (ER, bottom-right) direction, and its conditional histograms after 30-orbital periods of propagation in Molniya.

accurately in this case as well. The worst result in the table is the mean from the hybrid method based on the STM: it is about 7%. On the other hand, the relative errors of the mean from the STTs are almost 100 times smaller; thus, we can also conclude that the hybrid method based on the STTs is necessary. Finally, we can see that the hybrid methods defined with the second and third order STTs map the uncertainty with similar accuracy in this highly elliptic case. As

Table 7.4: Central moments and relative errors on x-axis after 30-orbital periods of propagation (Molniya)

	Mean		Variance		Skewness		Kurtosis	
	μ_1	Δ (%)	μ_2	Δ (%)	$\overline{\mu}_3$	Δ (%)	$\overline{\mu}_4$	Δ (%)
STM	2.1018	7.6028	4.1792e5	1.0382e-1	8.0660e-3	1.3802e1	2.3972	1.0533e-3
2^{nd} STT	1.9546	6.3190e-2	4.1796e5	9.3720e-2	7.1024e-3	2.0742e-1	2.3972	9.0759e-5
3^{rd} STT	1.9546	6.3206e-2	4.1796e5	9.3699e-2	7.1024e-3	2.0747e-1	2.3972	1.0740e-4

seen in the previous case, the mean and the covariance after 15 days later are calculated with with Equation (3.26), and Table 7.5 presents the propagated values with the STM and STTs. This result

Table 7.5: Errors in the analytically propagated mean with respect to the truth (Molniya)

	STM	STT (2nd order)	STT (3rd order)
$\Delta\delta l$	-14.9890e-6	-13.5673e-9	-13.5729e-9
$\Delta\delta g$	-23.9734e-9	-15.7318e-9	-15.7317e-9
$\Delta\delta h$	102.1294e-9	-11.7265e-9	-11.7276e-9
$\Delta\delta L$	-5.5091e-3	-5.5091e-3	-5.5091e-3
$\Delta\delta G$	116.4601e-3	116.4601e-3	116.4601e-3
$\Delta\delta H$	-58.6631e-3	-58.6285e-3	-58.6285e-3

also clarifies that the hybrid method based on the STM is less accurate than that based on the STTs, as well as shows that the third order STT makes no improvement in the accuracy. Figure 7.6 depicts a ratio of corrections from the second and the third order STTs; this figure implies that the correction from the third order STT is negligible. Therefore, as before, we can suggest the optimal combination of the hybrid method.

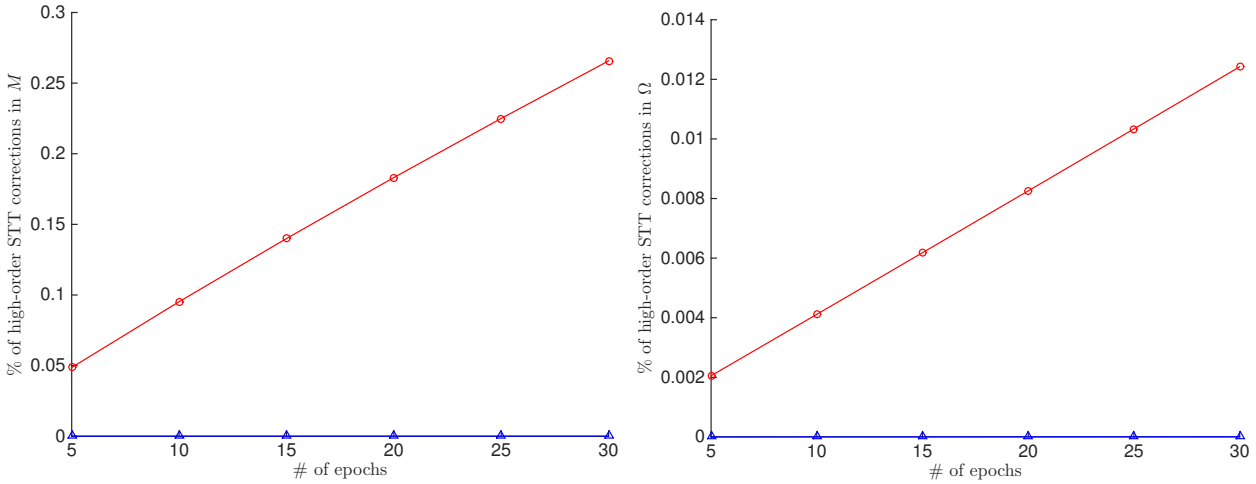

(a) Corrections of the mean anomaly in time

(b) Corrections of longitude of the ascending node in time

Figure 7.6: Time history of a ratio of correction values from the second and third-order STTs with respect to the short-period variation. Figure 7.6(a) shows the corrections in the mean anomaly in time. As seen in the figure, the correction of the mean anomaly from the third-order STT is negligible. Figure 7.6(b) depicts an evolution of longitude of the ascending node, and it represents that the corrections from the STTs are less than 0.03%. This angle changes slowly, i.e., almost the constant, in time in the given dynamical system, i.e., almost linear evolution; thus, the high order STTs are meaningless for this angle.

7.3.2.2 Statistical Energy Test

As in the previous example, the p-value is calculated at every five orbital periods. The same conditions, e.g., significance level and orbital periods of propagation, are applied to this case. Similarly, p-values for all considered epochs are larger than the significance level, shown in Figure 7.7; thus, we conclude that the propagated uncertainties with the hybrid method for the highly elliptic orbit case are equal to the truth with a 95% confidence level.

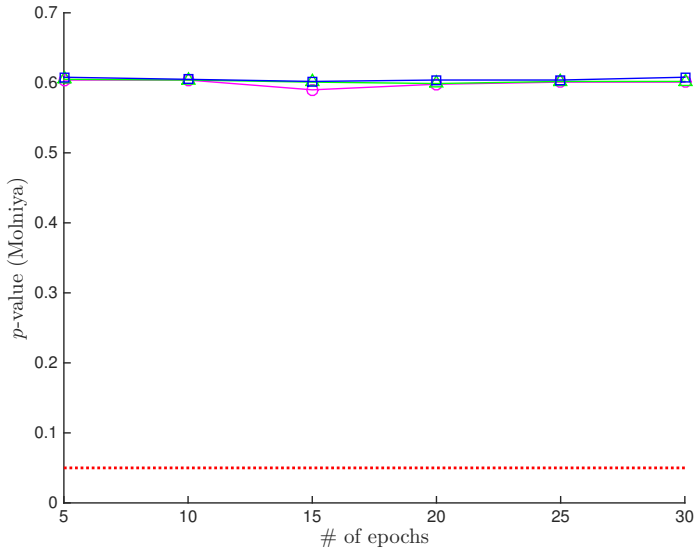

Figure 7.7: Time histories of the p-value from the STM (circles in magenta), the second (triangles in green), and third (squares in blue) order STT with the SDS and the designated significance level, α (dottedline)

7.4 Performance Improvement of the Hybrid Method

For the sake of showing the improvement in computational efficiency, we observe the elapsed time it takes to map the initial uncertainty over 15 days. The number of samples is 300,000. The ephemerides of the Sun and moon at each integration epoch are linearly interpolated with the MATLAB internal function '*interp1*.' Three approaches are used: 1) Monte Carlo simulations with the numerical integration, 2) Monte Carlo simulations with the SDS, and 3) the hybrid method. All computations are performed on a laptop, 2.8 GHz Intel® Core i7 and 4 GB 1067 MHz DDR3. The

elapsed time is the average value acquired from 10 runs (the M-C with the numerical integration is from 2 runs.)

Table 7.6: Comparison of elapsed time in propagating the uncertainty

Method		elapsed time (seconds)	Remarks
Numerical M-C		5.6598e6 ($\approx$ 65.5 days)	–
SDS M-C		7.1184e4 ($\approx$ .8 days)	–
Hybrid method	2nd STT	80.7167	include elapsed time
	3rd STT	111.3365	for computing STTs

As seen in Table 7.6, the hybrid method extremely improves the performance in propagating the uncertainty. The elapsed times for the hybrid method are less than 0.002 % with respect to that for Monte Carlo simulations with the full dynamical system.

7.5 Conclusion

The hybrid method is inspired by a question how we can avoid to use Monte Carlo simulations in mapping uncertainty without losing accuracy. A fundamental idea of the hybrid method is to combine the advantages of the State Transition Tensors (STTs) and the Simplified Dynamical System (SDS). The most remarkable advantage of the STT is that it maps an initial deviation directly to that at any desired epoch, as well as that it captures nonlinearity of the dynamical system. Because of these strengths, the STT is selected as the answer. The hybrid method is defined through two steps: 1) expanding the SDS as a form of the Taylor series expansion, and then 2) generating the STT up to an order where we want. This combined method, ideally, is expected to have the advantages of the two fundamental ideas, i.e., SDS and STT.

In this chapter, we generate the STT up to third order to define the hybrid method and apply them to the two non-Keplerian motions under multiple perturbations, i.e., J_2 gravity field harmonics, a direct Solar Radiation Pressure (SRP), and gravitational attractions due to the Sun and moon (lunisolar perturbation). The accuracy of the propagated uncertainty and the improvement of a performance are verified through the two statistical methods and through the comparison

of elapsed times. From the test, the hybrid method is verified as a more efficient method while maintaining the accuracy for uncertainty propagation.

Lastly, we also proposed that the optimal combination for the hybrid method for the given cases. As shown in Figures 7.3 and 7.6, the second order STT is the dominant part to improve the accuracy for mapping uncertainty. This implies that the second order STT is enough to capture the nonlinearity of the SDS. Related to this result, it is also worth considering the optimal combination for the SDS that has higher nonlinearity, such as a Low Earth Orbit (LEO) case.

Chapter 8

Conclusion and Future Works

8.1 Conclusion

In recent years, Space Situational Awareness (SSA) has become increasingly important as the number of tracked Resident Space Objects (RSOs) continues their growth. In order to keep pace with this situation, various methods have been proposed to propagate uncertainty accurately by capturing the nonlinearity of the dynamical system. The methods mostly focus on expressing motion of the RSOs with more realistic mathematical descriptions. However, to understand the evolution of uncertainty more rigorously and to propose a new method for mapping uncertainty, an investigation of the dynamical system itself should be fruitful. This idea can be clarified with the motivational question of this research, which is

"How much precision is needed in describing the dynamical motion of a spacecraft to ensure an accurate determination of propagated orbit uncertainty?"

In this dissertation, we examine the question by verifying the dynamical realism in propagating uncertainty accurately, and then we ultimately apply the answer to develop the more efficient method while maintaining the accuracy.

In Chapter 3, an analytic method of nonlinear uncertainty propagation and of an evolution of PDF are discussed. A special solution to the Fokker-Planck equations for deterministic systems

and the State Transition Tensors (STTs) concept are combined so that, given an analytical expression of both the initial probability distribution and the dynamics, the probability distribution may be expressed analytically for all time. Moreover, the analytic expressions for calculating the third and fourth order moments are introduced. In order to understand the STTs more clearly, the two-body dynamics is applied to the above framework. Consequently, the results demonstrate the potential efficiency and accuracy of analytical uncertainty propagation even when compared to numerical results employing realistic parameter models and the good agreement between the analytic and Monte Carlo results implies that further investigation in analytic uncertainty propagation may indeed be beneficial.

In Chapter 4, we reviewed the Deprit-Lie transformation method and its the generalized expressions. One of the most advantageous property of this transformation is the systematic process, such as obtaining the generating functions. The algorithms for converting the variables' spaces and for restoring the periodic variations are also addressed. Then, the symplecticity of the transformation is verified. Lastly, for practical applications, a procedure for deriving the (semi) analytic solutions was presented; and the feasibility and the improvement of accuracy of the transformation method were verified by revisiting the problem of the artificial satellite theory.

In Chapter 5, the idea of the weak solution for stochastic partial differential equations[29] motivates us to identify a dominant variation and explore the Simplified Dynamical System (SDS) for uncertainty propagation. For the first verification of the motivational question, we have focused on the dynamical realism in mapping uncertainty and verified the accuracy and the performance improvement of the SDS, as well as identified the dominant variation in uncertainty propagation. Throughout this chapter, we show that the SDS is capable of propagating the initial PDF while maintaining accuracy even though the short-period variations are regarded as constants. It is worth mentioning that we also investigate the influence of the short-period variations in mapping uncertainty by comparing distributions within one period. The replacement of periodic variations

apparently make an offset in the orbit element space; however, it is verified that there is a negligible effect in mapping uncertainty in the Cartesian coordinates space. In conclusion, the most dominant variation for the accurate propagation of uncertainty is the secular variation of the dynamical system of the orbiting bodies. Moreover, we have introduced a new statistical method, called the statistical energy test, for comparing multivariate PDFs more rigorously[2, 3]. Based on this test, we conclude that the propagated uncertainty with the SDS describes the true uncertainty accurately with 95% of confidence level for every test scenario.

In Chapter 6, the property of the Deprit-Lie transformation method[19] inspires us to expand the SDS and to replace the initial offset correction algorithm with a fully analytic method. The expanded SDS, based on the second-order secular (averaged) dynamics, considers multiple perturbations, such as J_2 gravity field harmonics, gravitational attraction of the moon, and a direct Solar Radiation Pressure (SRP). And the analytic initial correction algorithm is implemented based on the generating functions. Thus, the main goal of this chapter is to verify the capability of the expanded SDS in two aspects, i.e., accuracy and efficiency. Throughout this chapter, we describe how the Deprit-Lie transformation method is applied to define the expanded SDS and the analytic initial offset correction algorithm. Then, we have verified the accuracy and the improvement of computational efficiency through the statistical approaches and through the comparison of processing times, respectively. In particular, an evolution of uncertainty of high area-to-mass ratio (HAMR) objects is tested as a more extreme case. Through this test, we verify that the expanded SDS is applicable to map uncertainty for the HAMR objects accurately and efficiently. Lastly, we define the new initial offset correction algorithm based on the generating function and show that it successfully replaces the previous methods. This should be another advantage of an application of the Deprit-Lie transformation method.

In Chapter 7, the hybrid method is proposed based on a question “How can we avoid using Monte Carlo simulations in mapping uncertainty without losing accuracy?” A fundamental idea of the

hybrid method is to combine the advantages of the STTs and the SDS. The most remarkable advantages of the STT are that it maps an initial deviation directly to that at any desired epoch and that it captures nonlinearity of the dynamical system. Because of these strengths, the STT is selected as the answer. The hybrid method is defined through two steps: 1) expanding the SDS as a form of the Taylor series expansion, and then 2) generating the STT up to an order where we want. This combined method, ideally, is expected to have the advantages of the two fundamental ideas, i.e., SDS and STT. In this chapter, we generate the STTs up to third order to define the hybrid method and apply each order of the STTs to the two non-Keplerian motions under multiple perturbations, i.e., J_2 gravity field harmonics, a direct SRP, and gravitational attractions due to the Sun and moon (lunisolar perturbation). The accuracy of the propagated uncertainty and the improvement of the computational efficiency are verified through the two statistical methods and through the comparison of elapsed times. From the test, the hybrid method is verified as a more efficient method while maintaining the accuracy for uncertainty propagation. Lastly, we also proposed the optimal combination of the both ideas for the hybrid method for the given examples. As shown in Figures 7.3 and 7.6, the second order STT is the dominant part to improve the accuracy for mapping uncertainty. This implies that the second order STT is sufficient to capture the nonlinearity of the SDS. Related to this result, it is also worth considering the optimal combination for the SDS that has higher nonlinearity, such as a Low Earth Orbit (LEO) case.

8.2 Future Works

We will briefly mention about planned follow-up studies. The future works can be classified to twofold. At first, we will explore more practical applications based on the SDS. Next, based on (semi) analytic solutions, various celestial mechanics problems would be investigated, such as resonances, frozen orbits, and so on. Following is a short summary:

■ We are planning to expand the current hybrid method by incorporating additional perturbations relevant to Earth-orbiting objects to the uncertainty propagation, such as the full effect

due to the oblateness or the tesseral harmonics of the Earth or drag. As well as it is also investigated to generate the hybrid method for more practical problems, which include a control law, a filtering, and so on. Brief descriptions about these works are given below:

- Expansion of the SDS to non-autonomous Hamiltonian case

  · Incorporate of drag force in the SDS [8, 11, 16].

  · According to Two Line Elements (TLE) released by North American Aerospace Defense Command (NORAD), there are many known objects on a low altitude ($\leq$ 2.0 ER.)

  · Introduce practical measurements data such as GPS occultation, radiosonde, etc.

- Estimation with sparse tracking for space debris

  · Some space debris, such as the fragments of the Chinese Fengyun-1C satellite, have stable orbits: thus, they need to be monitored over long-period of time.

  · Nonlinear mapping of uncertainty becomes diluted after some period of propagation.

  · Study map to incorporate measurements into highly distorted uncertainty distributions.

  · Use my methods of uncertainty mapping and representation from my thesis.

  · Apply modern estimation approaches, e.g., particle filter.

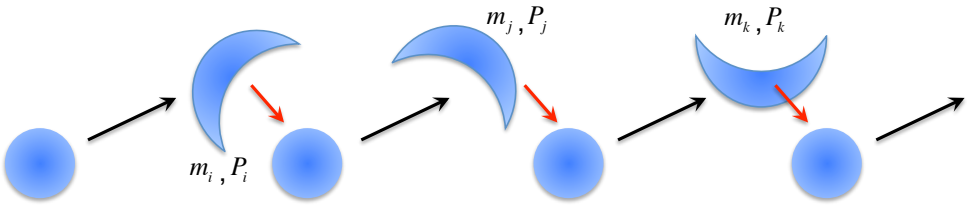

Figure 8.1: Incorporation of the tracking date to update the propagated uncertainty: Aa region of the propagated uncertainty spreads over time. After some time later, everywhere in a trajectory is under the propagated uncertainty region. By updating this region with sparse tracking data, the uncertainty region may be prevented from an infinite inflation.

- Collision assessment and avoidance strategy

  · The hybrid method propagate uncertainty more efficiently while keeping accuracy [60]

  · Map uncertainties of a satellite and potentially hazardous objects analytically.

· Assess if propagated uncertainty had any overlap by applying Bayes' theorem.

· One could design an avoidance strategy by applying the statistically correct trajectory and nonlinear statistical targeting [62, 64].

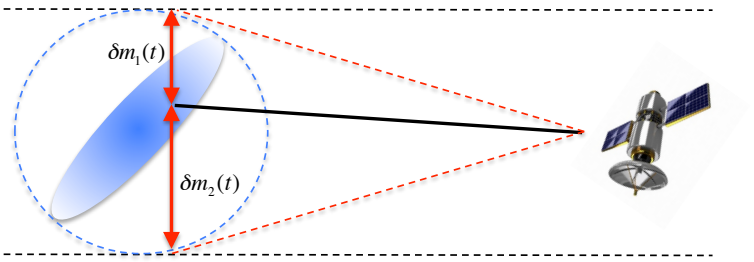

Figure 8.2: Collision assessment and avoidance strategy

■ The (semi) analytic solutions and the generating functions, derived from the Deprit-Lie transformation, can provide more insight to analyze resonances or to understand trajectories of celestial bodies itself (or those around small bodies.) Thus, this approach would be useful to explore resonant orbits for space debris removal as well as to study a long-term evolution of celestial bodies, such as a formation of the Saturn's ring or a motion of particles within a galactic disk.

Bibliography

[1] M. K. M. Ahmed. On the normalization of perturbed keplerian systems. The Astronomical Journal, 107(5):1900–1903, 1994.

[2] B. Aslan. The concept of energy in nonparametric statistics - Goodness-of-Fit problems and deconvolution. PhD thesis, Universitat Siegen, 2004.

[3] B. Aslan and G. Zech. Statistical energy as a tool for binning-free, multivariate goodness-of-fit tests, two-sample comparison and unfolding. Nuclear Instruments and Methods in Physics Research, 537:626–636, 2005.

[4] Roger R. Bate, Donald D. Muller, and Jerry E. White. Fundamentals of Astrodynamics. Dover Publications, Inc., 1971.

[5] J. S. Bay. Fundamentals of Linear State Space Systems. McGraw-Hill, 1999.

[6] Gerhard Beutler. Methods of Celestial Mechanics I: Physical, Mathematical, and Numerical Principles, volume 1. Springer, 2005.

[7] D. Boccaletti and G. Pucacco. Theory of Orbits, volume 2: Perturbative and Geometrical Methods. Springer.

[8] Slawomir Breiter and Gilles Mètris. Symplectic mapping for satellites and space debris including nongravitational forces. Celest Mech Dyn Astr, 71:79–94, 1999.

[9] Dirk Brouwer. Solution of the problem of artificial satellite theory without drag. The Astronomical Journal, 64(1274):378–396, 1959.

[10] Dirk Brouwer and Gerald M. Clemence. Methods of Celestial Mechanics. Academic Press, 1961.

[11] Dirk Brouwer and Gen-Ichiro Hori. Theoretical evaluation of atmospheric drag effects in the motion of an artificial satellite. The Astronomical Journal, 66:193–225, 1961.

[12] Barbara J. Cain. Determination of mean elements for brouwer's satellite theory. The Astronomical Journal, 67(6):391–392, 1962.

[13] J. A. Campbell and W. H. Jefferys. Equivalence of the perturbation theories of hori and deprit. Celestial Mechanics, 2:467–473, 1970.

[14] Shannon L. Coffey and Andrè Deprit. Third-order solution for artificial satellites. Journal of Guidance, Control, and Dynamics, 5, July-August 1982.

[15] D. A. Danielson, B. Neta, and L. W. Early. Semianalytic satellite theory (sst): Mathematical algorithms. Technical report, Naval Postgraduate School, 1994.

[16] FABIENNE DELHAISE. Analyical treatment of air drag and earth oblateness effects upon an artificial satellite. Celestial Mechanics and Dynamical Astronomy, 52:85–103, 1991.

[17] Kyle Jordan DeMars. Nonlinear Orbit Uncertainty Prediction and Rectification for Space Situational Awareness. thesis, University of Texas at Austin, December 2010.

[18] A. Deprit. The elimination of the parallax in satellite theory. Celestial Mechanics, 24:111–153, 1981.

[19] Andre Deprit. Canonical transformations depending on a small parameter. Celestial Mechanics, 1:12–30, 1969.

[20] Andrè Deprit. Delaunay normalisations. Celestial Mechanics, 26:9–21, 1982.

[21] R. Deutsch. Nonlinear Transformations of Random Processes. Prentice Hall, 1962.

[22] R. C. Domingos, A. F. Bertachini de Almeida Prado, and R Vilhena de Moraes. Studying the behaviour of averaged models in the third body perturbation problem. Journal of Physics, 465, 2013.

[23] R. C. Domingos, R. Vilhena de Moraes, and F. Bertachini De Almeida Prado. Third-body perturbation in the case of elliptic orbits for the disturbing body. Mathematical Problems in Engineering, 2008, April 2008.

[24] Bradley Efron and R.J. Tibshirani. An Introduction to the Bootstrap. Chapman and Hall, New York, 1993.

[25] P. Exertier, G. Metris, Y. Boudon, and F. Barlier. Long Term Evolution of Mean Orbital Elements of Artificial Satellites, volume 82 of Geophysical Monograph Series. American Geophysical Union, March 2013.

[26] Space Foundation. Space situational awareness, November 2015.

[27] Kohei Fujimoto and Daniel J. Scheeres. Analytical nonlinear propagation of uncertainty in the two-body problem. Journal of Guidance, Control, and Dynamics, 35(2):497–509, 2012.

[28] Daniel Giza, Puneet Singla, and Moriba Jah. An approach for nonlinear uncertainty propagation: Application to orbital mechanics. Number AIAA 2009-6082. AIAA, 2009.

[29] Eric Daniel Gustafson. Stochastic Optimal Control of Spacecraft. PhD thesis, The University of Michigan, 2010.

[30] Liam M. Healy. Orbit propagation with lie transfer maps in the perturbed kepler problem. Celest Mech Dyn Astr, 85:175–207, 2003.

[31] Keric Hill and Brandon A. Jones. TurboProp Version 4.0. Colorado Center for Astrodynamics Research, University of Colorado at Boulder, May 2009.

[32] G. I Hori. The effect of radiation pressure on the motion of an artificial satellite. In J. Barkley Rosser, editor, Space Mathematics Part 3, volume 7, pages 167–182. American Mathematical Society, 1966.

[33] G. I Hori. Theory of general perturbations with unspecified canonical variables. Astronomy Society of Japan, 18:287–296, 1966.

[34] Joel L. Horowitz. Handbook of Econometrics, Chapter 52 - The Bootstrap, volume 5. North-Holland, 2001.

[35] J. Horwood, N. D. Aragon, and A. B. Poore. Estimation of drag and its uncertainty in initial orbit determination using gauss-hermite quadrature. In AAS Born Symposium, 2010.

[36] J. T. Horwood, N. D. Aragon, and A. B. Poore. Gaussian sum filters for space surveillance: Theory and simulations. Journal of Guidance, Control, and Dynamics, 34(6):1839–1851, December 2011.

[37] William H. Jefferys. Automated, closed form integration of formulas in elliptic motion. Celestial Mechanics, 3:390–394, 1971.

[38] Brandon A. Jones, Alireza Doostan, and George H. Born. Nonlinear propagation of orbit uncertainty using non-intrusive polynomial chaos. Journal of Guidance, Control, and Dynamics, 36(2):430–444, Marck-April 2013.

[39] J. Junkins and P. Singla. How nonlinear is it? a tutorial on nonlinearity of orbit and attitude dynamics. Journal of the Astronautical Sciences, 52(1):7–60, 2004.

[40] J. L. Junkins, M. R. Akella, and K. T. Alfriend. Non-gaussian error propagation in orbital mechanics. Journal of Astronautical Sciences, 44(4):541–563, October-December 1996.

[41] Ahmed Aly Kamel. Expansion formulae in canonical transformations depending on a small parameter. Celestial Mechanics, 1:190–199, 1969.

[42] Ahmed Aly Kamel. Perturbation method in the theory of nonlinear oscillations. Celestial Mechanics, 3:90–106, 1970.

[43] Hiroshi Kinoshita. Third-order solution of an artificial-satellite theory. SAO special report 379, Smithsonian Astrophysical Observatory, Smithsonian Institution, Astrophysical Observatory, Cambridge, Massachusetts 02138, July 1977.

[44] Yoshihide Kozai. The motion of a close earth satellite. The Astronomical Journal, 64:367–377, 1959.

[45] Yoshihide Kozai. Second-order solution of artificial satellite theory without air drag. The Astronomical Journal, 67(7):446–461, 1962.

[46] Martin Lara, Juan F. San Juan, and Luis M. Lopez. Semianalytic integration of high-altitude orbits under lunisolar effects. Mathematical Problems in Engineering, 2012(Article ID 659396), 2012.

[47] Martin Lara, Juan F. San-Juan, and Luis M. Lòpez-Ochoa. Efficient semi-analytic integration of gnss orbits under tesseral effects. Acta Astronautica, 2013.

[48] Martin Lara, Juan F. San-Juan, and Luis M. Lòpez-Ochoa. Delaunay variables approach to the elimination of the perigee in artificial satellite theory. Celest Mech Dyn Astr, 2014.

[49] Martin Lara, Juan F. San-Juan, and Luis M. Lòpez-Ochoa. Proper averaging via parallax elimination. Adv. Astronaut. Sci., 150:315–331, 2014.

[50] R. H. Lyddane. Small eccentricities or inclinations in the brouwer theory of the artificial satellite. The Astronomical Journal, 68(8):555–558, October 1963.

[51] Peter S. Maybeck. Stochastic Models, Estimation and Control, volume 2. Academic Press, New York, NY, 1982.

[52] P. McCullagh. Tensor Methods in Statistics. Chapman and Hall, 1987.

[53] Jason R. W. Mclaren, John C. Thomas, Jessica L. Mackintosh, Kerry A. Mudge, Kenneth J. Grant, Cradley A. Clare, and William G. Cowley. Comparison of probability density functions for analyzing irradiance statistics due to atmospheric turbulence. Applied Optics, 51(25):5996–6002, Sep. 2012.

[54] Jay W. McMahon. An Analytical Theory for the Perturbative Effect of Solar Radiation Pressure on Natural and Artificial Satellites. PhD thesis, University of Colorado, 2011.

[55] G. Metris. Mean values of particular functions in the elliptic motion. Celestial Mechanics and Dynamical Astronomy, 52:79–84, 1991.

[56] G. Metris and P. Exertier. Semi-analytical theory of the mean orbital motion. Astronomy and Astrophysics, 294:278–286, 1995.

[57] F. R. Moulton. Differential Equations. The MacMillan Company, 1930.

[58] NASA Orbital Debris Program Office. Orbital debris quarterly news, 2013.

[59] Inkwan Park and Daniel J. Scheeres. Simplified propagation of uncertainty in the non-keplerian problem. September 2014.

[60] Inkwan Park and Daniel J. Scheeres. The effect of dynamical accuracy for uncertainty propagation (accepted). Journal of Guidance, Control, and Dynamics, 2015.

[61] Inkwan Park, Daniel J. Scheeres, and Kohei Fujimoto. The effect of dynamical accuracy for uncertainty propagation. In Stephen B. Broschart, James D. Turner, Kathleen C. Howell, and Felix R. Hoots, editors, Astrodynamics 2013, volume 150, August 2013.

[62] R. S. Park and D. J. Scheeres. Nonlinear mapping of gaussian statistics: Theory and applications to spacecraft trajectory design. Journal of Guidance, Control, and Dynamics, 29(6):1367–1375, November-December 2006.

[63] Ryan S. Park and Daniel J. Scheeres. Nonlinear semi-analytci methods for trajectory estimation. Journal of Guidance, Control, and Dynamics, 30(6), 2007.

[64] Sang H. Park. Nonlinear Trajectory Navigation. PhD thesis, University of Michigan, 2007.

[65] William H. Press, Saul A. Teukolsky, William T. Vetterling, and Brian P. Flannery. Numerical Recipes in C: The Art of Scientific Computing. CAMBRIDGE UNIVERSITY PRESS, second edition, 1988.

[66] Jeremy D. Price and Robert Wood. Comparison of probability density functions for total specific humidity and saturation deficit humidity, and consequences for cloud parametrization. Quarterly Journal of the Royal Meteorological Society, 128:2059–2072, 2002.

[67] A E Roy. Orbital Motion. Taylor and Francis Group, fourth edition, 2005.

[68] D. Roy. A weak form of stochastic newmark method with applications to engineering dynamical systems. Applied Mathematical Modelling, 27(6):421–436, 2003.

[69] D. Roy and M. K. Dash. A stochastic newmark method for engineering dynamical systems. Jouranl of Sound and Vibration, 249(1):83–100, 2002.

[70] Nadia A. Saad, Kh. I. Khalil, and Magdy Y. Amin. Analytical solution for the combined solar radiation pressure and luni-solar effects on the orbits of high altitude satellites. The Open Astronomy Journal, 3:113–122, 2010.

[71] Bernard De Saedeleer and Jacques Henrard. Analytical theory of an artificial satellite of the moon. Ann N Y Acad Sci., 1017:434–449, 2004.

[72] Daniel J. Scheeres. Orbital Motion in Strongly Perturbed Environments. Springer, 2012.

[73] Carlos Renato Huaura Solòrzano and Antonio Fernando Bertachini de Almeida. Third-body perturbation using a single averaged model: Application in nonsingular variables. Mathematical Problems in Engineering, 2007, 2007.

[74] T.T. Soong. Random Differential Equations in Science and Engineering, volume 103. Academic Press Inc., 1973.

[75] Gàbor J. Szèkely and Maria L. Rizzo. Energy statistics: A class of statistics based on distances. Journal of Statistical Planning and Interference, 143:1249–1272, 2013.

[76] B. D. Tapley, B. E. Schutz, and G. H. Born. Statistical Orbit Determination. Elsevier Academic Press, Burlington, MA, 1 edition, 2004.

[77] Gabriel Terejanu, Puneet Singla, Tarunraj Singh, and Peter D. Scott. Uncertainty propagation for nonlinear dynamic systems using gaussian mixture models. Journal of Guidance, Control, and Dynamics, 31(6):1623–1633, November-December 2008.

[78] M. Valli, R. Armellin, R. Di Lizia, and M. R. Lavagna. Nonlinear mapping of uncertainties in celestial mechanics. Journal of Guidance, Control, and Dynamics, 36(1):48–63, 2013.

[79] C. Wiedemann, S. Flegel, J. Gelhaus, M. Möckel, H. Klinkrad, H. Krag, , and P. Vörsmann. The space debris environment model MASTER-2009. In the 28th International Symposium on Space Technology and Science, 2011.

[80] Guochang Xu and Jia Xu. Orbits: 2nd Order Singularity-free Solutions. Springer, second edition, 2013.

[81] G. Zech and B. Aslan. New test for the multivariate two-sample problem based on the concept of minimum energy. Journal of Statistical Computation and Simulation, 75(2):109–119, Feb. 2005.

Appendix A

Useful Mathematical Techniques

A.1 Calculus of Derivatives

Taking partial derivatives to any given orbital dynamics are necessary not only for deriving the Lagrange Planetary Equations, but also for applying the Deprit-Lie transformation method. In particular, implicit relations between phase variables have to be considered when we use the dynamical system for an orbiting object, such as a relation between the mean and true anomalies. Before discussing the partial derivatives, we clarify basic relations between the mean, the true, and the eccentric anomalies in the orbiting motion as follows [72]:

$$\begin{aligned}
\cos E &= \frac{e + \cos f}{1 + e\cos f}, \\
\sin E &= \frac{\sqrt{1-e^2}\sin f}{1 + e\cos f}, \\
\cos f &= \frac{\cos E - e}{1 - e\cos E}, \\
\sin f &= \frac{\sqrt{1-e^2}\sin E}{1 - e\cos E}.
\end{aligned} \tag{A.1}$$

Next are the associated differential relationships of the anomalies.

$$\begin{aligned}
dM &= (1 - e\cos E)dE, \\
dM &= \frac{(1-e^2)^{3/2}}{(1 + e\cos f)^2}df, \\
dE &= \frac{\sqrt{1-e^2}}{1 + e\cos f}df, \\
df &= \frac{\sqrt{1-e^2}}{1 - e\cos E}dE
\end{aligned} \tag{A.2}$$

From the relations defined in Equations (A.1) and (A.2), we can get

$$
\begin{aligned}
&\frac{\partial E}{\partial(e,\, M)} = \left(\frac{a}{r}\sin E,\, \frac{a}{r}\right), \\
&\frac{\partial f}{\partial(e,\, M)} = \left(\frac{2+e\cos f}{1-e^2}\sin f,\, \left(\frac{a}{r}\right)^2\sqrt{1-e^2}\right), \\
&\frac{\partial r}{\partial M} = ae\sin E\frac{\partial E}{\partial M} = \frac{a^2 e}{r}\sin E = \frac{ae}{\sqrt{1-e^2}}\sin f, \\
&\frac{\partial r}{\partial(a,\, e,\, i,\, \Omega,\, \omega)} = \left(\frac{r}{a},\, -a\cos f,\, 0,\, 0,\, 0\right), \\
&\frac{\partial u}{\partial e} = \frac{\partial u}{\partial f}\frac{\partial f}{\partial e} = \frac{2+e\cos f}{1-e^2}\sin f, \\
&\frac{\partial u}{\partial M} = \frac{\partial u}{\partial f}\frac{\partial f}{\partial M} = \left(\frac{a}{r}\right)^2\sqrt{1-e^2}, \\
&\frac{\partial u}{\partial(a,\, i,\, \Omega,\, \omega)} = (0,\, 0,\, 0,\, 1),
\end{aligned}
\tag{A.3}
$$

where $u = f + \omega$. It is worth mentioning that these results are useful when we define the implicit relations between the Delaunay variables since the Deprit-LIe transformation method in this study is defined in the Delaunay variables space. More detailed derivation procedure is presented in Beutler[6].

We can obtain another useful partial derivatives based on the relationships listed below:

$$\tan\frac{f}{2} = \sqrt{\frac{1+e}{1-e}}\tan\frac{E}{2}, \tag{A.4a}$$

$$E = M(t) + e\sin E, \tag{A.4b}$$

$$M(t) = n(t - T_0). \tag{A.4c}$$

From Eq. (A.4), we can find dependencies between the variables as

$$
\begin{aligned}
f &= f(e,\, E), \\
E &= E(M,\, e), \\
M &= M(a,\, T_0).
\end{aligned}
\tag{A.5}
$$

Then,

$$\frac{\partial f}{\partial a} = \frac{\partial f}{\partial E}\frac{\partial E}{\partial M}\frac{\partial M}{\partial a}, \tag{A.6a}$$

$$\frac{\partial f}{\partial e} = \{f\}_e + \frac{\partial f}{\partial E}\frac{\partial E}{\partial e}, \tag{A.6b}$$

$$\frac{\partial f}{\partial T_0} = \frac{\partial f}{\partial E}\frac{\partial E}{\partial M}\frac{\partial M}{\partial T_0}, \tag{A.6c}$$

where $\{f\}_e$ specially designates the partial derivative of the true anomaly with respect to e, ignoring the dependency of E on e. T_0 can be replaced with M_0 or $M(T_0)$ or σ_0 [80]. Here are additional results:

$$\frac{\partial f}{\partial E} = \frac{1}{\sqrt{1-e^2}}\frac{p}{r}, \tag{A.7a}$$

$$\frac{\partial M}{\partial a} = -\frac{3}{2a}M(t), \tag{A.7b}$$

$$\frac{\partial f}{\partial a} = -\frac{3a\sqrt{1-e^2}}{2r^2}M(t), \tag{A.7c}$$

$$\frac{\partial f}{\partial e} = \frac{1}{1-e^2}\frac{p}{r}\sin f, \tag{A.7d}$$

$$\frac{\partial f}{\partial T_0} = -\frac{nap}{r^2\sqrt{1-e^2}}. \tag{A.7e}$$

Lastly, as demonstrated, the Deprit-Lie transformation method uses the Delaunay variables defined in Equation (6.4). In this study, auxiliary variables, (ξ, f, g, h, a, n, e, η, s, c), are introduced to express the semi-analytic solutions in the closed-form by rewriting the given dynamical system. These variables are defined as follows:

$$\begin{array}{ll}
\xi = \dfrac{a}{r} = \dfrac{1+e\cos f}{1-e^2} = \dfrac{1}{1-e\cos E} & f \\
a = \dfrac{L^2}{\mu} & n = \dfrac{\mu^2}{L^3} \\
e = \sqrt{1-\left(\dfrac{G}{L}\right)^2} & \eta = \sqrt{1-e^2} = \dfrac{G}{L} \\
s = \sin I = \sqrt{1-\left(\dfrac{H}{G}\right)^2} & c = \cos I = \dfrac{H}{G} \\
g & h
\end{array} \tag{A.8}$$

Table A.1 shows partial derivatives of the auxiliary variables with respect to the Delaunay variables. For the sake of solving the higher-order homological equations, Equation (A.8) and the relations in

Table A.1: Table of partial derivatives

	$\partial/\partial L$	$\partial/\partial G$	$\partial/\partial H$	$\partial/\partial l$
ξ	$\frac{\xi^2\eta^2}{na^2e}\cos f$	$-\frac{\xi^2\eta}{na^2e}\cos f$	0	$-\frac{\xi^2 e}{\eta}\sin f$
a	$\frac{2}{an}$	0	0	0
n	$-\frac{3}{a^2}$	0	0	0
s	0	$\frac{c^2}{na^2\eta s}$	$-\frac{c}{na^2\eta s}$	0
c	0	$-\frac{c}{na^2\eta}$	$\frac{1}{na^2\eta}$	0
e	$\frac{\eta^2}{na^2e}$	$-\frac{\eta}{na^2e}$	0	0
η	$\frac{\eta}{na^2}$	$\frac{1}{na^2}$	0	0
f	$\frac{1+\xi\eta^2}{na^2e}\sin f$	$-\frac{1+\xi\eta^2}{\eta na^2e}\sin f$	0	$\xi^2\eta$

the table are applied. For instance, the second-partial derivatives for computing $\mathcal{L}_1^2\mathcal{H}_{0,0}$ are defined as:

$$\frac{\partial^2\xi}{\partial l^2} = \frac{\partial}{\partial l}\left(-\frac{\xi^2 e}{\eta}\sin f\right) = -2\frac{e^2\xi}{\eta}\left(\frac{\partial\xi}{\partial l}\right)\sin f - \frac{\xi^2 e}{\eta}\left(\frac{\partial \sin f}{\partial l}\right) = \frac{\xi^3 e^3}{\eta^2}(1-\cos 2f) - \frac{\xi^4 ne}{\eta}\cos f. \tag{A.9}$$

With the same idea, we also get

$$\frac{\partial^2 f}{\partial l^2} = \frac{\partial}{\partial l}(\xi^2\eta) = -2\xi^3 e\sin f, \tag{A.10a}$$

$$\frac{\partial^2}{\partial l^2}(a, n, s, c, e, \eta) = 0. \tag{A.10b}$$

A.2 Averaging of Orbital Dynamics

The simplified dynamical system eliminates the short-period variations from the full dynamical system. Even when the Deprit-Lie transformation is applied, an averaging of orbital dynamics is necessarily applied. In this section, useful mathematical approaches are summarized to make results in a closed-form.

The expansion of quantities of the form r^n and $1/r^n$ in terms of Fourier series coefficients is useful to carry out averaging equations [72].

$$(1+e\cos\tau)^n = \sum_{m=0}^{\infty} a_m^n \cos(m\tau) \tag{A.11a}$$

$$\frac{1}{(1+e\cos\tau)^n} = \sum_{m=0}^{\infty} b_m^n \cos(m\tau) \tag{A.11b}$$

where the coefficients are defined as follows:

$$a_0^n = c_0^n \tag{A.12a}$$

$$a_k^n = 2\left(\frac{e}{2}\right)^k c_k^n \tag{A.12b}$$

$$b_0^n = \frac{\sqrt{1-e^2}}{(1-e^2)^n} f_0^n \tag{A.12c}$$

$$b_k^n = (-1)^k 2\left(\frac{e}{2}\right)^k \frac{\sqrt{1-e^2}}{(1-e^2)^n} f_k^n \tag{A.12d}$$

The coefficients c_k^n and f_k^n have the general definitions:

$$c_k^n = \begin{cases} \sum_{l=0}^{[(n-k)/2]} \frac{n!}{l!(l+k)!(n-k-2l)!} \left(\frac{e}{2}\right)^{2l} & n \geq k \\ \\ 0 & n < k \end{cases} \tag{A.13a}$$

$$f_k^{n+1} = \begin{cases} \frac{(n-k)!(n+k)!}{(n!)^2} \sum_{l=0}^{[(n-k)/2]} \frac{n!}{l!(l+k)!(n-k-2l)!} \left(\frac{e}{2}\right)^{2l} & n+1 > k \\ \\ \frac{n-k}{n}(1-e^2) f_k^n + 2 f_{k-1}^{n+1} & n+1 \leq k \end{cases} \tag{A.13b}$$

$$f_k^1 = \left(\frac{2}{1+\sqrt{1-e^2}}\right)^k \tag{A.13c}$$

where $[a] = \text{floor}(a)$, integer part in a. A practical application of the above relations are given in Equation A.14 [44].

$$\overline{\left(\frac{a}{r}\right)^3} = \frac{1}{2\pi} \int_0^{2\pi} \left(\frac{a}{r}\right)^3 dM = (1-e^2)^{-3/2} \tag{A.14a}$$

$$\overline{\left(\frac{a}{r}\right)^3 \sin(2f)} = \overline{\left(\frac{a}{r}\right)^3 \cos(2f)} = 0 \tag{A.14b}$$

$$\overline{\left(\frac{a}{r}\right)^4 \cos(f)} = e(1-e^2)^{-5/2} \tag{A.14c}$$

$$\overline{\left(\frac{a}{r}\right)^4 \sin(f)} = \overline{\left(\frac{a}{r}\right)^4 \cos(3f)} = \overline{\left(\frac{a}{r}\right)^4 \sin(3f)} = 0 \tag{A.14d}$$

$$\overline{\left(\frac{a}{r}\right)^5} = (1-e^2)^{-7/2} \left(1 + \frac{3}{2}e^2\right) \tag{A.14e}$$

$$\overline{\left(\frac{a}{r}\right)^5 \cos(2f)} = \frac{3}{4} e^2 (1-e^2)^{-7/2} \tag{A.14f}$$

$$\overline{\left(\frac{a}{r}\right)^5 \sin(2f)} = \overline{\left(\frac{a}{r}\right)^5 \cos(4f)} = \overline{\left(\frac{a}{r}\right)^5 \sin(4f)} = 0 \tag{A.14g}$$

$$\tag{A.14h}$$

$$\overline{\left(\frac{a}{r}\right)^6} = (1-e^2)^{-9/2}\left(1+3e^2+\frac{3}{8}e^4\right) \tag{A.15a}$$

$$\overline{\left(\frac{a}{r}\right)^6\cos(f)} = 2e(1-e^2)^{-9/2}\left(1+\frac{3}{4}e^2\right) \tag{A.15b}$$

$$\overline{\left(\frac{a}{r}\right)^6\cos(2f)} = \frac{3}{2}e^2(1-e^2)^{-9/2}\left(1+\frac{1}{6}e^2\right) \tag{A.15c}$$

$$\overline{\left(\frac{a}{r}\right)^6\cos(3f)} = \frac{e^3}{2}(1-e^2)^{-9/2} \tag{A.15d}$$

$$\overline{\left(\frac{a}{r}\right)^6\cos(4f)} = \frac{e^4}{16}(1-e^2)^{-9/2} \tag{A.15e}$$

$$\overline{\left(\frac{a}{r}\right)^6\cos(jf)} = 0, \quad (j>4) \tag{A.15f}$$

(A.15g)

Note that the mean values of $\cos j\,f$ $(j=1,2,\ldots)$ with respect to the mean anomaly do not become zero, but it can be generalized as [44]

$$\overline{\cos jf} = \left[\frac{-e}{\left(1+\sqrt{1-e^2}\right)}\right]^j (1+j\sqrt{1-e^2}). \tag{A.16}$$

Throughout this section, we shortly present the useful mathematical expressions applied in this study. There are a lot of additional useful expressions that are not summarized here. We recommend to review a works by Ahmed [1], Jefferys [37], and Metris [55].

Appendix B

Taylor Series Expansion of Orbital Dynmaics

The state transition tensor is defined by taking higher-order terms in an expanded dynamical system. In general, the Taylor series expansion is applied to rewrite the dynamical system with respect to the initial conditions or the reference trajectory. Here, we summarize the Taylor series expansion for a single variable and multiple variables.

$$
\begin{aligned}
f(x^* + \delta x) &= \sum_{n=0}^{\infty} \frac{f^{(n)}(x)}{n!} \delta x^n \Bigg|_{x=x^*} \\
&= \left[f(x^*) + \frac{\partial f(x)}{\partial x}\delta x + \frac{1}{2!}\frac{\partial^2 f(x)}{\partial x^2}(\delta x)^2 + \frac{1}{3!}\frac{\partial^3 f(x)}{\partial x^3}(\delta x)^3 + \text{H.O.T.} \right]_{x=x^*}
\end{aligned}
$$

Figure B.1: Example of the Taylor series expansion for a single variable

Figure B.1 shows the basic form of the Taylor series expansion. As mentioned briefly, the state transition tensors take higher-order terms of this expansion for capturing the nonlinearity of the dynamical system. The traditional linearized mapping matrix, i.e., state transition matrix, uses only the first-order expansion plotted in red line. On the other hand, the state transition tensors include additional terms up to any desired order. As an example, we show the second and third-order state transition tensors which are depicted in green and blue, respectively.

The Taylor series expansion in multivariate phase space have much more complicate form since one has to consider correlation between each variable. Equation (B.1) shows the expansion when

the number of variables is two.

$$
\begin{aligned}
f(x,y) = {} & f(x^*,y^*) + \frac{\partial f}{\partial x}(x-x^*) + \frac{\partial f}{\partial y}(y-y^*) \\
& + \frac{1}{2!}\left[\frac{\partial^2 f}{\partial x^2}(x-x^*)^2 + \frac{2\partial^2 f}{\partial x \partial y}(x-x^*)(y-y^*) + \frac{\partial^2 f}{\partial y^2}(y-y^*)^2\right] \\
& + \frac{1}{3!}\left[\frac{\partial^3 f}{\partial x^3}(x-x^*)^3 + \frac{3\partial^3 f}{\partial x^2 \partial y}(x-x^*)^2(y-y^*) + \frac{3\partial^3 f}{\partial x \partial y^2}(x-x^*)(y-y^*)^2 + \frac{\partial^3 f}{\partial y^3}(y-y^*)^3\right] \\
& + \frac{1}{4!}\left[\frac{\partial^4 f}{\partial x^4}(x-x^*)^4 + \frac{4\partial^4 f}{\partial x^3 \partial y}(x-x^*)^3(y-y^*) + \frac{6\partial^4 f}{\partial x^2 \partial y^2}(x-x^*)^2(y-y^*)^2 + \right. \\
& \qquad \left. \frac{4\partial^4 f}{\partial x \partial y^3}(x-x^*)(y-y^*)^3 + \frac{\partial^4 f}{\partial y^4}(y-y^*)^4\right] + H.O.T.
\end{aligned}
\tag{B.1}
$$

We can use a compact expression of the Taylor series expansion with multivariate variables. Suppose that $\boldsymbol{x} = (x,\, y)$ and $\boldsymbol{a} = (a,\, b)$. Then, the expansion around $\boldsymbol{x}^* = \boldsymbol{a}$ becomes

$$
\begin{aligned}
f(x,\, y) = {} & f(a,\, b) + f_x(a,\, b)(x-a) + f_y(a,\, b)(y-b) \\
& + \frac{1}{2!}\left[f_{xx}(a,\, b)(x-a)^2 + 2f_{xy}(a,\, b)(x-a)(y-b) + f_{yy}(y-b)^2\right] + \ldots,
\end{aligned}
\tag{B.2}
$$

which is the compact form of Equation (B.1).

For any given number of variables, the Taylor series expansion can be generalized [4, 5, 57],. Let us assume that a given function $\boldsymbol{f}(\boldsymbol{x})$ is an infinitely differentiable and real function with $\boldsymbol{f},\, \boldsymbol{x} \in \mathbb{R}^n$. Then, the expansion about a point $\boldsymbol{x} = \boldsymbol{a}$ is defined as follows:

$$
f^i\left(x^1,\, \ldots,\, x^{\mathrm{N}}\right) = \sum_{j\geq 0} \frac{1}{j!}\left[\sum_{k=1}^{\mathrm{N}} \left(x^k - a^k\right) \frac{\partial}{\partial \xi}^{k}\right]^j f^i\left(\xi^1,\, \ldots,\, \xi^{\mathrm{N}}\right)\Bigg|_{\xi^m = a^m}, \tag{B.3}
$$

where ξ denotes a dummy variables. If one introduces a vector form, this expression becomes a compacter as:

$$
f^i(\boldsymbol{x}) = \sum_{j\geq 0} \frac{1}{j!}\left[\,(\boldsymbol{x}-\boldsymbol{a})\cdot \nabla_\xi\,\right]^j f^i(\boldsymbol{\xi})\Big|_{\boldsymbol{\xi}=\boldsymbol{a}}, \tag{B.4}
$$

where ∇ represents a gradient operator.

Appendix C

Lie Series and Transformation

C.1 Lie Series

C.1.1 Properties of the Lie Operator

The primary feature of the Deprit-Lie transformation is the application of the Lie transformation operator to construct a canonical transformation in expanded form.

Definition 18 (Lie Operator). For given two analytic functions $f(\boldsymbol{q}, \boldsymbol{p})$ and $\mathcal{W}(\boldsymbol{q}, \boldsymbol{p})$ bounded in a domain Ω of phase space, *Lie derivative* of the function f generated by $\mathcal{W}$ is defined as a form of the Poisson bracket $\{f, \mathcal{W}\}$, which we now denote by the symbol

$$\mathcal{L}_{\mathcal{W}} f = \{f, \mathcal{W}\} = \sum_{i=1}^{n} \left(\frac{\partial f}{\partial q_i} \frac{\partial \mathcal{W}}{\partial p_i} - \frac{\partial f}{\partial p_i} \frac{\partial \mathcal{W}}{\partial q_i} \right), \tag{C.1}$$

where $\mathcal{L}_{\mathcal{W}}$ is called the *Lie operator*.

The Lie operator satisfies below relations

$$\mathcal{L}_{\mathcal{W}}(\alpha \cdot f + \beta \cdot g) = \alpha \cdot \mathcal{L}_{\mathcal{W}} f + \beta \cdot \mathcal{L}_{\mathcal{W}} g, \tag{C.2a}$$

$$\mathcal{L}_{\mathcal{W}}(f \cdot g) = f \cdot \mathcal{L}_{\mathcal{W}} g + g \cdot \mathcal{L}_{\mathcal{W}} f, \tag{C.2b}$$

$$\mathcal{L}_{\mathcal{W}}\{f\,;\, g\} = \{f\,;\, \mathcal{L}_{\mathcal{W}} g\} + \{\mathcal{L}_{\mathcal{W}} f\,;\, g\}, \tag{C.2c}$$

based on the properties of the Poisson brackets shown in Equations (2.35) - (2.37), and

$$\mathcal{L}_{\mathcal{V}} \mathcal{L}_{\mathcal{W}} f = \mathcal{L}_{\{\mathcal{W}\,;\,\mathcal{V}\}} f + \mathcal{L}_{\mathcal{W}} \mathcal{L}_{\mathcal{V}} f, \tag{C.3}$$

from the *Jacobi's identity* in Equation for given real constants α, β, and any analytic function $V(\boldsymbol{q}, \boldsymbol{p})$ in the domain Ω. By recurrence over n, Equations (C.2a) - (C.2c) can be extended to become

$$\mathcal{L}_{\mathcal{W}}^{n}(\alpha \cdot f + \beta \cdot g) = \alpha \cdot \mathcal{L}_{\mathcal{W}}^{n} f + \beta \cdot \mathcal{L}_{\mathcal{W}}^{n} g, \tag{C.4a}$$

$$\mathcal{L}_{\mathcal{W}}^{n}(f \cdot g) = \sum_{0 \le m \le n} \binom{n}{m} \mathcal{L}_{\mathcal{W}}^{m} f \cdot \mathcal{L}_{\mathcal{W}}^{n-m} g, \tag{C.4b}$$

$$\mathcal{L}_{\mathcal{W}}^{n}\{f\,;\, g\} = \sum_{0 \le m \le n} \binom{n}{m} \{\mathcal{L}_{\mathcal{W}}^{m} f\,;\, \mathcal{L}_{\mathcal{W}}^{n-m} g\}, \tag{C.4c}$$

where

$$\binom{n}{m} = \frac{n!}{(n-m)!\, m!}$$

is the binomial coefficient.

C.1.2 Generating Function for the Inverse Transformation

Let the function $\mathcal{W}(y, Y)$ satisfy conditions sufficient to ensure a relation

$$\exp(\epsilon \mathcal{L}_{\mathcal{W}}) f = \sum_{n \ge 0}^{\infty} \frac{\epsilon^n}{n!} \mathcal{L}_{\mathcal{W}}^{n} f, \tag{C.5}$$

one can get a derivative

$$\frac{d}{d\epsilon} \exp(\epsilon \mathcal{L}_{\mathcal{W}}) f = \exp(\epsilon \mathcal{L}_{\mathcal{W}}) \mathcal{L}_{\mathcal{W}} f$$

and express in a general form, called the *commutation theorem*[7] as follows.

Theorem 1 (The Commutation Theorem) If $\boldsymbol{z} \equiv (\boldsymbol{q}, \boldsymbol{p})$ denotes the generic point of Ω and $Z_i = \exp(\epsilon \mathcal{L}_{\mathcal{W}}) z_i$ $(i = 1, 2, \ldots, 2n)$, then, for any function $F(\boldsymbol{z})$ analytic in the domain Ω, one has

$$\exp(\epsilon \mathcal{L}_{W}) F(z_1,\, z_2,\, \ldots, z_{2n}) = F(Z_1,\, Z_2,\, \ldots, Z_{2n}), \tag{C.6}$$

and, in particular,

$$\exp(\epsilon \mathcal{L}_{\mathcal{W}})(f,\, g) = \big(\exp(\epsilon \mathcal{L}_{\mathcal{W}}) f,\, \exp(\epsilon \mathcal{L}_{\mathcal{W}}) g\big). \tag{C.7}$$

If one differentiate the functions Z_i with respect to ϵ, then

$$\frac{dZ_i}{d\epsilon} = \exp(\epsilon\mathcal{L}_{\mathcal{W}})(\mathcal{L}_{\mathcal{W}} Z_i) = \exp(\epsilon\mathcal{L}_{\mathcal{W}})\,\Theta_i(\boldsymbol{z}). \tag{C.8}$$

By applying the commutation theorem,

$$\frac{dZ_i}{d\epsilon} = \exp(\epsilon\mathcal{L}_{\mathcal{W}})\,\Theta_i(Z_1,\, Z_2,\, \ldots,\, Z_{2n}). \tag{C.9}$$

Therefore we can say that the solutions of Equation (C.9), which satisfy the initial conditions $Z_i|_{\epsilon=0} = z_i$, are represented by the Lie series $Z_i = \exp(\epsilon\mathcal{L}_{\mathcal{W}})z_i$. Lastly, by Equation (C.7), *Lie's theorem* is defined as follows.

Theorem 2 (The Lie's Theorem) Let the transformation $\boldsymbol{z} = \boldsymbol{z}(\boldsymbol{\zeta})$ be given, from the $2n$-dimensional vector $\boldsymbol{z} = (\boldsymbol{q},\, \boldsymbol{p})$, where q_i and p_i are generalized coordinates and conjugate momenta, to the $2n$-dimensional vector $\boldsymbol{\zeta} = (\boldsymbol{\xi},\, \boldsymbol{\eta})$. If ϵ is a constant parameter and an analytic function $\mathcal{W}(\boldsymbol{z})$ exists such that the series

$$\boldsymbol{\zeta}(\epsilon) = \exp(\epsilon\mathcal{L}_{\mathcal{W}})\boldsymbol{z} \tag{C.10}$$

converges on a domain of the space $\boldsymbol{z}$, then the transformation $\boldsymbol{z} = \boldsymbol{z}(\boldsymbol{\zeta})$ is a canonical.

The function $\mathcal{W}$ is the *generating function* for the canonical transformation in Equation (C.10). If an analytic function $\mathcal{V}$ is sufficient to satisfy the inverse transformation $\boldsymbol{z} = \exp(\epsilon\mathcal{L}_{\mathcal{V}})\boldsymbol{\zeta}$, then

$$\begin{aligned} \exp(\epsilon\mathcal{L}_{\mathcal{V}})\boldsymbol{\zeta} &= \exp(\epsilon\mathcal{L}_{\mathcal{V}})\,[\,\exp(\epsilon\mathcal{L}_{\mathcal{W}})\boldsymbol{z}\,] \\ &= \exp\,[\,\epsilon(\mathcal{L}_{\mathcal{W}} + \mathcal{L}_{\mathcal{V}})\,]\,\boldsymbol{z} = \boldsymbol{z}. \end{aligned} \tag{C.11}$$

Therefore, the operator $\exp\,[\,\epsilon(\mathcal{L}_{\mathcal{W}} + \mathcal{L}_{\mathcal{V}})\,]$ must be the identity operator. i.e., : that is $\mathcal{L}_{\mathcal{W}} + \mathcal{L}_{\mathcal{V}} = 0$, from which $\mathcal{V} = -\mathcal{W}$.

C.2 Lie Transformation

The *Lie transfromation* is a "contaminated Lie series" by the methods of perturbation theory. The canonical transformation represented by the Lie series will have to differ by a small amount from the identity transformation. In particular, Deprit[19] proposed this transformation by defining

the generating functions $\mathcal{W}$ as a function of the generalized coordinates, conjugate momenta, and a smal parameter ϵ. For a given function $\mathcal{W}(\boldsymbol{\zeta}\,;\,\epsilon)$, the Lie transformation operator[19] is defined by

$$f \;\rightarrow\; \Delta_{\mathcal{W}} f = \mathcal{L}_{\mathcal{W}}\, f + \frac{\partial f}{\partial \epsilon}. \tag{C.12}$$

C.2.1 Properties of the Lie Transformation Operator

The transformation operator also has similar properties to the Lie series operator as follows.

$$\Delta_{\mathcal{W}}(\alpha \cdot f + \beta \cdot g) = \alpha \Delta_{\mathcal{W}} f + \beta \Delta_{\mathcal{W}} g, \tag{C.13a}$$

$$\Delta_{\mathcal{W}}(f\, g) = f \cdot \Delta_{\mathcal{W}} g + g \cdot \Delta_{\mathcal{W}} f, \tag{C.13b}$$

$$\Delta_{\mathcal{W}}\{f\,;\,g\} = \{\Delta_{\mathcal{W}} f\,;\,g\} + \{f\,;\,\Delta_{\mathcal{W}} g\}, \tag{C.13c}$$

$$\Delta_{\mathcal{V}}\Delta_{\mathcal{W}} = \Delta_{\mathcal{W}}\Delta_{\mathcal{V}} + \mathcal{L}_{\{\mathcal{W}\,;\,\mathcal{V}\}} + \mathcal{L}_{\partial\mathcal{W}/\partial\epsilon - \partial\mathcal{V}/\partial\epsilon}. \tag{C.13d}$$

As well as there exist similar properties in a recursive application of the operator

$$\Delta^n_{\mathcal{W}}(\alpha \cdot f + \beta \cdot g) = \alpha \cdot \Delta^n_{\mathcal{W}} f + \beta \cdot \Delta^n_{\mathcal{W}} g, \tag{C.14a}$$

$$\Delta^n_{\mathcal{W}}(f \cdot g) = \sum_{0 \le m \le n} \binom{n}{m} \Delta^m_{\mathcal{W}} f \cdot \Delta^{n-m}_{\mathcal{W}} g, \tag{C.14b}$$

$$\Delta^n_{\mathcal{W}}\{f\,;\,g\} = \sum_{0 \le m \le n} \binom{n}{m} \{\Delta^m_{\mathcal{W}} f\,;\,\Delta^{n-m}_{\mathcal{W}} g\}, \tag{C.14c}$$

In order to simplify the expressions in Equations (C.14a) - (C.14c), the function of $\boldsymbol{\zeta}$ which results from $\epsilon = 0$ in the expression $\Delta^n_{\mathcal{W}(\boldsymbol{\zeta}\,;\,\epsilon)} f(\boldsymbol{\zeta}\,;\,\epsilon)$, will be more simply written as $f^{(n)}(\boldsymbol{\zeta}\,;\,0)$.

C.2.2 Specific Derivation of the Lie Transformation Operator

Consider the formal power series

$$E_{\mathcal{W}}(f) = \sum_{n \ge 0} \frac{1}{n!} \epsilon^n f^{(n)}(\boldsymbol{\zeta}\,;\,\epsilon)\bigg|_{\epsilon=0} = \sum_{n \ge 0} \frac{1}{n!} \epsilon^n f^{(n)}(\boldsymbol{\zeta}; 0). \tag{C.15}$$

The mapping $E_{\mathcal{W}} : f \longmapsto E_{\mathcal{W}}(f)$ is called the Lie transformation generated by $\mathcal{W}$ [19]. Similar to the properties given in Equations (C.14a) - (C.14c), one can obtain

$$E_{\mathcal{W}}(\alpha \cdot f + \beta \cdot g) = \alpha \cdot E_{\mathcal{W}}(f) + \beta \cdot E_{\mathcal{W}}(g), \tag{C.16a}$$

$$E_{\mathcal{W}}(f \cdot g) = E_{\mathcal{W}}(f) \cdot E_{\mathcal{W}}(g), \tag{C.16b}$$

$$E_{\mathcal{W}}\{f\,;\, g\} = \{E_{\mathcal{W}}(f)\,;\, E_{\mathcal{W}}(g)\}. \tag{C.16c}$$

Equation (C.16c) defines the formal power series

$$\boldsymbol{\zeta}' = E_{\mathcal{W}}(\boldsymbol{\zeta}) = \sum_{n=0}^{\infty} \frac{1}{n!} \epsilon^n \boldsymbol{\zeta}^{(n)}(\boldsymbol{\zeta}\,;\, 0) \tag{C.17}$$

define a canonical transformation $(\boldsymbol{\zeta},\, \epsilon) \longmapsto \boldsymbol{\zeta}'$. If $\boldsymbol{\zeta}$ is a vector $(\boldsymbol{\xi},\, \boldsymbol{\eta})$, where $\boldsymbol{\xi}$ and $\boldsymbol{\eta}$ represent the generalized coordinates and the conjugate momenta, Deprit demonstrated Equation (C.17) can be interpreted based on a condition $\boldsymbol{\zeta}' = \boldsymbol{\zeta}$ at the point $\epsilon = 0$ as follows [19]:

$$\frac{d\boldsymbol{\xi}}{d\epsilon} = \frac{\partial}{\partial \boldsymbol{\eta}} \mathcal{W}(\boldsymbol{\xi},\, \boldsymbol{\eta}\,;\, \epsilon), \;\; \frac{d\boldsymbol{\eta}}{d\epsilon} = -\frac{\partial}{\partial \boldsymbol{\xi}} \mathcal{W}(\boldsymbol{\xi},\, \boldsymbol{\eta}\,;\, \epsilon) \tag{C.18}$$

Then, from Equations (C.14a) - (C.14c), we also obtain the relations

$$\frac{dx}{d\epsilon} = (x; W) = \Delta_w x, \quad \frac{d^2x}{d\epsilon^2} = ((x; W); W) + \left(x; \frac{\partial W}{\partial \epsilon}\right) = \Delta_w^2 x, \quad \ldots \tag{C.19}$$

Consequently, an expansion of $\boldsymbol{\zeta}'$ in power series of a small parameter ϵ can be expressed in Equation (C.17). For a given function $f\,(\boldsymbol{\xi}',\, \boldsymbol{\eta}',\, \epsilon)$, Equation (C.18) could be generalized along the solution $(\boldsymbol{\xi}'(\boldsymbol{\xi},\, \boldsymbol{\eta},\, \epsilon),\, \boldsymbol{\eta}'(\boldsymbol{\xi},\, \boldsymbol{\eta},\, \epsilon))$ as

$$\frac{df}{d\epsilon} = \Delta_{\mathcal{W}} f, \quad \frac{d^2 f}{d\epsilon^2} = \Delta_{\mathcal{W}}^2 f, \quad \ldots. \tag{C.20}$$

In the same idea, this becomes

$$f\left(\boldsymbol{\xi}'(\boldsymbol{\xi},\, \boldsymbol{\eta},\, \epsilon),\, \boldsymbol{\eta}'(\boldsymbol{\xi},\, \boldsymbol{\eta},\, \epsilon)\right) = \sum_{n=0}^{\infty} \frac{1}{n!} \epsilon^n \left(\Delta_{\mathcal{W}}^n f\right)_{\epsilon=0}, \tag{C.21}$$

which can be expressed symbolically in

$$f(E_{\mathcal{W}}(\boldsymbol{\xi}),\, E_{\mathcal{W}}(\boldsymbol{\eta})\,;\, \epsilon) = (E_{\mathcal{W}}(f))(\boldsymbol{\xi},\, \boldsymbol{\eta}\,;\, \epsilon). \tag{C.22}$$

Equation (C.22) shows the rule to convert a function of ($\boldsymbol{\xi}'$, $\boldsymbol{\eta}'$, ϵ) into that of ($\boldsymbol{\xi}$, $\boldsymbol{\eta}$, ϵ) through the canonical transformation given in Equation (C.18).

$$
\begin{aligned}
f\left(\boldsymbol{\xi}'(\boldsymbol{\xi},\,\boldsymbol{\eta},\,\epsilon),\,\boldsymbol{\eta}'(\boldsymbol{\xi},\,\boldsymbol{\eta},\,\epsilon)\right) &= f(E_{\mathcal{W}}(\boldsymbol{\xi}), E_{\mathcal{W}}(\boldsymbol{\eta});\epsilon) \\
&= (E_{\mathcal{W}} f)(\boldsymbol{\xi},\boldsymbol{\eta};\epsilon) \\
&= \sum_{n\geq 0} \frac{1}{n!}\epsilon^n \underbrace{(\Delta^n_{\mathcal{W}} f)_{\epsilon=0}}_{f^{(n)}} \\
&= \underbrace{\left(\Delta^0_{\mathcal{W}} f\right)_{\epsilon=0}}_{f^{(0)}} + \frac{1}{1!}\epsilon \underbrace{\left(\Delta^1_{\mathcal{W}} f\right)_{\epsilon=0}}_{f^{(1)}} + \frac{1}{2!}\epsilon^2 \underbrace{\left(\Delta^2_{\mathcal{W}} f\right)_{\epsilon=0}}_{f^{(2)}} + \frac{1}{3!}\epsilon^3 \underbrace{\left(\Delta^3_{\mathcal{W}} f\right)_{\epsilon=0}}_{f^{(3)}} + \dots
\end{aligned}
\tag{C.23}
$$

Each term in the series expansion in Equation (C.18), e.g., $\boldsymbol{\zeta}^{(k)}$, can be defined at the point $\epsilon = 0$ as follows:

$$
\begin{aligned}
&\Delta^{(k)}_W f = \sum_{n\geq 0} \frac{1}{n!}\epsilon^n f^{(k)}_n \\
&\Rightarrow \Delta^0_W = f^{(0)}_0 + \frac{1}{1!}\epsilon f^{(0)}_1 + \frac{1}{2!}\epsilon f^{(0)}_2 + \frac{1}{3!}\epsilon f^{(0)}_3 + \dots = f^{(0)}_0 = f^{(0)} \quad \text{where, } \epsilon = 0 \\
&\Rightarrow \Delta^1_W = f^{(1)}_0 + \frac{1}{1!}\epsilon f^{(1)}_1 + \frac{1}{2!}\epsilon f^{(1)}_2 + \frac{1}{3!}\epsilon f^{(1)}_3 + \dots = f^{(1)}_0 = f^{(1)} \quad \text{where, } \epsilon = 0 \\
&\qquad\qquad\qquad\qquad \vdots \\
&\Rightarrow \Delta^k_W = f^{(k)}_0 + \frac{1}{1!}\epsilon f^{(k)}_1 + \frac{1}{2!}\epsilon f^{(k)}_2 + \frac{1}{3!}\epsilon f^{(k)}_3 + \dots = f^{(k)}_0 = f^{(k)} \quad \text{where, } \epsilon = 0
\end{aligned}
\tag{C.24}
$$

Thus, the symbolic expression, Equation (C.22), can be rewritten by using Equation C.24 in

$$
f\left(\boldsymbol{\xi}'(\boldsymbol{\xi},\,\boldsymbol{\eta},\,\epsilon),\,\boldsymbol{\eta}'(\boldsymbol{\xi},\,\boldsymbol{\eta},\,\epsilon)\right) = f^{(0)}_0 + \frac{1}{1!}\epsilon f^{(1)}_0 + \frac{1}{2!}\epsilon^2 f^{(2)}_0 + \frac{1}{3!}\epsilon^3 f^{(3)}_0 + \dots \tag{C.25}
$$

From the above discussion, the generalized expression describing the Deprit's triangle, Equation (4.6), is obtained from a given formal series, Equations (4.2). Here we present a detailed procedure of this mapping. Suppose that we have

$$
W(\boldsymbol{y},\boldsymbol{Y};\epsilon) = \sum_{n\geq 0} \frac{1}{n!}\epsilon^n W_{n+1}(\boldsymbol{y},\boldsymbol{Y}), \tag{C.26a}
$$

$$
f(\boldsymbol{y},\boldsymbol{Y};\epsilon) = \sum_{n\geq 0} \frac{1}{n!}\epsilon^n f_n(\boldsymbol{y},\boldsymbol{Y}). \tag{C.26b}
$$

Then, we get each term of the right-hand side on Equation (C.12) as

$$\frac{\partial f}{\partial \epsilon}(\boldsymbol{y}, \boldsymbol{Y}; \epsilon) = \sum_{n \geq 0} \frac{1}{n!} \epsilon^n f_{n+1}(\boldsymbol{y}, \boldsymbol{Y}), \tag{C.27a}$$

$$\mathcal{L}_{\mathcal{W}} f(\boldsymbol{y}, \boldsymbol{Y}; \epsilon) = \sum_{n \geq 0} \frac{1}{n!} \epsilon^n \sum_{0 \leq m \leq n} \binom{n}{m} L_{m+1} f_{n-m}(\boldsymbol{y}, \boldsymbol{Y}). \tag{C.27b}$$

Let us use a concise form $\mathcal{L}_{\mathcal{W}_p} = L_p$ for convenience. Trom Equations (C.23) and (C.27), the first transformation of a function f is

$$\Delta_{\mathcal{W}} f = \Delta^1_{\mathcal{W}} f = \mathcal{L}_{\mathcal{W}} f(\boldsymbol{y}, \boldsymbol{Y}; \epsilon) + \frac{\partial f}{\partial \epsilon}(\boldsymbol{y}, \boldsymbol{Y}; \epsilon) = \sum_{n \geq 0} \frac{1}{n!} \epsilon^n f_n^{(1)}(\boldsymbol{y}, \boldsymbol{Y}), \tag{C.28}$$

Then, by an iteration,

$$\begin{aligned} \Delta^2_{\mathcal{W}} f &= \sum_{n \geq 0} \frac{1}{n!} \epsilon^n f_n^{(2)}(\boldsymbol{y}, \boldsymbol{Y}), \\ &\vdots \\ \Delta^k_{\mathcal{W}} f &= \sum_{n \geq 0} \frac{1}{n!} \epsilon^n f_n^{(k)}(\boldsymbol{y}, \boldsymbol{Y}). \end{aligned} \tag{C.29}$$

Since previous papers [19, 42] only provides or applies the generalized expression of this iteration, we address details as follows:

$$f(\boldsymbol{y}, \boldsymbol{Y}; \epsilon) = f_0(\boldsymbol{y}, \boldsymbol{Y}) + \frac{1}{1!}\epsilon f_1(\boldsymbol{y}, \boldsymbol{Y}) + \frac{1}{2!}\epsilon^2 f(\boldsymbol{y}, \boldsymbol{Y}) + \frac{1}{3!}\epsilon^3 f(\boldsymbol{y}, \boldsymbol{Y}) + \dots \tag{C.30a}$$

$$\begin{aligned} \Delta^1_{\mathcal{W}} f(\boldsymbol{y}, \boldsymbol{Y}; \epsilon) &= \Delta^1_{\mathcal{W}} f_0(\boldsymbol{y}, \boldsymbol{Y}) + \frac{1}{1!}\epsilon \left(\Delta^1_{\mathcal{W}} f(\boldsymbol{y}, \boldsymbol{Y})\right) + \frac{1}{2!}\epsilon^2 \left(\Delta^1_{\mathcal{W}} f(\boldsymbol{y}, \boldsymbol{Y})\right) + \frac{1}{3!}\epsilon^3 \left(\Delta^1_{\mathcal{W}} f(\boldsymbol{y}, \boldsymbol{Y})\right) + \dots \\ &= \underbrace{\left(\frac{\partial f_0}{\partial \epsilon} + \mathcal{L}_{\mathcal{W}} f_0\right)}_{f_0^{(1)}} + \underbrace{\frac{1}{1!}\epsilon \left(\frac{\partial f_1}{\partial \epsilon} + \mathcal{L}_{\mathcal{W}} f_1\right)}_{f_1^{(1)}} + \underbrace{\frac{1}{2!}\epsilon^2 \left(\frac{\partial f_2}{\partial \epsilon} + \mathcal{L}_{\mathcal{W}} f_2\right)}_{f_2^{(1)}} + \underbrace{\frac{1}{3!}\epsilon^3 \left(\frac{\partial f_3}{\partial \epsilon} + \mathcal{L}_{\mathcal{W}} f_3\right)}_{f_3^{(1)}} + \dots \\ &= \sum_{n \geq 0} \frac{1}{n!} \epsilon^n f_n^{(1)} \end{aligned} \tag{C.30b}$$

Note that we consider the expansion at the point of $\epsilon = 0$. Then, only one term $f_0^{(1)}$ is remained in Equation C.30b, which can be generalized as

$$E_{\mathcal{W}} f = (\Delta^k_{\mathcal{W}} f)_{\epsilon=0} = \left[f_0^{(k)} + \frac{1}{1!}\epsilon f_1^{(k)} + \frac{1}{2!}\epsilon^2 f_2^{(k)} + \frac{1}{3!}\epsilon^3 f_3^{(k)} + \dots + \frac{1}{n!}\epsilon^n f_n^{(k)} + \dots \right]_{\epsilon=0} = f_0^{(k)}. \tag{C.31}$$

Therefore, higher-order transformations, i.e., $f_n^{(k)}$, are regularized as ($n \geq 0$)

$$f_n^{(k)}(\boldsymbol{y}, \boldsymbol{Y}) = f_{n+1}^{(k-1)} + \sum_{0 \leq m \leq n} \binom{n}{m} \mathcal{L}_{m+1} f_{n-m}^{(k-1)}, \tag{C.32}$$

which describes the Deprit's triangle. In particular, when $n = 0$, we can simply get

$$f^{(k)}(\boldsymbol{y}, \boldsymbol{Y}; 0) = f_0^{(k)}(\boldsymbol{y}, \boldsymbol{Y}; \epsilon) = f_1^{(k-1)} + \mathcal{L}_1 f_0^{(k-1)}. \tag{C.33}$$

Equation C.34 shows some examples of the regulation.

$$\begin{aligned} f_2^{(1)} &= f_3 + \mathcal{L}_1 f_2 + 2\mathcal{L}_2 f_1 + \mathcal{L}_3 f_0 \\ f_1^{(2)} &= f_2^{(1)} + \mathcal{L}_1 f_1^{(1)} + \mathcal{L}_2 f_0 \\ f^{(3)} &= f_0^{(3)} = f_1^{(2)} + \mathcal{L}_1 f_1 \\ &\vdots \end{aligned} \tag{C.34}$$

In summary, as shown in Equations C.25 and C.31, only the terms with 0 in the subscript, i.e., $f_0^{(k)}$, are necessary results for the transformation. Thus, we can mention that the others, i.e., $f_n^{(k)}$ ($n \neq 0$), are intermediate terms to calculate the last expressions, $f_0^{(k)}$.

Appendix D

Simplification and Normalization

In Chapter 6, we transform a given Hamiltonian with two steps, simplification and normalization, in order to eliminate the short-period variations. These approaches are originally proposed by Deprit [18, 20]. This section briefly summarizes each method with a focus on a practical implementation.

D.1 Simplification

The elimination of the parallax [18] invented by Deprit is the basis of simplification. This idea does not remove the coordinates from the Hamiltonian, but the Hamiltonian is reduced to a simpler one. We summarize a role of this method with the abstract in [18]: *"When the perturbation affecting a Keplerian motion is proportional to* $r^{-n}\,(n \geq 3)$*, a canonical transformation of Lie type will convert the system into one in which the perturbation is proportional to* r^{-2}*. Because it removes parallactic factors, the transformation is called the elimination of the parallax."*

We apply the Deprit-Lie transformation methods by replacing the polar-nodal variables, used in the original paper [18], with the Delaunay variables [49]. The primary technical contribution of the simplification is to reduce computations needed for performing further normalizations drastically. A main idea of this approach can be realized with

$$\frac{1}{r^m} \;\longmapsto\; \frac{1}{r^2}\left(\frac{1+e\,\cos f}{a\,(1-e^2)}\right)^{m-2}, \tag{D.1}$$

where r, a, e and f represent a distance from the Earth's center of mass to an orbiting object, the semi-major axis, the eccentricity, and the true anomaly. A term $\sqrt{1-e^2}$ is usually replaced with

η. Then, required computations in the transformation, such as integrations, can be simplified by

$$a^2\eta\, dl = r^2\, , df, \tag{D.2}$$

where l denotes the mean anomaly. Let us take the perturbation due to the earth oblateness as an example.

$$\mathcal{H}_{\mathrm{J}_2} = \frac{1}{2}\frac{\mu\,\alpha}{r^3}\mathrm{J}_2\left[\frac{3}{2}s^2 - \frac{3}{2}s^2\cos(2f+2g) - 1\right]. \tag{D.3}$$

In an implemented manipulator, Equation (D.1) converts the simplification is applied as follows:

$$\begin{aligned}\mathcal{H}_{\mathrm{J}_2} &= \frac{1}{2}\frac{\mu}{r}\left(\frac{\alpha}{r}\right)^2\mathrm{J}_2\left[\frac{3}{2}s^2 - \frac{3}{2}s^2\cos(2f+2g) - 1\right] \\ &= \frac{\mu}{2}\left(\frac{\alpha}{r}\right)^2\mathrm{J}_2\left[\frac{3}{2}s^2 - \frac{3}{2}s^2\cos(2f+2g) - 1\right]\left(\frac{1+e\,\cos f}{a\,\eta^2}\right).\end{aligned} \tag{D.4}$$

Then, by following the Deprit-Lie transformation procedure, one can redefine the given Hamiltonian to have $(1/r)^n$ $(n \leq 2)$ and get the generating functions, $\mathcal{W}_s$, from the homological equation. Figure D.1 depicts how the simplification and normalization are connected. The transformed Hamil-

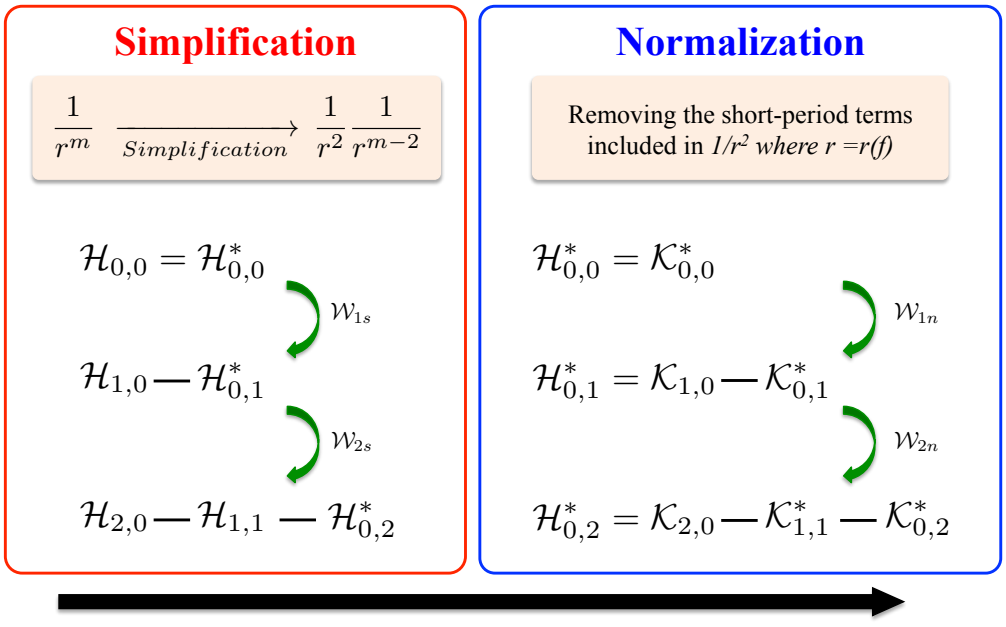

Figure D.1: Simplification and Normalization: the simplification (red box) reduces an order of $(1/r)$ in the given Hamiltonian to make calculations simpler. The normalization, a following step, removes the coordinates from the Hamiltonian, e.g., elimination of the short-period variations.

tonian in the simplification step (red box), $\mathcal{H}^*_{0,0}$, $\mathcal{H}^*_{0,1}$, and $\mathcal{H}^*_{0,2}$, are obtained by extracting terms

independent of the true anomaly from Equation (D.4). Then, one can get the generating functions by solving the homological equations. Let us use a subscript s to express the generating function for the simplification.

D.2 Normalization

A normalization represents a procedure to eliminate all the coordinates, i.e., angular variables, sequentially from the Hamiltonian [20, 48, 49]. The normalized Hamiltonian, i.e., $\mathcal{K}_{0,i}^{*}$ in Figure D.1, is the kernel of the Lie derivative about the unperturbed solution (the Keplerian motion), which is

$$\ker(\mathcal{L}_0) = \{F(l,\, g,\, h,\, L,\, G,\, H) \,|\, \mathcal{L}_0(F) = 0\}\,. \tag{D.5}$$

In summary, through the normalization, the Delaunay action L, an integral of $\mathcal{H}_0$, generates an infinitesimal contact transformation [20]. This local map replaces a perturbed Hamiltonian $\mathcal{R}$ by $\mathcal{R}'$ such that $\mathcal{R}' \in \ker(\mathcal{L}_0)$. Note that the normalization (green box) allows reducing the number of degrees of freedom by one unit, e.g., $\mathcal{K} = \mathcal{K}(-,\, g,\, h,\, L,\, G,\, H)$. This normalization can be simply carried out by

$$\mathcal{K}_n = \left\langle \widetilde{\mathcal{H}}_{0,n} \right\rangle = \frac{1}{2\pi} \int_0^{2\pi} \widetilde{\mathcal{H}}_{0,n}\, dl, \tag{D.6}$$

where $\widetilde{\mathcal{H}}_{0,n}$ is a combination of previous terms as discussed in Equation (4.9). The normalization can be preceded by a preparatory simplification which eliminates these kinds of terms, thus notably easing the normalization process.

We take special note that the generating function, $\mathcal{W}$, for the elimination of the short-period variations, i.e., STEP1 in Figure 4.2, is obtained by

$$\mathcal{W} = \mathcal{W}_{i\,s} + \mathcal{W}_{i\,n}. \tag{D.7}$$

Appendix E

Analytic Solutions and Generating Functions of the Problem of the Artificial Satellite Theory

The third-order analytic solutions after eliminating all periodic variations are given below:

$$
\begin{aligned}
\dot{l} = n &- \frac{3\alpha^2 \mathrm{J}_2 \mu \left(3s^2-2\right)}{4a^5\eta^3 n} - \frac{\alpha^4 \mathrm{J}_2^2 n}{128a^4 e\eta^{11}} \Big[4e^5 \left(2-3s^2\right)^2 - 16e^4 \left(2-3s^2\right)^2 - 16e^2 \left(2\eta^2-1\right)\left(2-3s^2\right)^2 \\
&-e\left\{48\eta^5\left(2-3s^2\right)^2 - 8\eta^2\left(2-3s^2\right)^2 + 4\left(2-3s^2\right)^2 + 15\eta^6\left(5s^4+8s^2-8\right) + \eta^4\left(351s^4-768s^2+376\right)\right\} \\
&-16\eta^2\left(\eta^2-1\right)\left(2-3s^2\right)^2\Big] + \frac{\alpha^6 \mathrm{J}_2^3 n}{2048a^6\left(5c^2-1\right)^3\eta^{11}} \Big[20c^6 \left\{84\eta^4 s^2\left(225s^4-315s^2+98\right)\right. \\
&-1650\eta^3\left(15s^6+14s^4-40s^2+16\right) + 5\eta^2\left(50175s^6-85790s^4+43048s^2-10000\right) \\
&\left.-4500\eta\left(21s^6-62s^4+56s^2-16\right) - 9\left(37975s^6-77590s^4+51408s^2-13200\right)\right\} \\
&-3c^4\left\{7\eta^4 s^2\left(14625s^6-21600s^4+5740s^2+1568\right) - 6600\eta^3\left(15s^6+14s^4-40s^2+16\right)\right. \\
&-18000\eta\left(21s^6-62s^4+56s^2-16\right) - 10\eta^2\left(19125s^8-141150s^6+196360s^4-89232s^2+20000\right) \\
&\left.+3\left(23625s^8-504900s^6+959780s^4-620032s^2+158400\right)\right\} \\
&+3c^2\left\{7\eta^4 s^4\left(1125s^6+2625s^4-7420s^2+3724\right) - 1320\eta^3\left(15s^6+14s^4-40s^2+16\right)\right. \\
&-3600\eta\left(21s^6-62s^4+56s^2-16\right) - 10\eta^2\left(2250s^{10}+1425s^8-30350s^6+41848s^4-18160s^2+4000\right) \\
&\left.+9\left(1125s^{10}+75s^8-34040s^6+64844s^4-41440s^2+10560\right)\right\} - 63\eta^4 s^6\left(14-15s^2\right)^2 \\
&+264\eta^3\left(15s^6+14s^4-40s^2+16\right) + 720\eta\left(21s^6-62s^4+56s^2-16\right) \\
&+20\eta^2\left(1350s^{10}-2520s^8-1047s^6+3734s^4-1816s^2+400\right) \\
&-9\left(1125s^{10}-2100s^8-5240s^6+12616s^4-8288s^2+2112\right)\Big], \qquad \text{(E.1a)}
\end{aligned}
$$

$$\dot{g} = -\frac{3\alpha^2 \mathrm{J}_2 n \left(5s^2-4\right)}{4a^2\eta^4 n} + \frac{\alpha^4 \mathrm{J}_2^2 n}{128a^4 e\eta^{12}} \left[4e^5 \left(135s^4-192s^2+68\right) \right.$$

$$-16e^4 \left(135s^4-192s^2+68\right) - 16e^2 \left(3s^2-2\right) \left(-36\eta^2+\left(48\eta^2-45\right)s^2+34\right)$$

$$+e\left\{-8\left(21\eta^6-72\eta^5-131\eta^4-68\eta^2+34\right)+15\left(9\eta^6+72\eta^5+41\eta^4+72\eta^2-36\right)s^4\right.$$

$$\left.+12\left(9\eta^6-132\eta^5-151\eta^4-128\eta^2+64\right)s^2\right\} - 16\eta^2\left(\eta^2-1\right)\left(2-3s^2\right)^2 \Big]$$

$$+\frac{\alpha^6 \mathrm{J}_2^3 n}{2048a^6\eta^{12}\left(4-5s^2\right)^4}\left[-200c^{10}\left\{8\left(147\eta^4+1375\eta^3+5381\eta^2-7875\eta-19278\right)\right.\right.$$

$$\left.+225\left(36\eta^4-55\eta^3+669\eta^2-315\eta-1519\right)s^4-20\left(378\eta^4+385\eta^3+8579\eta^2-6975\eta-23277\right)s^2\right\}$$

$$+20c^8\left\{16\left(294\eta^4-5500\eta^3-6013\eta^2+24750\eta+58719\right)+375\left(486\eta^4-440\eta^3+5409\eta^2-3150\eta\right.\right.$$

$$\left.-16331\right)s^6-50\left(4266\eta^4+5060\eta^3+45783\eta^2-58410\eta-196935\right)s^4+20\left(2163\eta^4+18920\eta^3\right.$$

$$\left.\left.+20792\eta^2-101700\eta-233595\right)s^2\right\}+c^6\left\{-64\left(147\eta^4-35750\eta^3-78744\eta^2+177750\eta+428097\right)\right.$$

$$-16875\left(75\eta^4-278\eta^2+219\right)s^8+6000\left(42\eta^4+440\eta^3-7239\eta^2+3150\eta+17717\right)s^6$$

$$+100\left(16089\eta^4+30580\eta^3+564282\eta^2-523980\eta-1904331\right)s^4-160\left(4473\eta^4+41690\eta^3\right.$$

$$\left.+136992\eta^2-273150\eta-705945\right)s^2\right\}+c^4\left\{-640\left(1210\eta^3+2921\eta^2-6120\eta-14781\right)\right.$$

$$+16875\left(3\eta^4-20\eta^2+21\right)s^{10}+2250\left(327\eta^4-938\eta^2+603\right)s^8-300\left(3783\eta^4+2640\eta^3-52990\eta^2\right.$$

$$\left.+18900\eta+112299\right)s^6+120\left(2303\eta^4-6820\eta^3-169792\eta^2+135720\eta+510885\right)s^4$$

$$\left.+16\left(6027\eta^4+128920\eta^3+523814\eta^2-889200\eta-2366481\right)s^2\right\}+64\left(1617\eta^3+4048\eta^2-8235\eta\right.$$

$$\left.-19914\right)+13500\left(3\eta^4-17\eta^2+16\right)s^{12}+450\left(102\eta^4+409\eta^2-653\right)s^{10}$$

$$-15\left(21363\eta^4+7040\eta^3-148942\eta^2+50400\eta+292027\right)s^8+4\left(86310\eta^4-550\eta^3-1267437\eta^2\right.$$

$$\left.+731880\eta+3172947\right)s^6-4\left(27783\eta^4-94182\eta^3-1018558\eta^2+1017270\eta+3335247\right)s^4$$

$$\left.-32\left(11693\eta^3+45496\eta^2-75825\eta-199668\right)s^2\right], \tag{E.1b}$$

$$\dot{h} = -\frac{3c\alpha^2 \mathrm{J}_2 n}{2a^2\eta^4} + \frac{3c\alpha^4 \mathrm{J}_2^2 n}{32a^4\eta^{12}} \left[4e^4 \left(3s^2-2\right) + e^3 \left(32-48s^2\right) - 16e \left(\eta^2-1\right)\left(3s^2-2\right) \right.$$
$$\left. +4 \left(\eta^6 - 6\eta^5 - 8\eta^4 - 4\eta^2 + 2\right) + \left(5\eta^6 + 36\eta^5 + 23\eta^4 + 24\eta^2 - 12\right) s^2 \right]$$
$$+ \frac{c\alpha^6 \mathrm{J}_2^3 n}{512a^6\eta^{12}\left(4-5s^2\right)^4} \left[50c^8 \left\{ 8 \left(147\eta^4 + 1375\eta^3 + 5381\eta^2 - 7875\eta - 19278\right) \right.\right.$$
$$\left. +225 \left(36\eta^4 - 55\eta^3 + 669\eta^2 - 315\eta - 1519\right) s^4 - 20 \left(378\eta^4 + 385\eta^3 + 8579\eta^2 - 6975\eta - 23277\right) s^2 \right\}$$
$$-10c^6 \left(16 \left(147\eta^4 + 2750\eta^3 + 11056\eta^2 - 15750\eta - 38703\right) + 3375 \left(13\eta^4 - 34\eta^2 + 21\right) s^6 \right.$$
$$\left. -900 \left(45\eta^4 + 55\eta^3 - 873\eta^2 + 315\eta + 1642\right) s^4 + 10 \left(105\eta^4 - 3080\eta^3 - 76066\eta^2 + 55800\eta + 190521\right) s^2 \right)$$
$$-3c^4 \left\{ -16 \left(49\eta^4 + 2750\eta^3 + 11252\eta^2 - 15750\eta - 38801\right) + 5625 \left(4\eta^4 - 7\eta^2 + 3\right) s^8 \right.$$
$$-1500 \left(91\eta^4 - 206\eta^2 + 115\right) s^6 + 100 \left(1402\eta^4 + 495\eta^3 - 10026\eta^2 + 2835\eta + 15950\right) s^4$$
$$\left. -40 \left(805\eta^4 - 770\eta^3 - 20672\eta^2 + 13950\eta + 48507\right) s^2 \right\} - 304 \left(55\eta^3 + 227\eta^2 - 315\eta - 777\right)$$
$$-16875 \left(\eta^4 - 4\eta^2 + 3\right) s^{12} + 1125 \left(37\eta^4 - 184\eta^2 + 147\right) s^{10} + 75 \left(314\eta^4 + 1333\eta^2 - 1647\right) s^8$$
$$-30 \left(3839\eta^4 + 660\eta^3 - 14718\eta^2 + 3780\eta + 20647\right) s^6 + 2 \left(41454\eta^4 + 3245\eta^3 - 362129\eta^2 + 165465\eta \right.$$
$$\left. +688989\right) s^4 - 12 \left(1323\eta^4 - 2442\eta^3 - 32740\eta^2 + 26070\eta + 82361\right) s^2 \Big] , \tag{E.1c}$$

$$\dot{L} = 0, \tag{E.1d}$$

$$\dot{G} = 0, \tag{E.1e}$$

$$\dot{H} = 0. \tag{E.1f}$$

The generating functions $\mathcal{W}_1$, $\mathcal{W}_2$, $\mathcal{W}_1^*$, and $\mathcal{W}_2^*$ are as follows:

$$\mathcal{W}_1 = \frac{\alpha^2 \mathrm{J}_2 n}{8\eta^3} \left[-3es^2 \sin(f+2g) - es^2 \sin(3f+2g) + 2e \left(3s^2-2\right) \sin f \right.$$
$$\left. -3s^2 \sin(2(f+g)) + 2 \left(3s^2-2\right)(f-l) \right] , \tag{E.2a}$$

$$\mathcal{W}_2 = \frac{\alpha^4 \mathrm{J}_2^2 n s^4}{256a^2 e\eta^7} \left[-24e^3 \sin(2f+2g) + 78e^3 \sin(4f+2g) - 15e^3 \sin(2f+4g) - 3e^3 \sin(4f+4g) \right.$$
$$+3e^3 \sin(6f+4g) - 360e^3 f \cos 2g + 60e^3 (f-l) + 30e^3 \sin(2f) + 360e^3 l \cos 2g$$
$$\left. -1344e^2 \sin(f+2g) + 128e^2 \sin(3f+2g) - 12e^2 \sin(3f+4g) + 12e^2 \sin(5f+4g) \right.$$

$$
\begin{aligned}
&-216e^2\sin f+72e\eta\sin 2f-336e\sin(2f+2g)+12e\sin(4f+4g)-480e(f-l)-72e\sin 2f\\
&+288\eta\sin f-288\sin f\,]+\frac{\alpha^4\mathrm{J}_2^2ns^2}{256a^2e\eta^7}\,[\,48e^3\sin(2f+2g)-60e^3\sin(4f+2g)+336e^3f\cos 2g\\
&+96e^3(f-l)+48e^3\sin 2f-336e^3l\cos 2g+1232e^2\sin(f+2g)-80e^2\sin(3f+2g)\\
&+864e^2\sin f-96e\eta\sin 2f+320e\sin(2f+2g)+864e(f-l)+96e\sin 2f-384\eta\sin f\\
&+384\sin f\,]+\frac{\alpha^4\mathrm{J}_2^2n}{256a^2e\eta^7}\,[\,-96e^3(f-l)-48e^3\sin 2f-512e^2\sin f+32e\eta\sin 2f\\
&-384e(f-l)-32e\sin 2f+128\eta\sin f-128\sin f\,],
\end{aligned}
\tag{E.2b}
$$

$$
\mathcal{W}_1^*=\frac{\alpha^2\mathrm{J}_2ns^2e^2\left(15s^2-14\right)}{32\eta^3\left(5s^2-4\right)}\sin 2g,
\tag{E.2c}
$$

$$
\begin{aligned}
\mathcal{W}_2^*=&-\frac{\alpha^4\mathrm{J}_2^2(\eta-1)ns^2}{1536a^2e\eta^{11}\left(4-5s^2\right)^2\left(5c^2-1\right)}\,\big[\,(\eta+1)\left(15s^2-14\right)c^2\,\big\{12\left(4e^5\left(15s^4-22s^2+8\right)\right.\\
&-16e^4\left(15s^4-22s^2+8\right)+e\left(-16\left(\eta^6-6\eta^5-8\eta^4-4\eta^2+2\right)+5\left(5\eta^6+36\eta^5+23\eta^4\right.\right.\\
&\left.\left.+24\eta^2-12\right)s^4-4\left(66\eta^5+63\eta^4+44\eta^2-22\right)s^2\right)+16\left(\eta^2-1\right)^2\left(15s^4-22s^2+8\right)\Big)\\
&-19e\eta^4\left(\eta^2-1\right)s^2\left(15s^2-14\right)\cos 2g\big\}-\left(5s^2-4\right)\Big\{44e^5(\eta+1)\left(2-3s^2\right)^2\left(15s^2-14\right)\\
&-176e^4(\eta+1)\left(2-3s^2\right)^2\left(15s^2-14\right)+e\left(16\left(105\eta^7+469\eta^6+55\eta^5-197\eta^4-308\eta^3\right.\right.\\
&\left.\left.-308\eta^2+154\eta+154\right)+45\left(25\eta^7-199\eta^6-81\eta^5+63\eta^4+264\eta^3+264\eta^2-132\eta-132\right)s^6\right.\\
&+6\left(125\eta^7+4373\eta^6+1277\eta^5-1531\eta^4-4488\eta^3-4488\eta^2+2244\eta+2244\right)s^4\\
&\left.-8\left(435\eta^7+3091\eta^6+603\eta^5-1197\eta^4-2508\eta^3-2508\eta^2+1254\eta+1254\right)s^2\right)\\
&+176(\eta-1)^2(\eta+1)^3\left(2-3s^2\right)^2\left(15s^2-14\right)\Big\}+2e(\eta-1)(\eta+1)^2\eta^4s^2\\
&\times\left(14-15s^2\right)^2\left(13s^2-10\right)\cos 2g\,\Big]\sin 2g
\end{aligned}
\tag{E.2d}
$$